FABRICATION AND ELECTRICAL/OPTICAL CHARACTERIZATION OF BULK GAN-BASED SCHOTTKY DIODES

Except where reference is made to the work of others, the work described in this dissertation is my own or was done in collaboration with my advisory committee. This dissertation does not include proprietary or classified information.

Hui Xu

Certificate of Approval:

Jianjun Dong
Associate Professor
Physics

Minseo Park, Chair
Associate Professor
Physics

John R. Williams
Professor
Physics

Michael J. Bozack
Professor
Physics

George T. Flowers
Dean
Graduate School

FABRICATION AND ELECTRICAL/OPTICAL CHARACTERIZATION OF BULK GAN-BASED SCHOTTKY DIODES

Hui Xu

A Dissertation

Submitted to

the Graduate Faculty of

Auburn University

In Partial Fulfillment of the

Requirements for the

Degree of

Doctor of Philosophy

Auburn, Alabama

August 10, 2009

FABRICATION AND ELECTRICAL/OPTICAL CHARACTERIZATION OF BULK GAN-BASED SCHOTTKY DIODES

Hui Xu

Signature of Author

Date of Graduation

VITA

Hui Xu, daughter of Renjun Xu and Guilan Zhong, was born on April 16, 1983, in Jiangyan, Jiangsu Province, People's Republic of China. In 2004, she received Bachelor of Science degree in Applied Physics from University of Science and Technology of China. After that she entered the graduate program at Physics Department of Auburn University in August, 2004, first worked as a Graduate Teaching Assistant and later a Graduate Research Assistant under the guide of Dr. Minseo Park. In 2007, she received a non-thesis Master of Science degree. She believes to learn is to change.

DISSERTATION ABSTRACT

FABRICATION AND ELECTRICAL/OPTICAL CHARACTERIZATION OF BULK GAN-BASED SCHOTTKY DIODES

Hui Xu

Doctor of Philosophy, August 10, 2009
(M.S. Auburn University 2007)
(B.S. University of Science and Technology of China, 2004)

129 Typed Pages

Directed by Minseo Park

As a wide bandgap semiconductor material, Gallium Nitride has long been considered as promising in blue and UV Light Emitting Diodes. And recently, its great potential in high power and high temperature applications is another area gaining lots of attention. Thanks to the fast development of crystal growth technology, high quality bulk Gallium Nitride substrate became available by Hydride Vapor Phase Epitaxy technique, which can greatly simplify fabrication process. With a fast switching speed and a low forward drop, Schottky diode is useful in high power electronic. Therefore, in this dissertation, the fabrication and characterization of Schottky diode based on bulk Gallium Nitride is discussed.

In order to achieve high breakdown voltage, while still keeping high forward current, vertical Schottky diodes were fabricated on low doping GaN epilayer grown on high doping bulk GaN substrate all by low cost HVPE. Device performance is discussed. Reliability of high power devices is always an issue. Self-heating is one of the concerns that limits the performance and lifetime of GaN devices. It is of great importance to monitor temperatures, especially when the devices are under operation. Raman spectroscopy offers the non-contact way method to diagnosis temperature. Therefore, it was used to probe Schottky diode temperature when the device was biased. Chemical stability of GaN makes it tolerant to harsh environment, such as high radiation. Diode degradation was observed after gamma ray irradiation, which gave information about intrinsic defects in GaN.

ACKNOWLEDGEMENTS

The author would like to give deepest appreciation to Dr. Minseo Park for his guidance, advice and support through the entire research work during the Ph.D period in Auburn University. The author also would like to give thanks to all the committee members, Dr. Jianjun Dong, Dr. John Williams, Dr. Michael J. Bozack and Dr. Kim for their participation in evaluating the work.

Additional, the author would like to thank Dr. Claude Ahyi for his kindly help and discussion every time. Thanks to Max Cichon for the help with gamma ray radiation and Tamara Isaacs-Smith for assistance any time. Thanks to Yi Zhou for the instruction with working on all kinds of fabrication equipments in the early part of the work. Thanks to An-jen Cheng for the help with Raman and PL characterization. Thanks to Zengjun Chen, Xingguang Zhu and Mingyu Li for discussion of problems met in device fabrication procedures.

Thank Kyma Technologies, Inc for providing the substrates.

Finally, the author would like to express special thanks to her boyfriend Chaokang Gu, without his patience, encourage and continuous support, the work could be much harder to finish. This dissertation is also dedicated to all the family members and friends.

Style manual or journal used: Applied Physics Letters with paper titles

Computer Software used: Microsoft Word 2007, Microsoft Excel 2007, Microsoft PowerPoint 2007, Origin Pro 7.5

TABLE OF CONTENTS

LIST OF TABLES

LIST OF FIGURES

CHAPTER 1

INTRODUCTION

1.1 GaN Material Properties

III-nitride semiconductor materials have been regarded as promising for semiconductor device applications during the past few decades. GaN is one of the III-nitride family members, which has received the most attention. The first GaN based light emitting diode was reported in early 1970s[1]. However, because there was no suitable substrate with close lattice match, the heteroepitaxial growth exhibited high defect density. The high n-type background carrier concentration is commonly thought to be from nitrogen vacancies. It was also not possible to grow p-type materials for a long time. These significant difficulties began to be overcome after the mid-1980s. High quality GaN films on sapphire substrates were achieved by metalorganic chemical vapor deposition (MOCVD) using AlN[2] or GaN[3] nucleation layers. As the background doping was reduced, it became possible to realize intentional doping. Si and Ge were found to be suitable for GaN n-type doping[4]. Si-doped GaN can have carrier concentrations as high as $2\times10^{19}/\text{cm}^3$, with smooth surface morphology. Since many device applications of GaN require p-n junction formation, great effects were made to dope p-type GaN.

The breakthrough was made by Amano *et al.* [5] who fabricated p-type GaN from Mg-doped GaN by low energy electron beam irradiation (LEEBI). However, the acceptor activation ratio was low because of the large binding energy of Mg. Later on, the hole concentration was increased to as high as $3\times10^{18}/cm^3$, with 0.2 Ω-cm resistivity[6]. In 1992, Nakamura discovered that thermal annealing at 700°C under N_2 ambient could achieve the same effect as LEEBI process[7]. Thereafter, Nichia offered the first commercial GaN based LEDs and laser diodes, which made GaN become the focus of increased research.

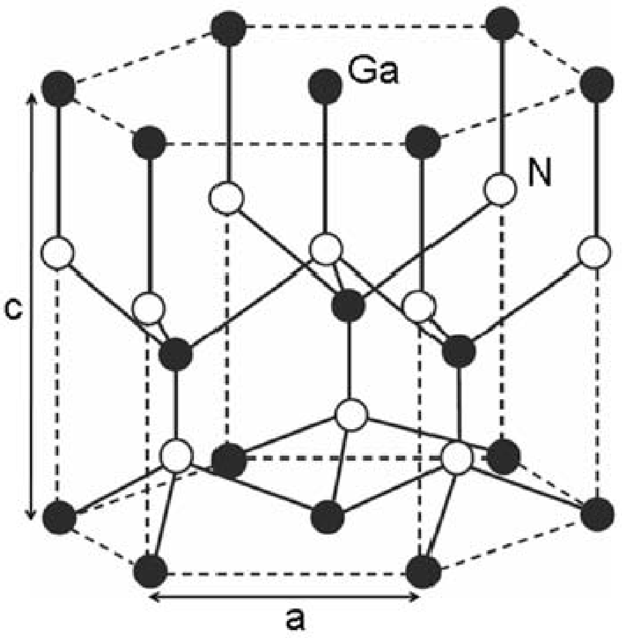

Figure 1.1.1 Wurtzite crystal with lattice constancts *a* and *c* [8]

This compound is a direct bandgap semiconductor material with Wurtzite or Zinc Blende crystal structure. However, the Wurtzite structure (as shown in figure 1.1.1) is more common than Zinc Blende. Under equilibrium, GaN crystallizes only in the Wurtzite structure[9]. Moreover, Zinc Blende polytypes have high defect densities due to large lattice mismatch. The basic parameters at room temperature for both Wurtzite and Zinc Blende crystal structures are provided in table 1.1.1.

Table 1.1.1 Material properties for Wurtzite and Zinc Blende GaN [10]

Crystal Structure	Wurtzite	Zinc Blende
Static dielectric constant	8.9	9.7
High frequency dielectric constant	5.35	5.3
Electron affinity (ev)	4.1	4.1
Lattice constants	a=3.189, c=5.186	4.52
Energy gap	3.4	3.2
Effective conduction band density of state (cm^{-3})	2.3×10^{18}	1.2×10^{19}
Effective valence band density of state (cm^{-3})	4.6×10^{19}	4.1×10^{19}
Electrical properties		
Breakdown field (MV/cm)	4	4
Hole mobility ($cm^2V^{-1}s^{-1}$)	200	350
Electrons mobility	1000	1000
Hole thermal velocity	9.4×10^4	9.5×10^4
Electron thermal velocity	2.6×10^5	3.2×10^5

The recent success of GaN semiconductor devices is much related to the unique material properties of GaN. It has a wide bandgap of 3.4 eV, making GaN attractive for high power and high temperature applications. Table 1.1.2 lists the material properties related to high temperature, high power and high frequency application of GaN and some other conventional semiconductors. The intrinsic carrier concentration of GaN at room temperature is 2×10^{-10} cm^{-3} calculated through this equation[11]:

$$n_i = \sqrt{N_C N_V} e^{-E_g/2kT}$$

where Nc and Nv are effective density of states at conduction band and valence band edge. Therefore, wide bandgap materials, like GaN or SiC, can go intrinsic at much higher temperatures compared to conventional materials such as Si, GaAs[12]. This property implies that GaN based power devices can operate with less cooling concerns and reduce the cost of processing for heat extraction. Meanwhile, another attractive property is the high critical breakdown field ~ 4 MV/cm, compared to 0.2 MV/cm for widely used Si. High critical breakdown field leads to a high breakdown voltage, which is required for high power devices obviously. Because the heat generation of intrinsic carriers at high temperatures is beyond control for conventional semiconductors, power electronics based on Si or GaAs are not able to tolerate elevated temperatures. Additional circuit designs for heat sinking makes packaging more complicated. Wide bandgap semiconductors, such as GaN and SiC, due to their inherent material advantages, can reduce the size of power stations and lower the cost for packaging[13].

GaN has shown a high saturation drift velocity; up to 3×10^7 cm/s. Theoretical calculations through monte carlo simulations all predicted that GaN with a doping level at 10^{17} cm^{-3} has a high saturation velocity and high electron mobility[14,15]. Recently, high electron mobility transistors (HEMT) based on AlGaN/GaN heterostructure is considered as the next generation mobile phone base station amplifiers[16]. Experimental data shows that the high electron mobility in two-dimensional (2D) electron gas is more pronounced than in GaAs[17]. Two types of polarizations exist in the heterostructure: spontaneous and piezoelectric, thanks to the lack of inversion symmetry of the wurtzite crystal structure and the high electronegativity of nitrogen atom[18].

From the beginning, GaN has been known for its application in light emitting diode (LED) due to its direct bandgap. Blue LEDs must emit more power in order to achieve comparable brightness, because the responsivity of human eye decreases significantly from green to other smaller wavelength color[19]. For indirect wide bandgap semiconductor material, such as SiC, it has difficulty achieve high output power because of the inherent inefficiency. This can be explained by radiative recombination, which an electron in the conduction band combines with a hole in the valence band and emits released energy through a photon. Moreover, even grown on highly lattice mismatched substrates and having a large dislocation defect density, GaN based LED can survive with high efficiency, which possibly comes from the ionic character of bonding in nitride materials[20]. These properties make GaN a good material for optoelectronics devices.

Table 1.1.2 Comparison of important semiconductor properties for high temperature electronics [12]

Property	Si	GaAs	4H SiC	GaN
Band Gap (eV)	1.12	1.42	3.25	3.4
Breakdown field (MV/cm)	0.25	0.4	2.2	4
Electron mobility (cm^2/V s)	1350	6000	800	1300
Thermal conductivity (W/cm K)	1.5	0.5	4.9	1.3
Saturation drift velocity (10^7 cm/s)	1	2	2	3
Dielectric constant	11.8	12.8	9.7	9
CFOM	1	8	458	489

CFOM: combined figure of merit for high temperature/high power/high frequency applications

Despite of the advantages of GaN materials, the difficulty of growth has impeded the development of GaN devices. The primary difficulty is the lack of GaN single crystal substrates for homoepitaxial growth[12]. Thus, GaN is forced to be grown by heteroepitaxy, mostly grown on sapphire or SiC, generating threading dislocations due to lattice mismatch. It is believed that the earliest report of GaN growth was by Johnson *et al.*[21]. The investigations of nitrides were made on small crystals or powders, which were first described as the conversion of metallic Ga in a NH_3 stream into GaN through the reaction:

$$2Ga + 2NH_3 = 2GaN + 3H_2$$

Then, the first single crystal GaN thin films were achieved by Maruska and Tietjen by a vapor transport CVD method[22]. Their approach was to flow HCl vapor onto metallic Ga, subsequently reacted with NH_3 at the sapphire substrate via this reaction:

$$GaCl + NH_3 = GaN + HCl + H_2$$

The growth rate of this technique was relatively high (0.5 μm/min). It allowed thick film growth, which was less influenced by thermal and lattice mismatches.

An ideal way to solve the lattice mismatch problem is to use a homoepitaxial substrate to grow GaN. Bulk GaN is a solution. Fast developing technology, hydride vapor phase epitaxy (HVPE) can be utilized to produce bulk GaN, due to the high growth rate[23]. Figure 1.1.2 shows the schematic figure of HVPE process[24]. In the process, group III nitrides, such as GaN or AlN, are formed by mixing hot gaseous metal chlorides GaCl or AlCl with ammonia gas (NH_3). The metal chlorides are generated by flowing hot HCl gas over the metal melt. The reactions involved are the same as the first epitaxial method used for the growth of single GaN crystal. The GaN templates are grown on substrates such as sapphire or SiC. P-type GaN can be achieved by using Mg during the growth and n-type GaN by silane gas. The thick GaN films can be separated from the growth substrate by a pulsed laser to thermally decompose a thin layer of GaN at the interface of the film and foreign substrate as seen in figure 1.1.3[23]. Chemical treatment and polishing of N-face surface is performed to remove the most defective region.

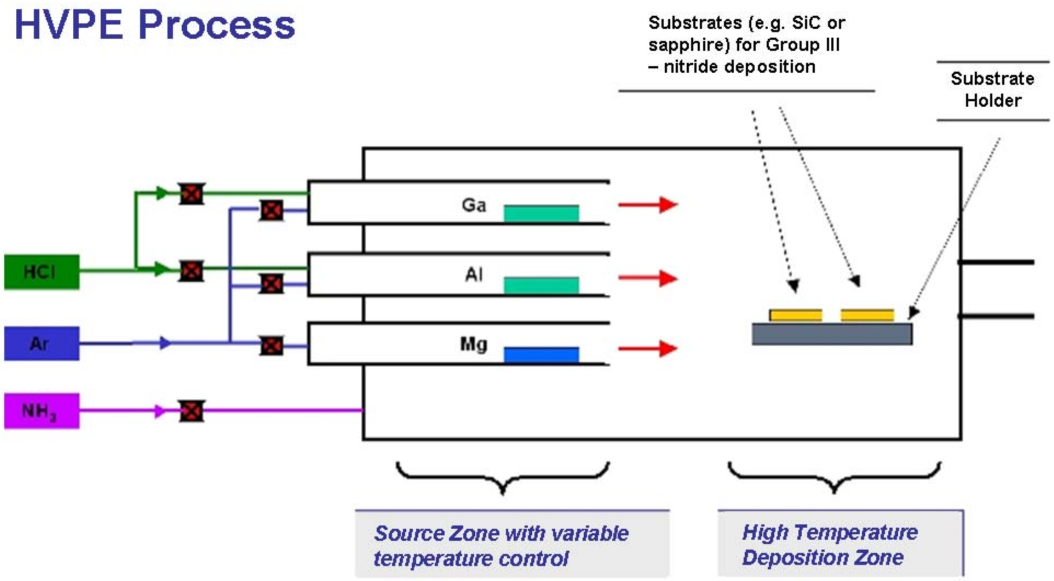

Figure 1.1.2 Schematic figure of HVPE process

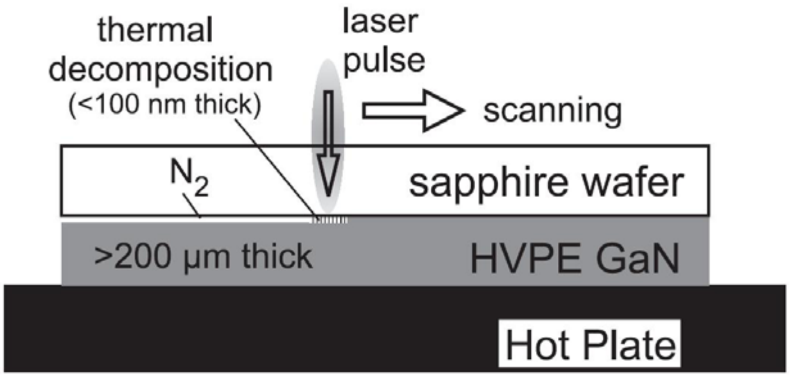

Figure 1.1.3 Schematic of laser induced liftoff to remove the substrate from GaN

Another method, such as metal-organic chemical vapor deposition (MOCVD) is also widely used to grow GaN thin film. It was first grown by S. Nakamura with GaN buffer layer[3]. The two gas flow system was shown in figure 1.1.4. The high velocity main flow transports the reactant gas to the substrate through the quartz nozzle, while the subflow goes in a perpendicular direction in order to assist the reactant gas in contact with the substrate. GaN buffer layer was grown at low temperature around 500°C. Then the desired GaN was grown at the high temperature between 1000°C and 1030°C. The surface morphology was greatly improved and the dislocation density was reduced with the GaN buffer layer[3,25]. The main reaction happened in the process was:

$$\text{TMG}(\text{Ga}(\text{CH}_3)_3) + \text{NH}_3 = \text{GaN} + 3\text{CH}_4$$

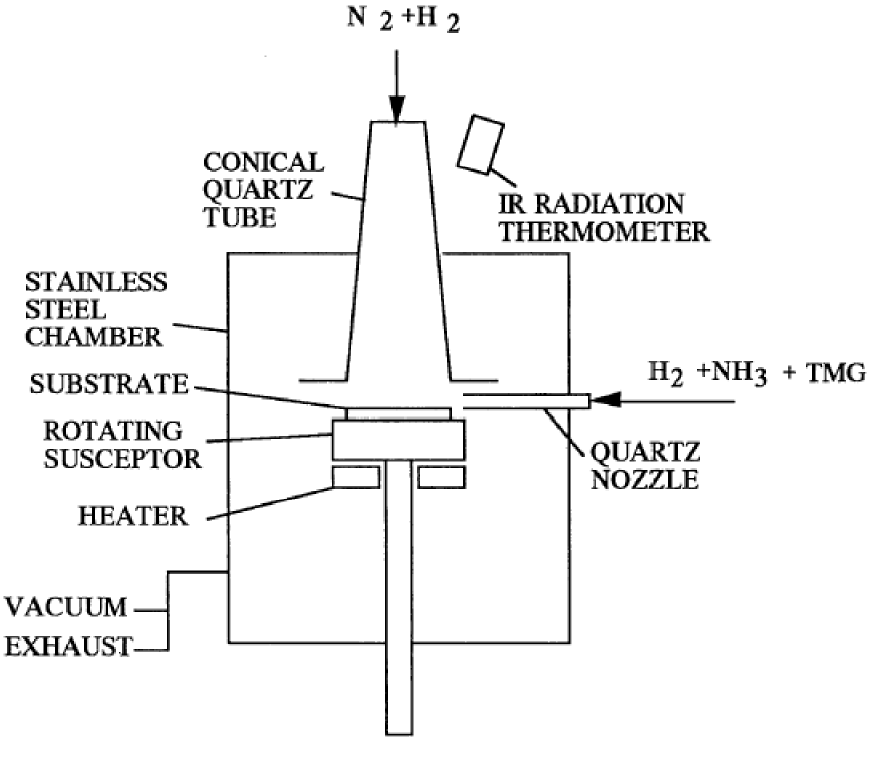

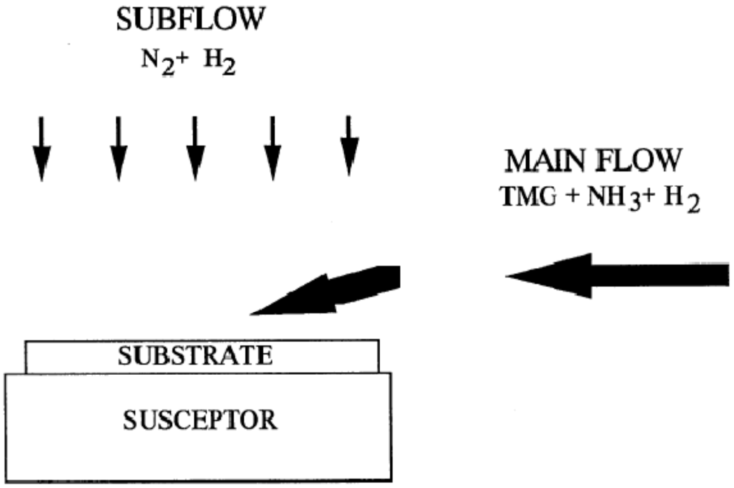

Figure 1.1.4 Schematic figure of two-flow MOCVD

In this dissertation, the primary focus is the study of Schottky diodes based on bulk GaN. Low leakage Schottky diodes have been fabricated with electrical properties discussed. Thermal management of devices is very important for device fabrication. Raman spectroscopy successfully indicated the temperature change of the GaN substrate when the Schottky diodes were under operation. Defects related to gamma-ray radiation on GaN were studied through the electrical characterization of Schottky diode. The discussions below are all based on N-type bulk GaN substrates.

1.2 GaN Schottky Diode Review

In the early 1980s, Schottky barrier diodes were fabricated on epitaxial GaN in order to determine the electrical properties of the thin GaN layer. For example, capacitance-voltage (C-V) measurements were widely utilized to determine the impurity profiles[26]. Until 1990s, it was possible to grown better quality single crystal GaN. Before that, it was difficult to have Schottky barrier diodes, from which the properties can be studied[27]. Hacke *et al.* successfully achieved low reverse leakage current below 1×10^{-10} A at the bias of 10 V[27]. Later on, much effect was put into charactering Schottky barrier diodes based on different contact metals by many groups. Aluminum and gold contacts were found to behave as ohmic and Schottky contacts on GaN[28]. High barrier height Schottky diodes of more than 1 eV were realized by using platinum (Pt)[29,30]. Varieties of metals of metals such as Pt, Pd, Au, Cr, Ni, Mo, and W were used as Schottky contact metal on GaN. Q. Z. Liu and S. S. Lau contributed a good review of metal GaN contact technology[31]. Stable and high performance metal contacts on GaN are crucial for device application. Theoretically, the Schottky barrier height is only the difference of metal work function and the electron affinity for a semiconductor material. Experimental results are inconsistent for the same metal[31]. General speaking, metals with higher work function can form a higher Schottky barrier height on GaN, which means there is a relationship between work function and barrier height. Making a low resistance ohmic contact on GaN is also very important for high performance Schottky diode. A detailed discussion concerning the metal stack for GaN ohmic contact is presented in Chapter 2.

An important characteristic of GaN based Schottky rectifiers is the measurement of critical field for electric breakdown. The critical breakdown field is a one of the most important parameters for high power devices[32]. Z. Z. Bandic *et al.* fabricated Schottky rectifiers with 450V standoff voltage based on HVPE grown GaN on sapphire substrate[32]. Their best devices had a turn on voltage (defined as the voltage where the corresponding current density is 100 A/cm^2) of 4.2 V. They also pointed out that the premature breakdown was related to corner and edge effects which severely limit the critical breakdown field.

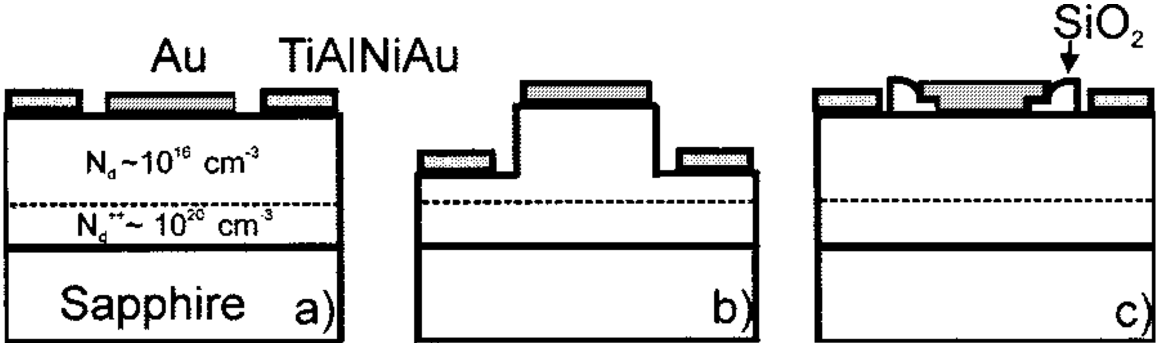

Figure 1.2.1 Device structures for GaN Schottky diodes (a) lateral Schottky rectifier (b) semi-vertical mesa structure (c) lateral Schottky rectifier with SiO_2 field plate.[32]

Figure 1.2.1 also from Bandic shows an example of GaN Schottky diodes with 3 different device geometries. Figure 1.2.1 a) is traditional lateral devices. Figure 1.2.1 b) shows devices with a mesa structures in the effect to decrease the ohmic resistivity because the ohmic contacts are closer to the region with higher electron concentration. However, the results were not as good as expected, mostly due to the mesa etching damage. Figure c) shows lateral device structure with SiO_2 field plate to lower the electric field crowding at the Schottky contact corner, which was found to be effective to achieve low reverse leakage current. To avoid damaging the top of the mesa structure while lowering the ohmic contact resistance, selective-area doping of the n^+ ohmic contact regions were formed by Si implantation[33]. With such lateral structure devices, > 2000 V breakdown voltage was realized, making GaN Schottky rectifiers comparable to the rectifiers on other wide band gap semiconductors, such as SiC. Breakdown voltage as high as 6350 V for GaN Schottky diodes was achieved in lateral geometry[34]. However, these devices have a high on-state voltage of >15 V and on-state resistance ~ 150 $m\Omega \cdot cm^2$. Although the breakdown behavior seems to be better in lateral geometry, it was found that the vertical mobility is about 6 times larger than the lateral mobility through the study of lateral and vertical current transport in GaN films[35]. With the contradiction that vertical is preferred for high electron mobility and the worry of mesa structure etching damage, it turns out that Schottky devices based on bulk GaN is the best solution. Due to the fast development of crystal growth technology, high quality bulk GaN is now available. Therefore in chapter 3, Schottky rectifiers with low on-state voltage and specific on-state resistance, fabricated based on n^- epi/n^+ bulk GaN substrates, are presented. The breakdown voltage is not as high as mentioned above, and this is likely caused by the premature breakdown at the corners of the contacts.

A brief introduction of the electrical properties of Schottky diodes is provided below.

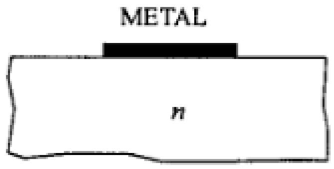

Figure 1.2.2 Simple metal-semiconductor contact

Figure 1.2.2 represents the structure of a Schottky contact. From the figure, it is obvious that the metal and the semiconductor substrate are in direct contact. So the Schottky barrier diode is also known as metal-semiconductor (MS) junction, which is used as building blocks for other devices. The direct MS junction results in low forward voltage drop and fast switching speed. Ideal Schottky diode does not have a recovery time, compared to typical p-n diode, when the diode switches from conducting state to non-conducting state (on and off). Sometimes, Schottky diode is called the "majority carrier" semiconductor device, because it is majority-carrier current dominant. The minority-carrier current is usually 4-6 orders of magnitude smaller than the majority-carrier current[36]. Thermionic emission of majority carriers over the barrier is the main current transport mechanism in a Schottky diode.

$$I = AA^{*}T^{2}\exp\left(\frac{-q\phi_b}{kT}\right)\left[\exp\left(\frac{qV_f}{nkT}-1\right)\right] = I_s\left[\exp\left(\frac{qV_f}{nkT}-1\right)\right] \qquad (1.2.1)$$

In this equation, A^{*} is effective Richardson constant.

$$A^{*} = \frac{4\pi q m^{*} k^{2}}{h^{3}}$$

T is the temperature, $\phi_b$is the Schottky barrier height, which will be introduced in details soon. k is Boltzmann constant, V_f is forward current. Is is the saturation current.

$$I_s = AA^*T^2 \exp\left(\frac{-q\phi_b}{kT}\right)$$

Typical I-V characteristic in different scale is:

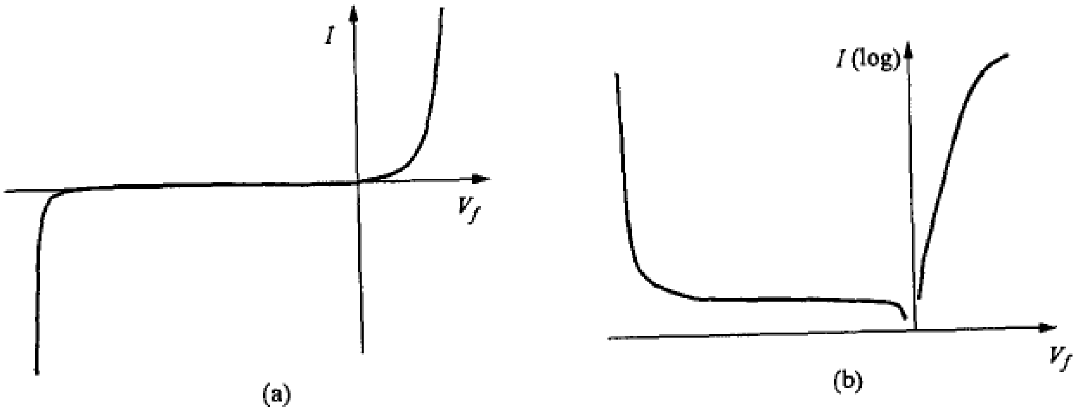

Figure 1.2.3 Typical I-V curve in linear and log scale [36]

(a) is plot in linear scale; (b) is plot in log scale.

The capacitance of the depletion-layer of a Schottky contact is:

$$\frac{A^2}{C^2} = \frac{2[\psi_{bi} - V - kT/q]}{q\varepsilon_s N} \tag{1.2.2}$$

where ψ_{bi} is the built-in potential, ε_s is the permittivity of semiconductor, N is the doping concentration, q is electron charge, k is Boltzmann constant. From the plot of $1/C^2$ vs. V, one can determine the barrier height as well as the doping concentration.

When a metal is in intimate contact with a semiconductor, a barrier is formed, which will control the current and capacitance behavior. It is important to understand the formation of the Schottky barrier in order to improve its performance. The formation of a Schottky barrier is shown by the energy band diagram.

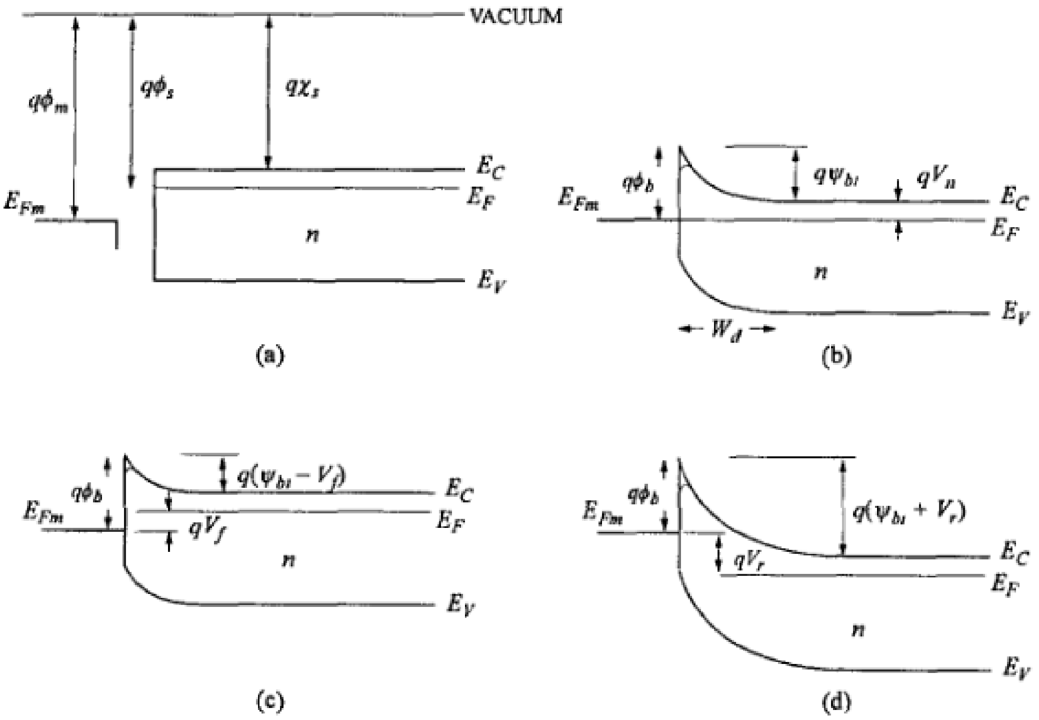

Figure 1.2.4 Band Structure of Schottky contact under bias [36]

(a) metal and semiconductor without contact

(b) metal and semiconductor in contact and under equilibrium

(c) under forward bias

(d) under reverse bias

For ideal interface, the barrier height is given by

$$\phi_b = \phi_m - \chi_s$$

ϕ_m the metal work function, it is the energy difference between the vacuum level to the Fermi level. χ_s is the electron affinity measured from the vacuum level to the bottom of the conduction band. This simple equation is never realized in reality. Experimentally, the measured Schottky barrier heights are a function of the difference between the metal work function and electron affinity of GaN[37].

As one of the important parameters representing the characteristics of the Schottky diode, barrier height needs to be measured after the fabrication of Schottky diode. There is more than one method to determine the barrier height. However, two major methods will be frequently used in this dissertation.

1. I-V curve: based on equation 1.2.1, a linear region of semilog I vesus V can be found for V>>kT/q.

   $$lnI = lnI_s + \frac{qV_f}{nkT} - 1$$

   When V_f is extrapolated to zero, the saturation current I_s is found. Then barrier height is calculated from the equation below.

   $$\phi_b = \frac{kT}{q} \ln \left(\frac{AA^2T^2}{I_s}\right)$$

2. C-V curve:

   $$\frac{A^2}{C^2} = \frac{2[\psi_{bi} - V - kT/q]}{q\varepsilon_s N}$$

   The built-in potential and the barrier height have the following relationship:

   $$\phi_b = \psi_{bi} + V_0$$

   where $V_0 = (kT/q)\ln(N_C/N_D)$, where N_C is the effective density of states in the conduction band. For GaN, $N_C = 2.3\times10^{18}$ cm^{-3} is normally used at room temperature. It is temperature dependent $N_C \propto T^{3/2}$.[38] If equation 1.2.2 is revised in this way,

$$1/C^2 = \left(\frac{2}{q\varepsilon_s N A^2}\right)[\psi_{bi} - kT/q - V]$$

$1/C^2$ has a linear relationship with V. The doping concentration N can be determined from the slope of the inverse capacitance squared vs. voltage plot as shown in figure 1.2.5. The intercept at the x axis enables us to calculate built-in potential.

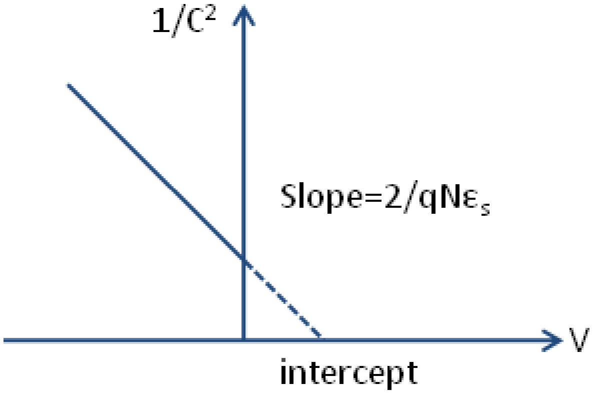

Figure 1.2.5 Linear relationship of inverse capacitance square and voltage

Therefore, the barrier height determined from C-V data is:

$$\phi_b = V(intercept) + kT/q + (kT/q)\ \ln(N_C/N_D)$$

Comparison of barrier heights determined from current-voltage (I-V), capacitance-voltage (C-V) and other methods have been studied. In one study, for instance, barrier height of Pt film was found to be 0.81V and 0.98V from I-V and C-V, respectively[39]. I-V behavior can be affected by any damage at the interface, since defects may act as recombination centers or intermediate state to assist tunneling current, which will increase n and decrease ϕ_b[40]. C-V measurements tend to be insensitive to such defects. It was observed that barrier height derived from I-V curve seems to be small than the value from C-V curve[41], the details will be discussed in Chapter 2.

The specific on-state resistance is another important parameter for GaN Schottky diodes. It is obtained through the inverse slope of the linear region in the forward I-V curve multiple the device area, usually with a unit of $m\Omega\cdot cm^2$ or $\Omega\cdot cm^2$.

1.3 Raman Spectroscopy

Raman Spectroscopy is a technique used to probe the surface structure and dynamics. It is widely used to study vibrational and rotational modes in a system. In the typical Raman experiment, a high intensity monochromatic light source, usually a laser is used to illuminate the sample. The incident photons interact with the sample. Most of the photons are elastically scattered, that is, the scattered light has the same frequency as the original incident light. This case is known as Rayleigh scattering. However, when the scattered light frequency is different from the incident frequency, it is known as Raman scattering. In Raman scattering, a molecule can absorb energy from the incident light, and thereby be excited from ground state to the higher vibrational energy state, which is called Stokes lines. If the molecule gives up energy to the incident phonons, causing the molecule return to its ground vibrational energy state, then anti-Stokes lines could be observed.

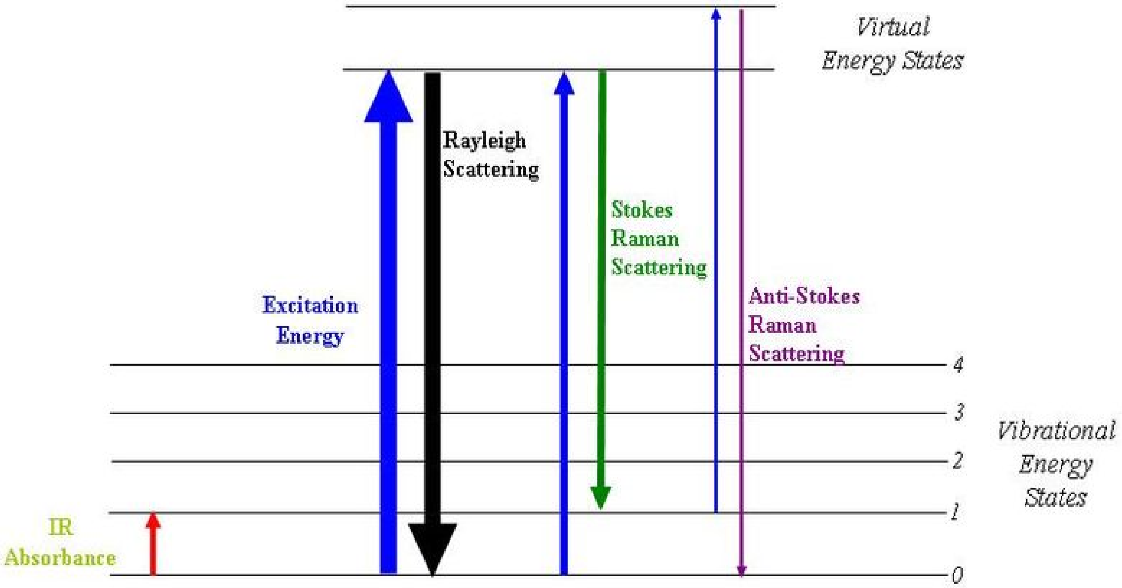

Figure1.3.1 Energy level diagram for Raman spectroscopy [42]

Figure 1.3.1 depicts the Raman process. The molecule is considered to be excited to a virtual energy state from the ground state by the incident photon, and return to a vibrational state, generating Stokes lines. In fact, the Raman effect occurs when the light interacts with the electron cloud of the sample molecule, leading to a change in molecular polarization potential.

In solid state physics, Raman spectroscopy is widely used to characterize materials, measure temperatures, and to find the crystallographic orientation. A given material has characteristic phonon modes, which act as a fingerprint for the material under investigation. Moreover, Raman spectroscopy can also be used to detect other low frequency excitation of the solid, such as plasmons, magnons, and superconducting gap excitations[42]. Raman scattering gives information about crystal orientation for an anisotropic crystal. If the crystal structure is provided, the polarization of Raman scattered light with respect to the crystal and the polarization of the laser light can be used to find the orientation of the crystal.

There are several advantages of utilizing Raman spectroscopy for microscopic analysis. Samples do not need to be sectioned, since it is a scattering technique. Almost no sample preparation is required. Only a very small amount of material is required for collecting the Raman data. Raman spectroscopy, in particular confocal microscopy, has very high spatial resolution along the z direction with good stability and repeatability. In addition, it is a non-contact, non-destructive method, excellent for sample reusability.

Raman phonon modes of GaN have received considerable attention due to the information provided is important in considering the electron transport and the non-radiative electron relaxation process[43]. It is interesting that in most of the Raman scattering measurements performed for GaN to date, similar phonon frequencies have been observed despite variations in sample quality. T. Azuhata *et al.* first successfully determined all of the Raman-active phonon frequencies from a high quality single-crystal GaN film grown on a sapphire substrate[43]. The crystalline structure of wurtzite-type GaN is described by the space group C^4_{6v}. Group theory predicts that the following Raman active phonons which are near-zero wave vectors[44]:

$$A_1(z) + E_1(x,y) + 2E_2$$

In the above, the polar $A_1(z)$ modes are polarized along the z axis, and the polar $E_1(x,y)$ modes are polarized in the xy plane. According to the direction of propagation, the polarity of the modes and the uniaxial structure of GaN will lead to frequency dispersion of the polar modes. Therefore, $A_1(z)$ phonon modes propagating along the z axis are purely longitudinal (LO), and due to the contribution of the electric field it has the highest frequency. On the other hand, phonons propagating in the xy plane are purely transverse (TO) and have the lowest frequency. For other propagation directions, longitudinal and transverse phonons exist simultaneously. Their frequencies will be between A_1(LO), E_1(LO) and A_1(TO), E_1(TO). $E_1(x, y)$ phonons are purely transverse along the z axis and propagating purely transverse or longitudinal in the xy plane.

For our scattering geometry, incident and scattered light propagates along the z axis and the c axis of GaN is along the z axis. Thus, only A_1(LO), E_1(TO), and $2E_2$ modes participate in the scattering according to the selection rule. Experimentally, Raman peaks due to E_2 high (568cm^{-1}) and A_1(LO) (732cm^{-1}) are observed easily because of their high intensity compared to other phonon modes.

Raman technology is a non-contact method widely applied for semiconductor characterization and the temperature dependent Raman effect on GaN Schottky diodes was studied and will be discussed in Chapter 4. In Raman measurement, temperature is deduced through the inelastic energy transfer between photons (light) and phonons (lattice vibrations)[45]. Because the incident light stays invariant during the device operation, all the Raman spectra changes observed are due to the phonon behavior of the crystal. Any phonon characteristic which varies with respect to temperature can then be utilized to study the thermal state of a device. Temperature measurements using Raman spectroscopy are generally performed by analyzing changes in the energy of optical phonons through analysis of the Stokes peak positions. From the experimental point of view, the phonon frequency shift of the peak is first monitored, and subsequently converted to a corresponding temperature difference using an appropriate calibration standard.

CHAPTER 2

DEVICE PROCESSING AND CHARACTERIZATION TECHNIQUES

2.1 Cleaning

Figure 2.1 Fabrication bench

The sample is cleaned upon receipt. Figure 2.1 shows the sample cleaning bench. For GaN, the cleaning procedure used is Acetone, Trichloroethylene(TCE), Acetone, Methanol, Methanol 5 minutes each in ultrasonic sequentially. First acetone and TCE is used for complete organic degreasing. Second acetone serves as the solvent to dissolve TCE. First methanol is the solvent for acetone. Last methanol is further cleaning organic solvent. Since methanol is dissolvable in water easily. Deionised water (DI water) rinse is next step. Next the samples are immersed into a dilute HCl solution (HCl:H_2O). A 1:1 HCl:Deionized(DI) water solution was found to be effective to remove oxide from GaN, and produces the lowest C/N ratio. Cl contamination was observed on the surface[46]. For HCl treatments, the oxygen surface coverage was inversely related to the amount of Cl detected on the surface, which means that higher Cl coverage leads to lower oxygen coverage[47]. Cl termination of GaN surfaces may be desirable, since the bond strengths of N, Ga and Cl are strong; binding dangling bonds at nitride surfaces with Cl should stabilize and inhibit reoxidation of the surface in air[47].

2.2 Sputtering

Sputtering is widely used for thin-film deposition. By bombardment of the target with energetic ions, atoms are ejected from a solid target material. Collision is the main mechanism of the physical sputtering. Momentum transfers between the atoms and ions. When the incident ions reach the target surface with the energy above the binding energy of the target atom, an atom can be ejected. The incident particles for the sputtering process are supplied by Ar plasma. Figure 2.2.1 and 2.2.2 show the exterior and interior appearance of the sputtering system. Ar plasma is created by high voltage and the Ar ions are accelerated through corresponding electric field. For vertical Schottky diodes on bulk GaN, an Ohmic contact is sputtered on the full backside of GaN wafer. In GaN based devices, reliable Ohmic contact formation is one of the critical issues. Ti is a low work function metal for GaN, and it is used as an Ohmic contact metal. Alternatively, Ti/Al bilayers were found to achieve a low contact resistance of 8×10^{-6} $\Omega\cdot cm^2$ after annealing at 900^oC for 30s[48]. One possible process involved is the solid phase reaction between Ti and GaN, where TiN is formed during high temperature annealing. N out-diffusion creates N vacancies near the contact. The region will be heavily doped n-GaN, because N vacancies act as donors for GaN[49]. However, the Ti/Al bilayers are not reliable upon high temperature annealing due to the tendency of oxidation of Ti or Al, as well as the propensity of Al to melt and "ball up"[50, 51]. During rapid thermal annealing (RTA), even with the presence of a very low concentration of oxygen (1 part per million), the contact suffers from oxygen contamination. The contact may become highly resistive due to alloying from the formation of Al_2O_3 coating on Al. Usually, the surface morphology of most Ti/Al contacts are quite rough. Al has a low melting temperature of 660^oC, which makes it very sensitive to RTA temperature. More complex multilayer systems, such as Ti/Al/Ni/Au, Ti/Al/Ti/Au, Ti/Al/Pt/Au, Ti/Al/Pd/Au, and Ti/Al/Mo/Au are suggested as better choice. In these different metal combinations, the last low resistance metal layer Au is employed to improve the resistance to oxidation of Ti/Al layer during high temperature annealing. As a third layer, different metals (Ni, Ti, Pt, Pd and Mo) between Au and Ti/Al are introduced to prevent the interdiffusion of Ti, Al and Au in order to improve the thermal stability of the contact.

Figure 2.2.1 Exterior of sputtering system

Figure 2.2.2 Interior of sputtering system

2.3 Rapid Thermal Annealing

Simple cleaning process is performed to remove the pasting organic used in sputtering step, by acetone, methanol and DI water. Subsequently, the samples are loaded into annealing system shown in figure 2.3.1. They are located in the center of the carbon strip, where heat is transferred. As you can see, there are some clips on top of the samples. Two purposes for this, one is to assist heat transfer to the top surface of the samples where it is not in direct contact with the heating source: carbon strip; second is that to help stable the sample when Nitrogen gas first comes through the chamber during the annealing time. Rapid thermal annealing is an important process used in semiconductor device fabrication industry. It consists of a heating a wafer in a timescale of seconds or minutes in order to affect its electrical properties. Ohmic contact annealing is essential in improving the electric properties, such as reducing the contact resistance and making better adhesion between metals and semiconductors. On n-type GaN, a nonalloyed Ti/Al metallization has been found to form a good ohmic contact[52]. The ohmic characteristic is believed to be caused by high temperature annealing which generates nitrogen vacancies that leave the surface heavily n-type, suitable for forming a tunneling junction.

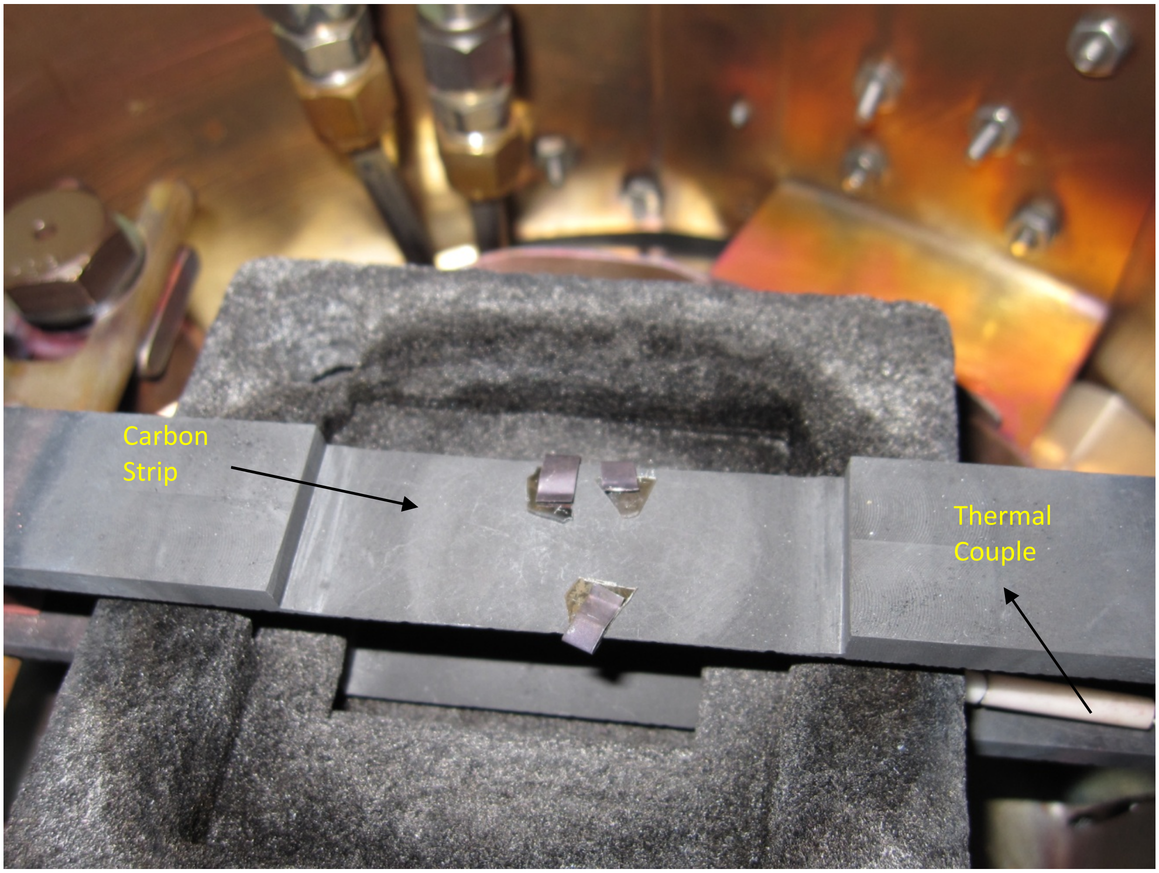

Figure 2.3.1Annealing system Sample holder

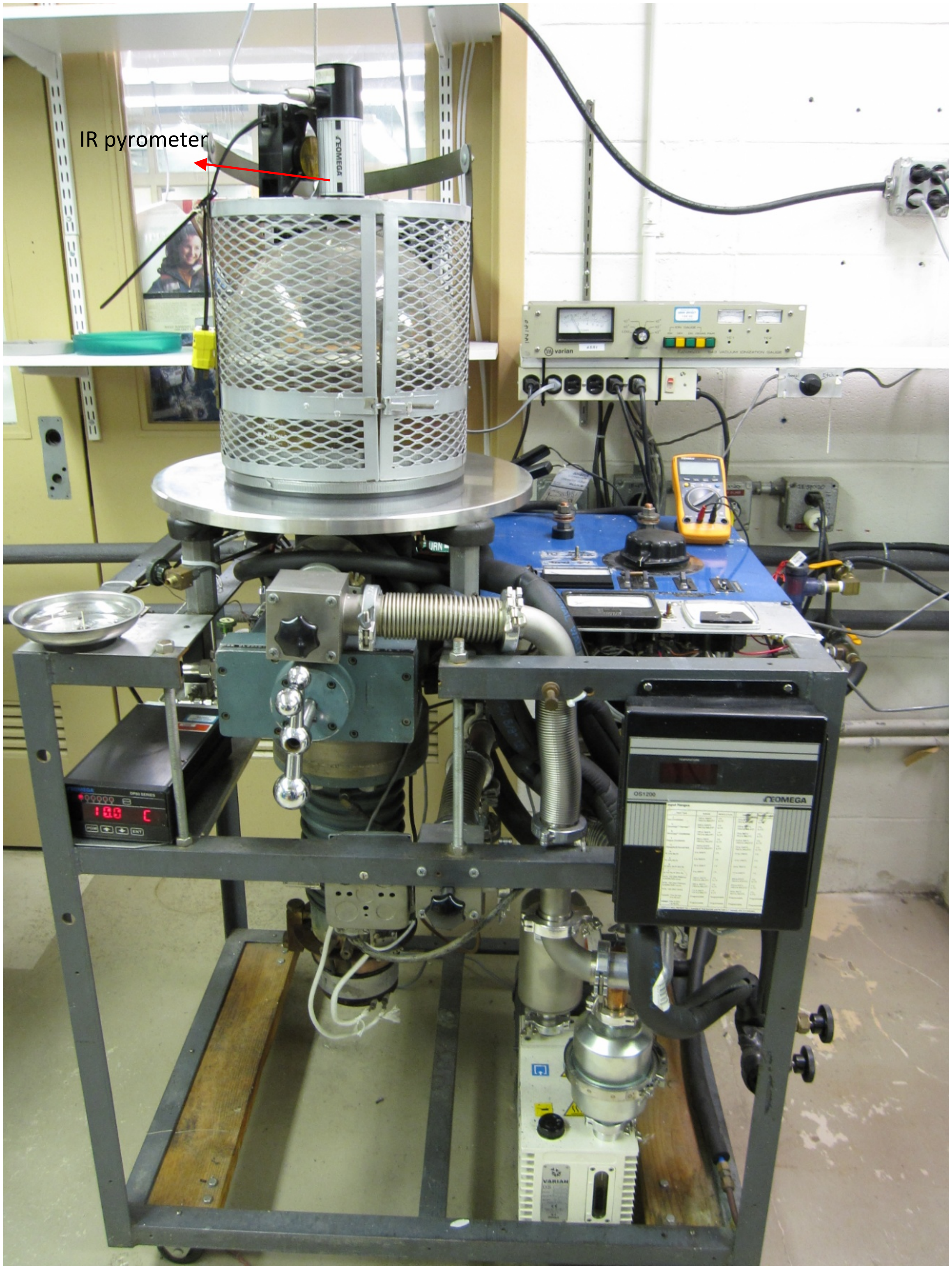

Figure 2.3.2 Overview of Annealing system

Figure 2.32 shows the annealing system. Usually a vacuum level of 2×10^{-7} torr is achieved prior to annealing. High purity nitrogen gas is introduced into the vacuum chamber during the heating procedure. The temperature is monitor through an OMEGASCOPE OS1100 infrared pyrometer located on top of the chamber shown in figure 2.3.2 and a thermal couple inside the chamber shown in figure 2.3.1.

2.4 Photolithography

Photolithography is an essential process used in device fabrication to selectively pattern a thin film. The pattern is transferred to the substrate from a photo mask to a light sensitive chemical, photoresist. A Karl Suss manual contact aligner for small volume processing photolithography system shown in figure 2.4 is used to effect the transfer. Shipley AZ5214E positive photoresist is used for photolithography in this work. Schottky contacts with patterns on the front Ga-face of the substrate, which is normally polished, are realized by photolithography. The wafer is covered with photoresist via spin coating at 4000 revolutions per minute for 30 seconds. The spin coat process results in a uniform, viscous thin layer of photoresist. The photoresist is prebaked to dry, typically at 90 ~ 100°C for 60 seconds on a hot plate. After the prebaking, it is exposed to a pattern of intense light through the photomask. Ultraviolet light is used as the light source. The common positive photoresist becomes soluble in the basic developer when exposed. As a result, after developing, the exposed photoresist parts are removed by the developer. The rest of the un-patterned area is still covered with photoresist. The developing time is variable, from 6 seconds to 30 seconds, based on the quality of photoresist, as well as the spin coat speed and time. Immediately before loading the samples to the sputtering system for Schottky metal contacts deposition, they are immersed into HCl: H_2O ratio 1:1 solution for 10s in order to remove new oxide on the surface of the exposed GaN part.

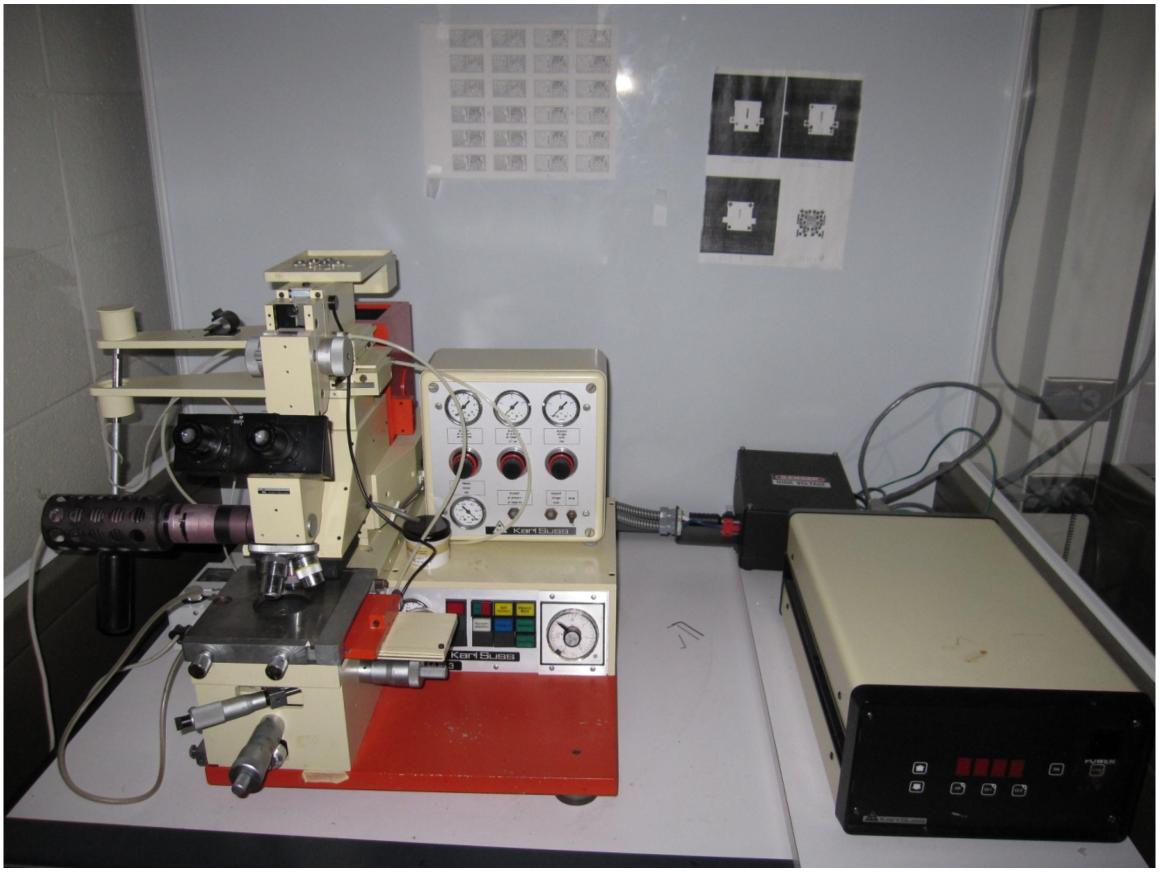

Figure 2.4 Photolithography system

2.5 Lift off

In the last section, photoresist is used to define the areas for metallization. The photoresist serves as sacrificial material, which is dissolved causing the metal to be removed from the area that needs no metal. The process is called lift off. Acetone is the solvent of choice. There are some major problems with lift-off. The worst problem for lift off is that the unwanted regions of the metal layer will remain on the wafer. This can be caused by different situations. For example, the photoresist below the parts is too thin so that it cannot dissolve properly. It is also possible that the metal adheres to the patterned parts preventing the lift-off. Au, for instance, its adhesion to itself is very good, however, bad to other materials. It is hard to lift-off pure Au metal. During the lift off process it is possible that metal become reattached to the surface at a random location. It is very difficult to remove these metals after the wafer has dried. In addition, during metal deposition, it can cover the sidewall of the photoresist. The metal along the sidewall extends upwards from the surface. It may fall over onto the surface, causing the unwanted shape on the wafer. Figure 2.5 shows the procedures from photolithography, metal deposition to lift off.

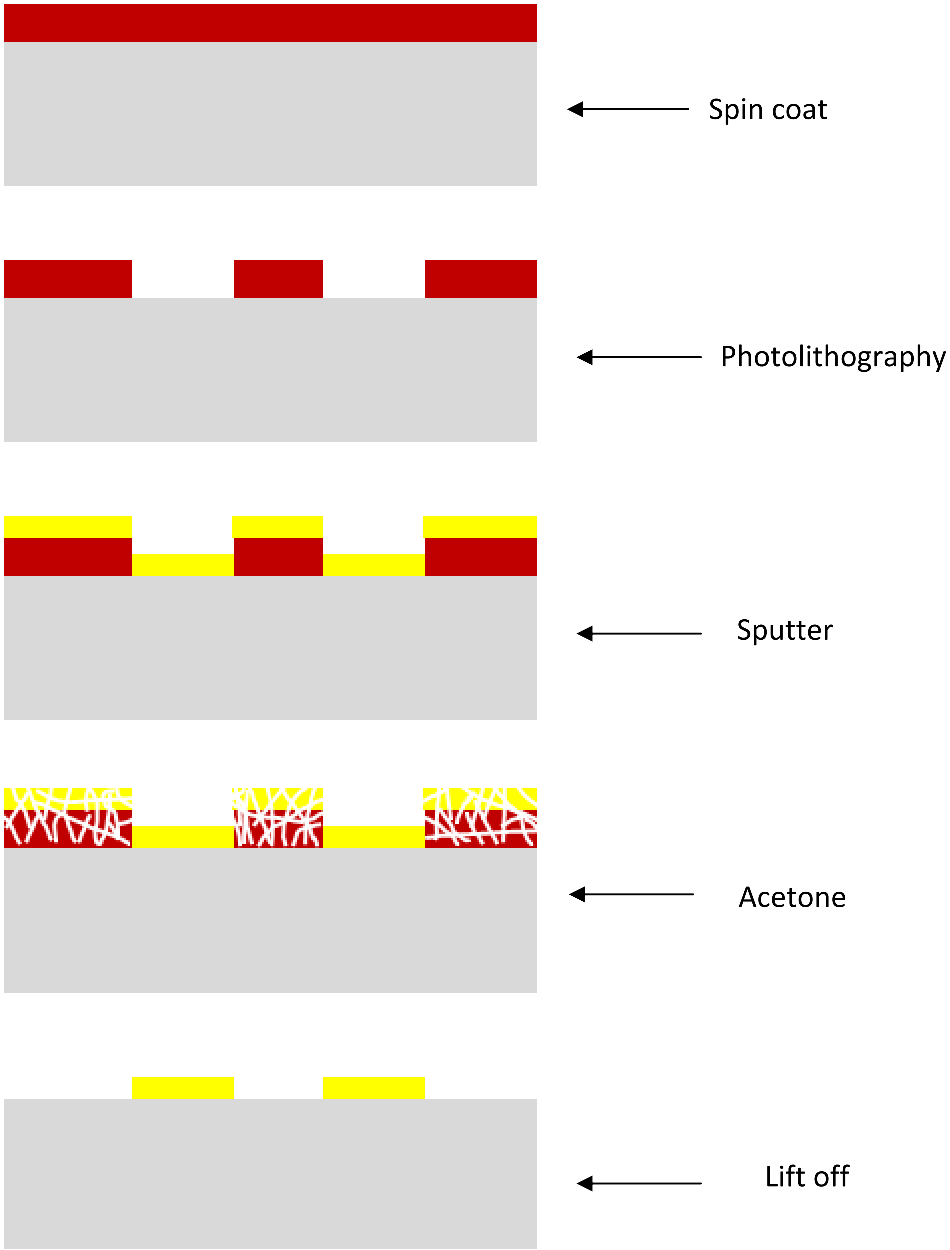

Figure 2.5 Lift off procedure

2.6 Reactive Ion Etching (RIE)

Generally, there are two etching processes: 1) wet etching where the target is dissolved when it is immersed in chemical solution, 2) dry etching where the target is dissolved by reactive ion or vapor phase etchant. Depending on the situation, one method may be preferred over the other. For wet etching, the simplest technology, only a container with liquid solution is required. However, usually a protection mask is needed to selectively etch the material. This will add complications to wet etching. First, a proper mask film must be found to make sure it will not dissolve or at least etches much slower than the target materials. Secondly, for certain materials, such as Si, it exhibits anisotropic etching in certain solutions. Anisotropic etching means different etch rates in different directions. Another case isotropic etching is also possible, where the etch rates are the same in all directions. Figure 2.6.1 shows the shape of materials under anisotropic and isotropic etching.

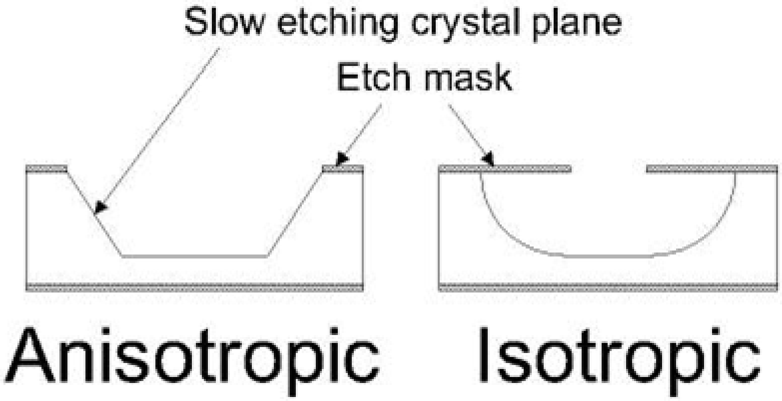

Figure 2.6.1 Difference between anisotropic and isotropic wet etching [53]

As shown in the above figure, isotropic processes will etch under the mask by the same depth as the vertical etch thickness. Anisotropic processes also causes loss of space. Dry etching provides some solutions to the problems. Dry etching makes it possible to etch almost straight down with no undercutting; however, the cost is much higher than wet etching. Reactive Ion Etching is one technique of dry etching.

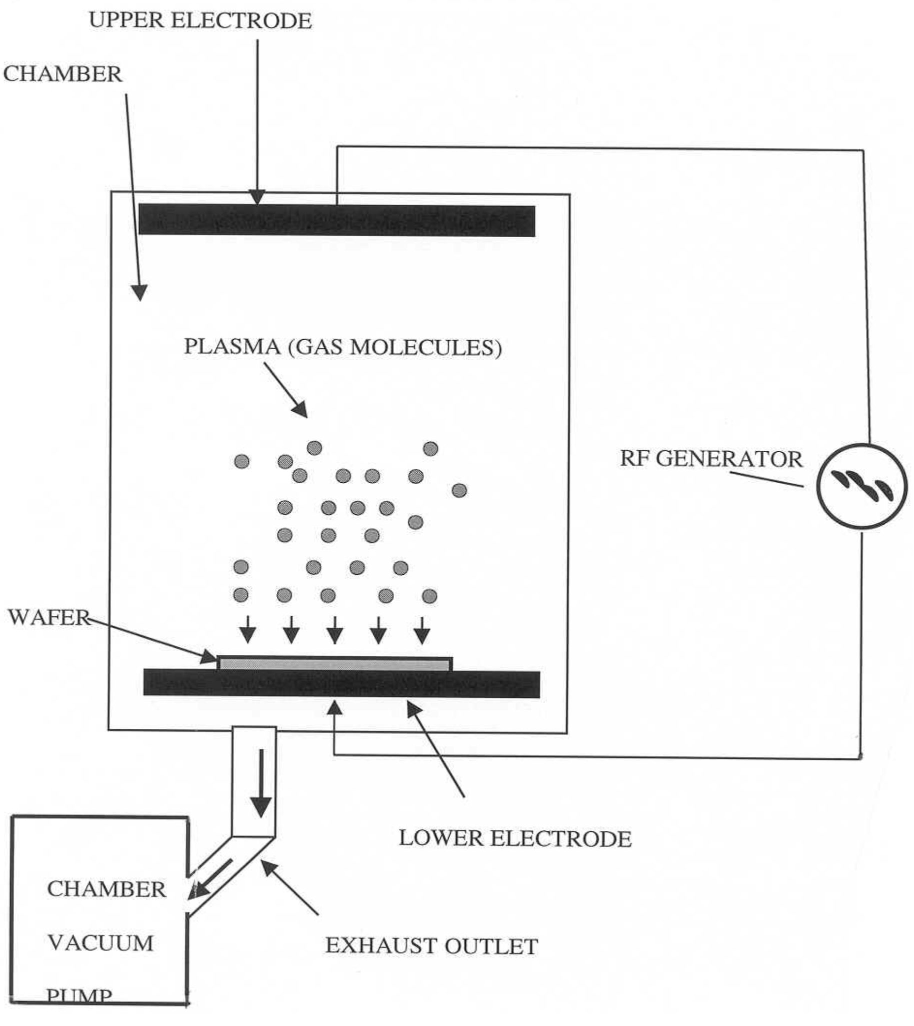

Figure 2.6.2 Schematic diagram for Reative ion etching [54]

Figure 2.6.2 is a typical parallel-plate reactive ion etching system. The gases enter through holes in the upper electrode. Plasma is generated using RF power source, breaking the gas molecules into ions. The wafer is located on the lower electrode. Plasma is attracted by the electric field to the wafer. The ions etch the unprotected pattern on the wafer. This is the chemical reaction etching. Physical etching which is similar to sputtering also exists. If the ions have energy high enough, they can bombard atoms out of the materials without a chemical reaction. For GaN or nitrides, dry etching has become the dominant technique. GaN is an extremely stable compound, and difficult to use conventional wet etching. It was reported that GaN was not soluble in acids, or bases at room temperature, but did dissolve in hot alkali solution at very slow rate[55]. High etching rate was observed, however, only effective on low quality GaN, which became a tool to identify defects and estimate defect density in GaN films[56, 57]. Much work has been devoted to dry etching, including reactive ion etching (RIE), electron cyclotron resonance (ECR)[58], inductively coupled plasma (ICP)[59] and *etc*. Figure 2.6.3 is the structure of the RIE system. I. Adesida *et al.* first reported GaN RIE in chlorine-based plasma has high etch rate[60]. Cl/Ar gas is used to etch GaN in this work. Etch rate increased rapidly with increasing power.

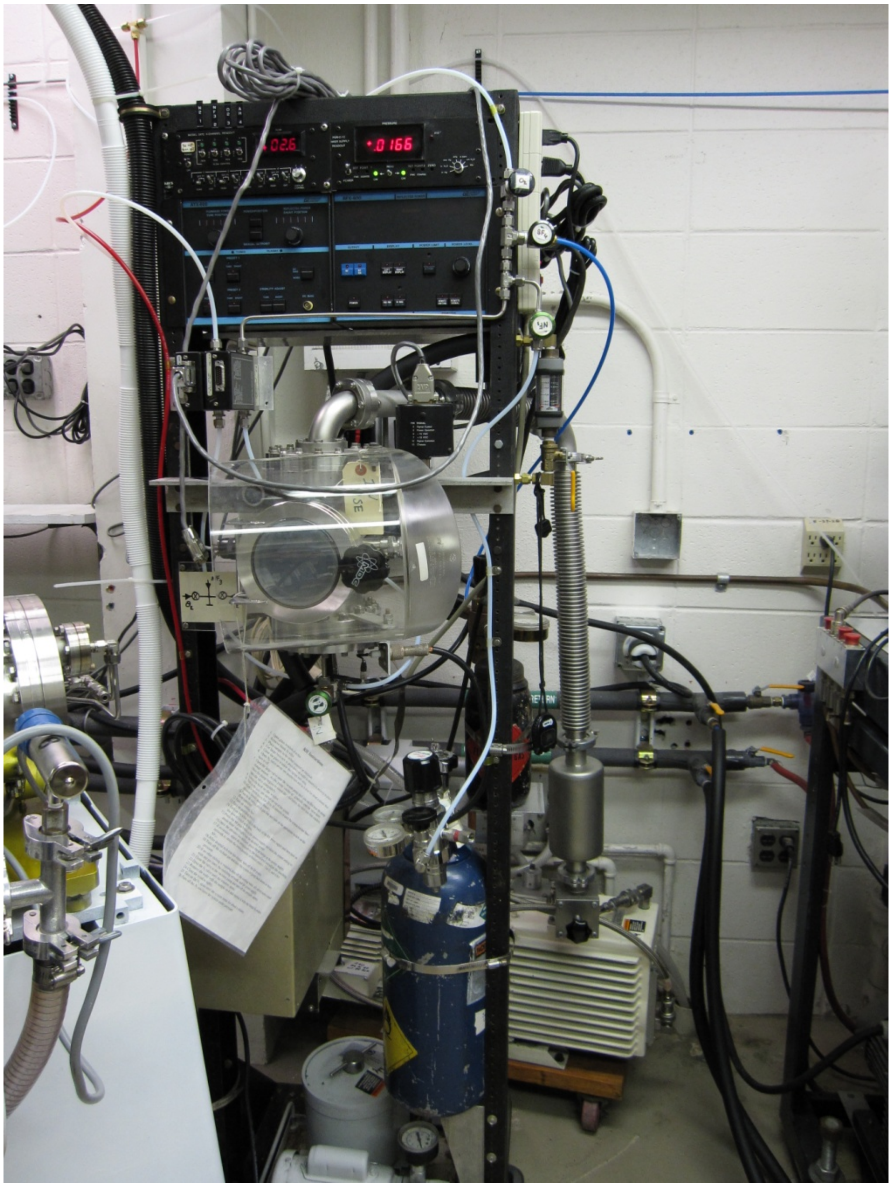

Figure 2.6.3 Reactive Ion Etching System

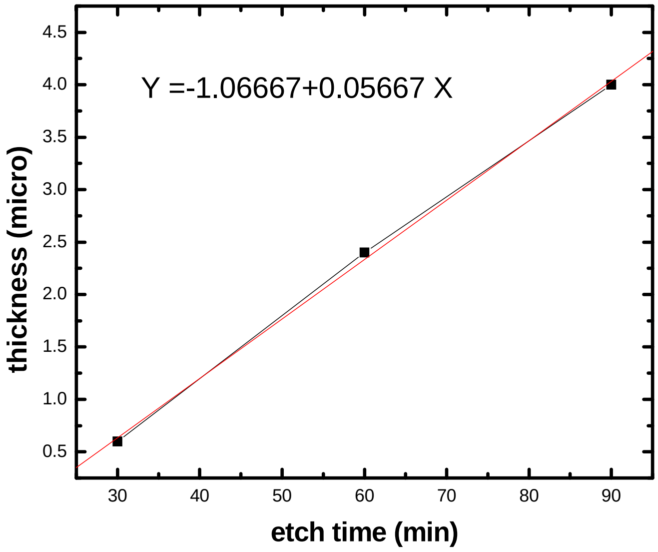

Figure 2.6.4 GaN etch rate using Cl/Ar

In order to have mesa isolation, effective etching on GaN is necessary. First, GaN top surface was patterned by photolithography, Ni serves as etch mask. The above figure shows the relationship of etch thickness and etch time. For 30 min, 60 min and 90 min, the GaN thickness etched is 0.6 μm, 2.4 μm and 4 μm, using the same power 30 W. Higher powers were also tested, however, with increasing power, the selectivity of etching on GaN is sacrificed.

2.7 Low field and high field I-V system

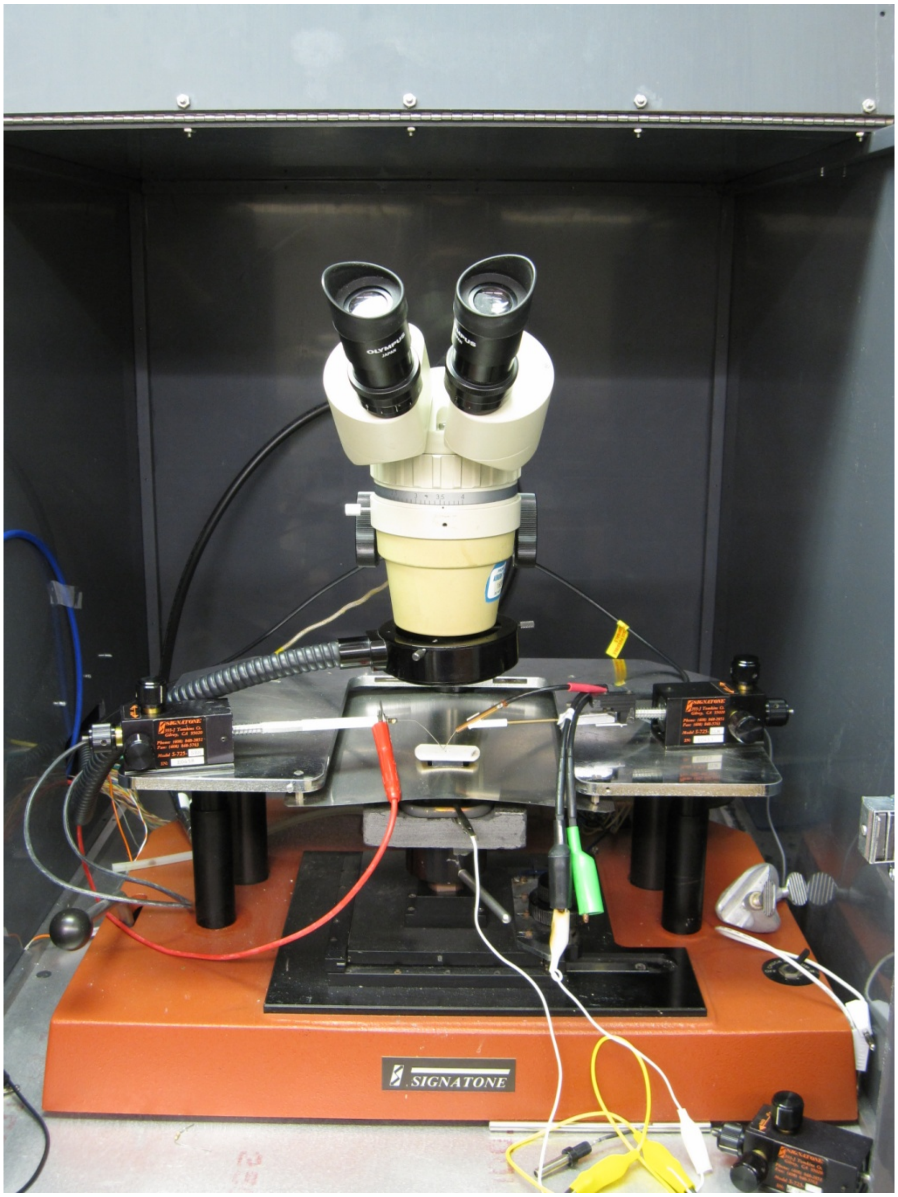

Figure 2.7.1 Low field I-V and breakdown measurement system

In electronics, the DC current and DC voltage across the terminals of a device is called current-voltage characteristic, also known as I-V curve. The system shown in figure 2.7.1 is used to measure the low field (low voltage with low electric field) I-V characteristic and breakdown voltages. The sample is placed in the square holder. The microscope is used to locate the Schottky and Ohmic contacts for the device, making placement of the probes possible. Keithley 6517 electrometer with embedded power source is connected to the probes. Under the sample station, is the heating source, making high temperature I-V measurement possible up to ~300^0C. The whole probe station is in a grounded black box to avoid light induced current, especially for a photodetector measurement. This system is used for the electric field breakdown measurement. One change in setup is required. One of probe needles (left one) is replaced by a needle with a resister attached on it. It is used to protect the electrometer. When the devices reach breakdown voltage, large current will be created. The resister helps to reduce the current in the circuit. A 62.5 kΩ resister is connected in series with the device to measure the breakdown voltage in this study. This I-V station can measure current as low as 10 fA. The upper current is limited to 10 mA. A system which can measure higher current is needed in figure 2.7.2. The forward current up to 2 A may be detected, and lower current limit is 10^{-5} A.

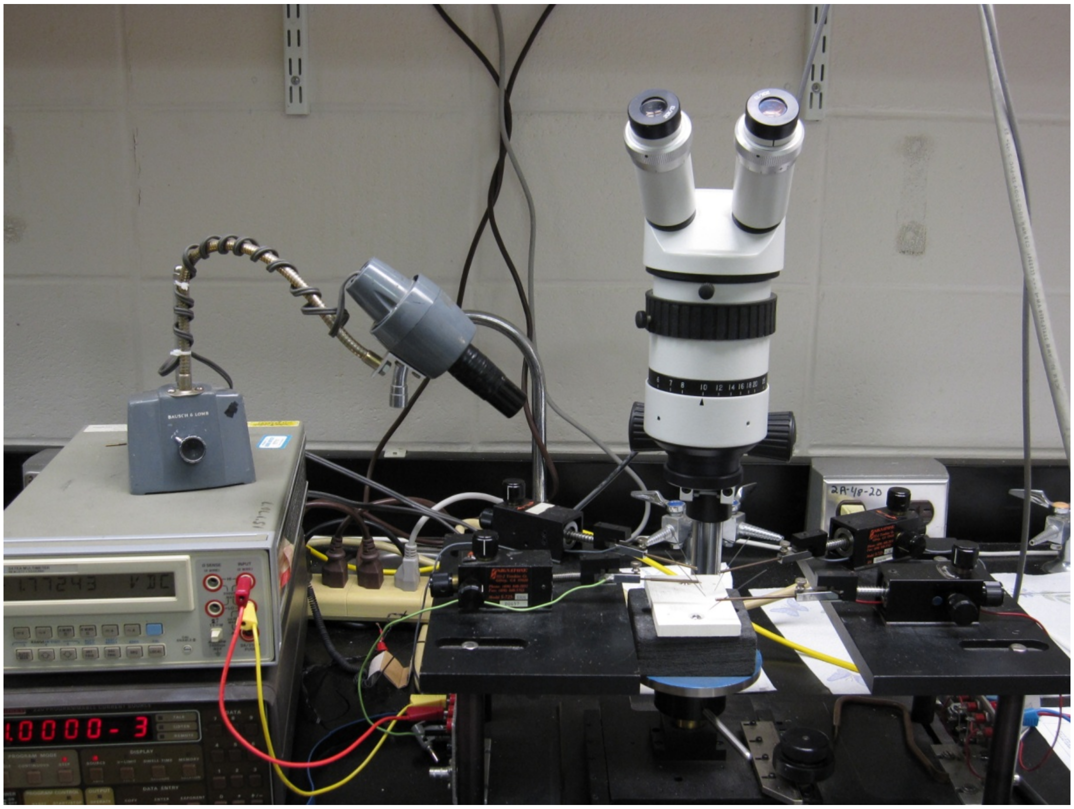

Figure 2.7.2 High field I-V measurement system

2.8 Capacitance-Voltage system

Capacitance-voltage (C-V), one of the most important techniques used for characterization of semiconductor materials and devices. This technique takes advantage of the depletion region. The depletion region is empty of conducting electrons and holes, but has electrically active defects and ionized donors. In the depletion region, the change of charge gives rise to capacitance[61]. The depletion width can be varied by changing the voltages applied to the metal-semiconductor contact. By solving the Poisson equations with boundary conditions, depletion width obtained[11]:

$$W_d = \sqrt{\frac{2\varepsilon_s}{qN_d}(\psi_{bi} - kT/q - V)}$$

The space charge per unit area in the depletion area is:

$$Q = qN_dW_d = \sqrt{2q\varepsilon_s N_d(\psi_{bi} - kT/q - V)}$$

and the depletion layer capacitance is related to width by:

$$C = \frac{\varepsilon_s A^2}{W_d} = A^2\sqrt{\frac{\varepsilon_s qN_d}{2(\psi_{bi} - kT/q - V)}}$$

Therefore, the dependence of depletion width on the applied voltage gives information about the device characteristics, such as doping profile and barrier height. C-V measurement is usually carried out by both DC and a small-signal AC for low frequency and high frequency dependencies. Keithley 590 quasi-static C-V meter is in measures of the low frequency, while Keithley 595 C-V analyzer controls the measurement for high frequency. The small AC signal is superimposed on the DC bias. Since the deep impurities can only follow slow signals, there is not enough time for the deep impurities to response to high frequency signals[11]. Therefore, the semiconductor parameters extracted from C-V curve are closer to ideal conditions. This explained why the barrier height derived from C-V curve is usually higher than the one from I-V curve mentioned in Chapter 1.

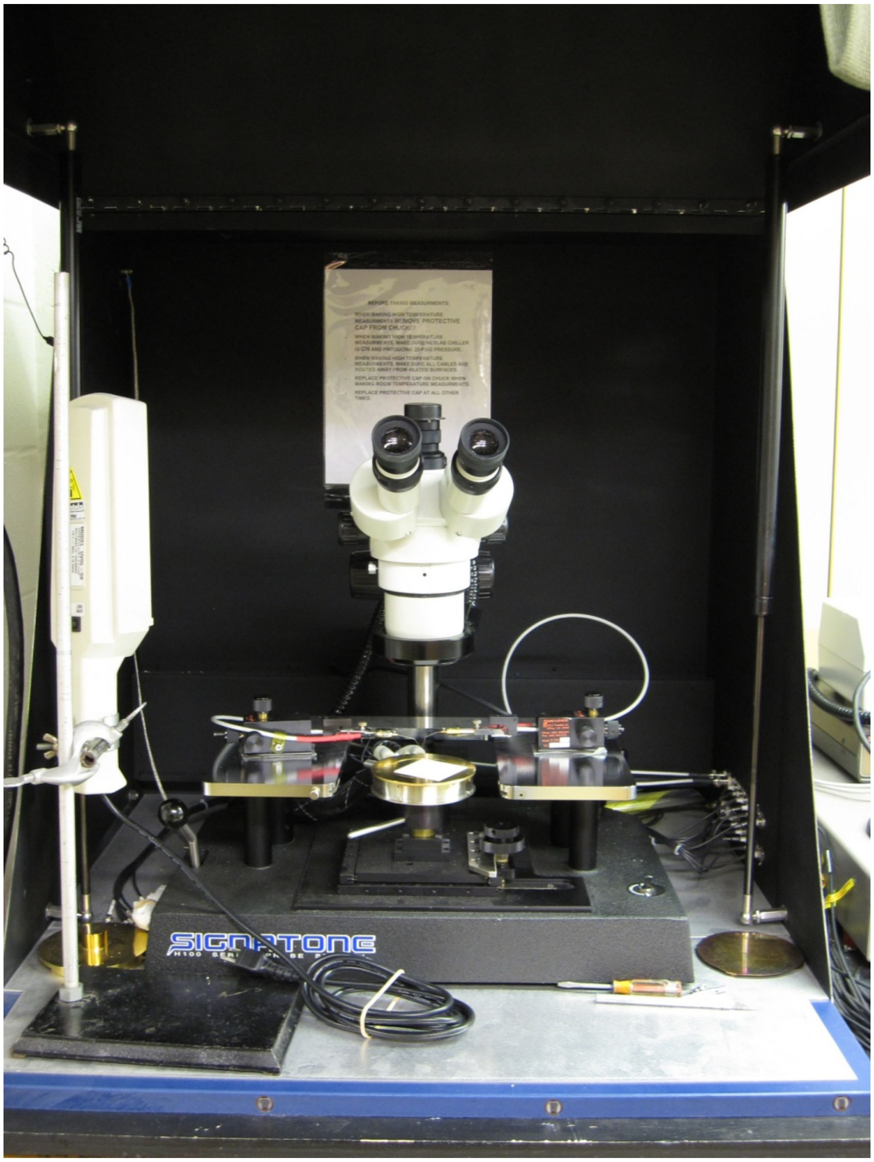

Figure 2.8.1 Capacitance-Voltage measurement system

2.9 Raman Spectroscopy

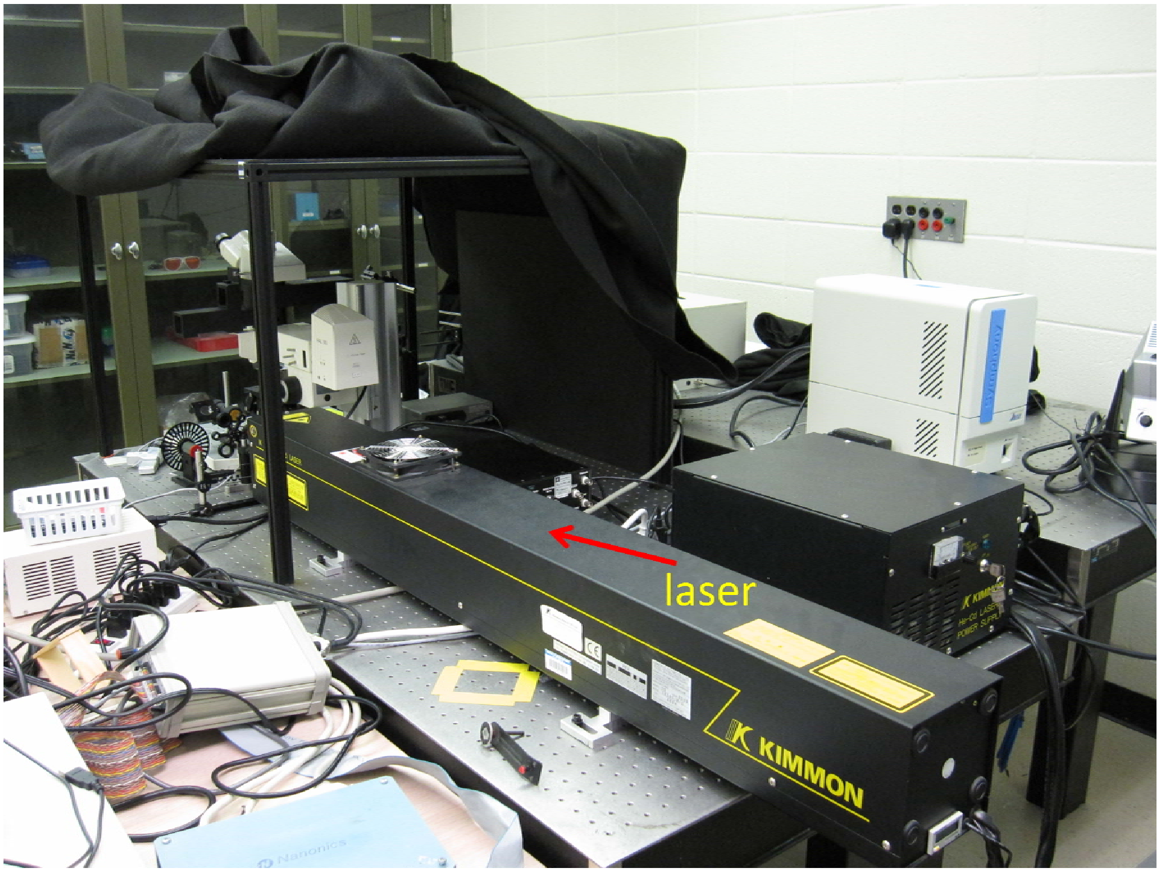

Figure 2.9.1 Back side of Raman System

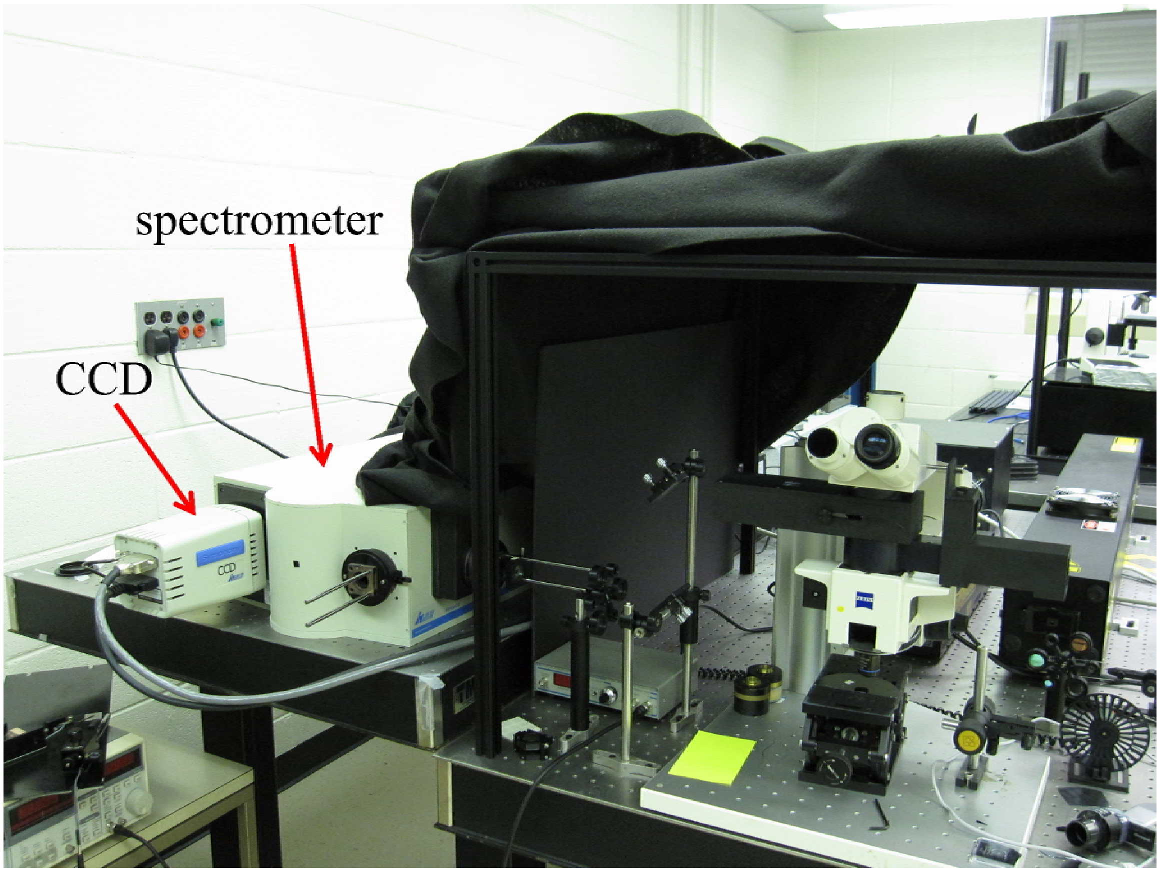

Figure 2.9.2 Front side of Raman system

Figure 2.9.1 and 2.9.2 shows the whole structure of the Raman system. Backside is the HeCd laser (Kimmon Electric) with 441.6 nm blue laser and 325 nm UV laser. The laser beam was focused onto a spot size of 5 ~ 10 μm in diameter. Laser line enters the microscope through several reflective mirrors and illuminates onto the sample. Then Raman Spectra are collected by a Jobin Yvon spectrometer and a thermally-cooled charge coupled device (CCD) detector (2048 by 512 pixels) after the laser interacts with the sample. A laser filter is applied to the entrance of the spectrometer to make sure only the Raman signal will be detected by the CCD. The spectrometer is embedded with two 3-inch holographic gratings 2400 lines/mm and 3600 lines/mm, corresponding to a resolution of 1 delta wave number and 0.2 delta wave number respectively. The Raman spectra are very sensitive to the location of the laser on the sample. For example, the intensity of Raman spectra can differ a lot depending on whether the laser is focused on the sample or not. The details of GaN Raman spectra are discussed in chapter 4.

CHAPTER 3

ELECTRICAL CHARACTERISTICS OF LOW LEAKAGE SCHOTTKY DIODE BASED ON EPI/BULK GAN WAFER ALL GROWN BY HYDRIDE VAPOR PHASE EPITAXY(HVPE)

3.1 Introduction

Great attention has been paid to Gallium Nitride (GaN) due to its application in high power high temperature electronics. Schottky rectifiers are essential components in a power electronic system (such as power inverters) due to its fast switching speed and a low switching loss. GaN-based Schottky diodes have been fabricated by many research groups. However, these are “lateral” devices which are based on GaN layers heteroepitaxially grown on foreign substrates such as sapphire. The problems with this device structure include high dislocation density due to heteroepitaxy, current limitation due to low thermal conductivity of sapphire, and limitation in the thickness of the epilayer, etc. With the advent of conductive bulk GaN wafers, it is now possible to fabricate a “vertical” Schottky rectifier. Until now, only a few research groups have reported a fabrication and device operation of the bulk GaN-based Schottky rectifiers.

In order to increase reverse breakdown voltage without reducing forward current output, it is desired to use a bi-layered structures (i.e., n^- epilayer on n^+ bulk). It is expected that forward current and reverse breakdown characteristics can be independently controlled. Pioneering work by Kang *et al.*[62] has produced Schottky rectifiers fabricated using n^-/n^+ GaN wafer, where the n+ bulk wafer and n^- epilayer were grown by HVPE and a metal-organic chemical vapor deposition (MOCVD), respectively. Their device exhibits power figure of merit, $(V_b)^2/R_{sp,on}$, of 11.5 $MWcm^{-2}$. Recently, Lewis and others[63] have fabricated Schottky rectifier using a Ni contact on n^-/n^+ GaN wafer. This diode showed a very low specific on-resistance of 0.57 $m\Omega cm^2$, but its breakdown properties were not reported. Lu *et al.*[64] have produced a Schottky rectifier with a low reverse-bias leakage current ($<3\times10^{-8}$ A @ -100 V) and a relatively low specific on-resistance (~ 5.3 $m\Omega cm^2$). The breakdown voltages of these devices were ranged between 260 and 430 V. Hashimoto and others[65] has also reported on the fabrication of Schottky diodes based on n^-/n^+ GaN wafer. This device exhibited a low specific on-state resistance of 1.3 $m\Omega cm^2$ and high reverse breakdown voltage of 580 V, producing corresponding $(V_b)^2/R_{sp,on}$ of 258.8 $MWcm^{-2}$.

Typically, MOCVD is a choice of epilayer growth technique for the deposition of high quality undoped or low-doped n^- drift layer while HVPE has been widely used for the preparation of bulk GaN wafer. In this research, the possibility of using all HVPE process both for the growth of bulk wafer and additional epilayer are explored due to the following reasons; 1) The HVPE process is relatively less expensive than that of MOCVD, and 2) By using this process, the extra step for device fabrication can be eliminated. Therefore, in this chapter the electrical characteristics of the GaN Schottky rectifiers fabricated on n- epi/n+ bulk GaN wafer, all grown by hydride vapor phase epitaxy (HVPE) are studied.

3.2 Experiment

Silicon-doped n-type bulk GaN wafers with a thickness of 385 µm were grown using a HVPE at Kyma Technologies, Inc. Nominally undoped GaN layer with a thickness of 80 µm was homoepitaxially grown on the Ga-face of the bulk GaN wafer *via* HVPE. The surface topography of the bi-layered wafer was analyzed using optical microscopy and atomic force microscopy (AFM). The wafer was cleaned sequentially using Trichloroethylene (TCE), Acetone, and Methanol, followed by etching in a heated HCl: H_2O solution (~100°C) for 10 min. As a full backside (N-face) ohmic contact, Ti (50 nm)/Al (100 nm)/Pt (50 nm)/Au (100 nm) multi-layered metallic contact was sputter deposited under a nitrogen atmosphere. Deposited ohmic contact was annealed at 750°C in N_2 for 30 seconds. As a Schottky contact metallization, Pt (250 nm) was deposited on the lithographically defined circular area (50 µm in diameter) using a direct-current (DC) magnetron sputtering. Some of the devices were additionally annealed at 500°C in N_2 for 10 seconds using a rapid thermal annealing (RTA). The schematic of the device structure is shown in Figure 3.1.

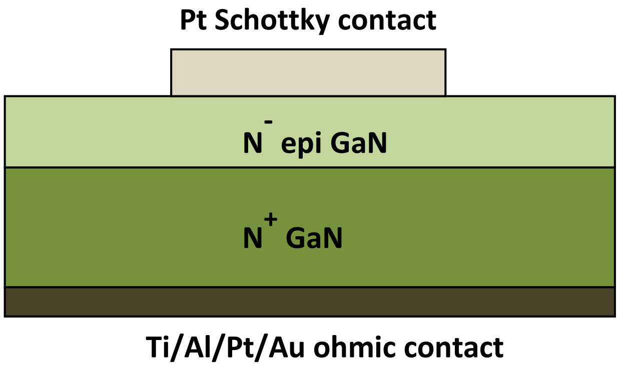

Figure 3.1 Schematic of Schottky diode structure on epi/bulk GaN substrate

Micro-Raman and photoluminescence spectroscopy were used to study the crystal quality of the wafer. Low-field Current-Voltage (I-V) measurement (from -5V to +5V) was carried out using an electrometer (Keithley 6517) with an embedded power source. I-V measurement at high forward bias regime was performed using a Tektronix 471 curve-tracer. Reverse-bias electrical breakdown characteristics were measured using Keithley 6517. Capacitance-Voltage (C-V) measurement was performed using a Keithley Mod 82-WIN Simultaneous C-V System at 100 kHz.

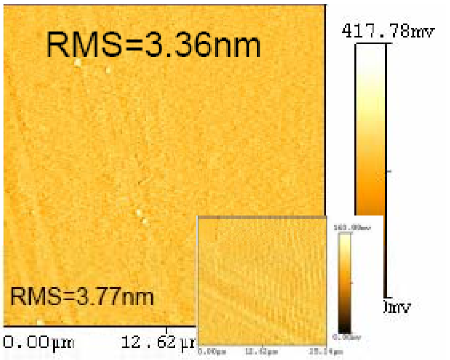

Figure 3.2 AFM topographic image of GaN

3.3 Results and discussion

Figure 3.2 exhibits AFM topographic image of the GaN epilayer grown by HVPE on bulk GaN. The RMS surface roughness of the Ga-face of the epilayer measured by AFM is 3-4 nm. The n-type doping level of the epilayer was determined from C-V measurement, and the value is ~10^{16} cm^{-3}. Figure 3.3 shows the low-field I-V characteristics of the Schottky diode fabricated.

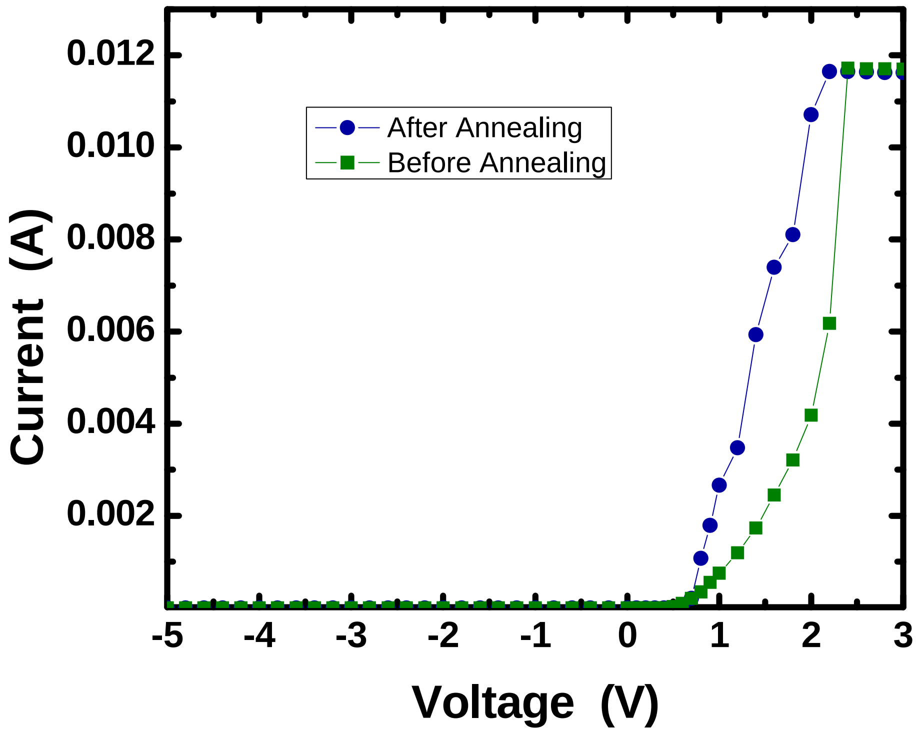

Figure 3.3 Low field I-V curve for Schottky diodes on epi/bulk GaN substrate

The I-V characteristics of Schottky diode is generally expressed by the following expression;

$$I = AA^{*}T^{2} \exp\left(-\frac{q\Phi_B}{k_B T}\right) \exp\left[\frac{qV}{nk_B T} - 1\right] = I_0 \exp\left[\frac{qV}{nk_B T} - 1\right] \qquad (3.1)$$

$$I_0 = AA^{*}T^{2} \exp\left(-\frac{q\Phi_B}{k_B T}\right) \qquad (3.2)$$

where A is the device area, A* is the effective Richardson constant, for GaN it is 26.4 A cm^{-1} K^{-2}, T is the temperature, Φ_B is the barrier height, and n is the diode ideality factor. If qV >> 3kT, equation 3.1 can be simplified as:

$$I = AA^{*}T^{2}\exp\left(-\frac{q\Phi_B}{k_BT}\right)\exp\left[\frac{qV}{nk_BT}\right] = I_0\exp\left[\frac{qV}{nk_BT}\right] \quad (3.1)'$$

For the devices without Schottky contact annealing, the turn on voltage is found to be as low as 1.5 V, with the specific on-state resistance 4.2 mΩ·cm^2. Turn on voltage is defined as the voltage at which the current density reaches 100 A/cm^2. The specific on-state resistance is the reciprocal of the slope for the linear region in the low field I-V curve. After annealing, the characteristics are greatly improved, the turn on voltage is decreased to ~ 0.95 eV and the specific on-state resistance becomes 2.6 mΩ·cm^2. That means the Schottky contact annealing helps improve the forward current transport.

An equivalent equation of equation 3.1' is

$$lnI = \ln I_0 + \frac{qV}{nk_BT} \quad (3.3)$$

Figure 3.4(a) shows lnI vs Voltage curve before annealing. From this curve, a linear region can be found. Non-ideal Schottky diodes with high series resistance can hardly have a linear region in semi-log plot of current versus voltage[66]. Therefore the ideality factor determined from this linear region is relatively reliable. It is calculated to be 1.13 through the slope of the fitting curve, corresponding to a barrier height 0.81 eV. At low forward bias region (voltage < 0.2 V), nonlinear behavior of the curve is mainly due to current transport mechanism other than thermionic emission exists, for example tunneling current. This is proved by ideality factor in that region is smaller than 1[63]. Meanwhile limitation of the instruments makes the current at this region not accurate. At higher bias region (voltage > 0.5 V), the series resistance greatly influence the forward current, causing the curve differ from linear. Thus, the thermionic current voltage equation with series resistance is needed:

$$I = AA^{*}T^{2}\exp\left(-\frac{q\Phi_B}{k_BT}\right)\exp\left[\frac{q(V-IR_S)}{nk_BT}-1\right] \tag{3.4}$$

If nature log function is taken on the above equation, it'll be found that;

$$I\frac{dV}{dI} = \frac{dV}{dlnI} = IR_s + \frac{nkT}{q} \tag{3.5}$$

in which R_s is the series resistance. Evidently, by plotting dV/dlnI vs I, the slope gives the series resistance. Before rapid thermal annealing, the data shows the series resistance is ~145 Ω. For comparison, similar calculation is done for the diode whose Schottky contact is annealed after fabrication. Three parameters ideality factor, barrier height and series resistance are 1.08, 0.9 eV, and 182 Ω, respectively. Figure 3.4 (b) indicate lnI vs. Voltage curve after annealing.

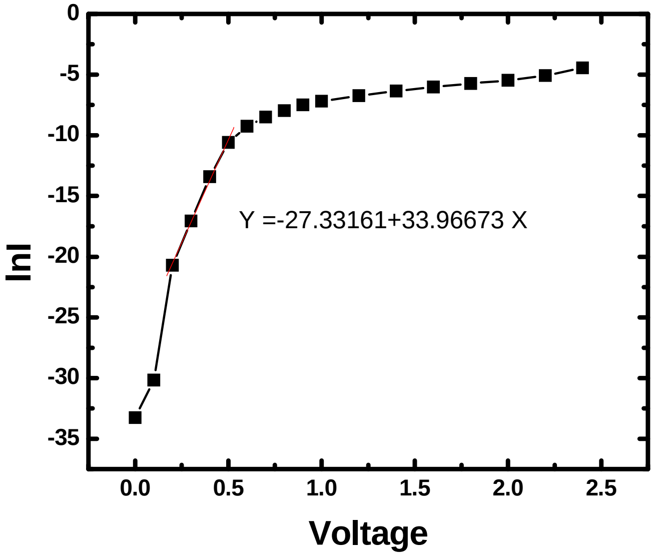

Figure 3.4 (a) I-V curve in log scale before Schottky contact annealing

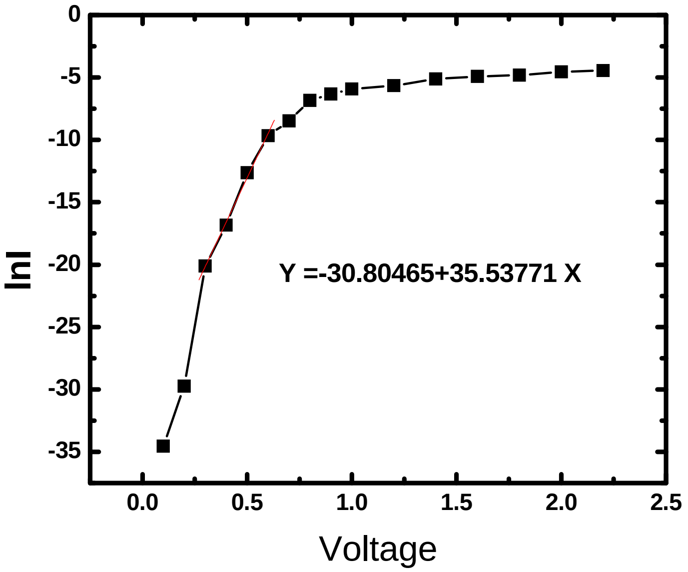

Figure 3.4 (b) I-V curve in log scale after Schottky contact annealing

Figure 3.5(a) and 3.5(b) show the high-field forward I-V characteristics in linear and log scale, respectively. It is easy to see that in the log scale at low voltage region, the curve is linear and at high voltage region, the current is limited by series resistance.

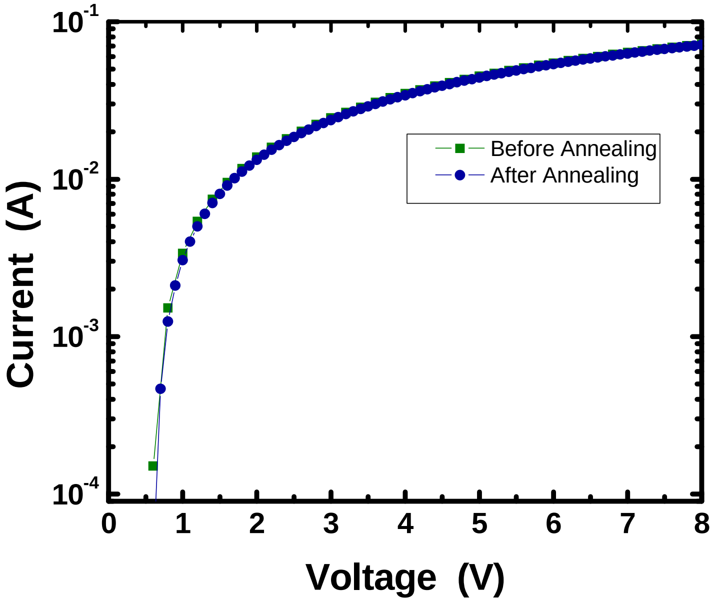

Figure 3.5 (a) High field I-V in linear scale

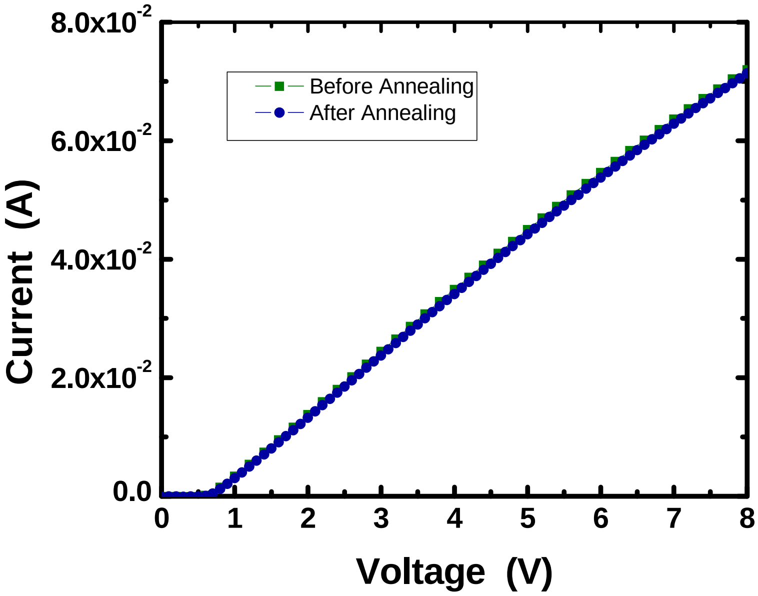

Figure 3.5 (b) High field I-V in log scale

The capacitance and voltage relationship is described by the following equation:

$$\frac{1}{C^2} = \frac{2(V_{bi} - V - kT/q)}{q\varepsilon\varepsilon_0 N_D A^2}$$

where V_{bi} is the build-in potential, k is the Boltzmann constant, T is the temperature, q is the elementary charge, ε_0 is the permittivity in vacuum, ε is the relative dielectric constant, for GaN it is 9.5, N_D is the impurity concentration and A is the contact area. C-V measurement is often served as a way to determine the Schottky barrier height. The intercept on the x axis of $1/C^2$ versus V plot can be used to get the build-in potential. Then the barrier height is the sumation of build-in potential and $(kT/q)\ln(N_C/N_D)$. N_C is the effective density of states in the conduction band, for GaN, this value is 2.24×10^{18} cm^{-3}. Therefore, the barrier height found from the C-V measurement is 1.31eV.

The Schottky diode shows a low reverse leakage current of 1.8×10^{-10} A at 90V. This low leakage current is achieved mainly due to the high quality of epilayer with low defect density. Notice that in Figure 3.6, the breakdown fields are ~350 V and ~200 V before and after annealing Schottky contact at $500^{o}C$ for 10s. It is expected to improve the adhesion of Pt contact on Ga surface. However, Q. Z. Liu et al. found that Pt Schottky diodes degraded after long annealing at $400^{o}C$.[67] Bubbles were found on their Pt contact, which might lead to the degradation in the electrical properties. The diodes may also suffer from high temperature, which causes the breakdown voltages reduced.

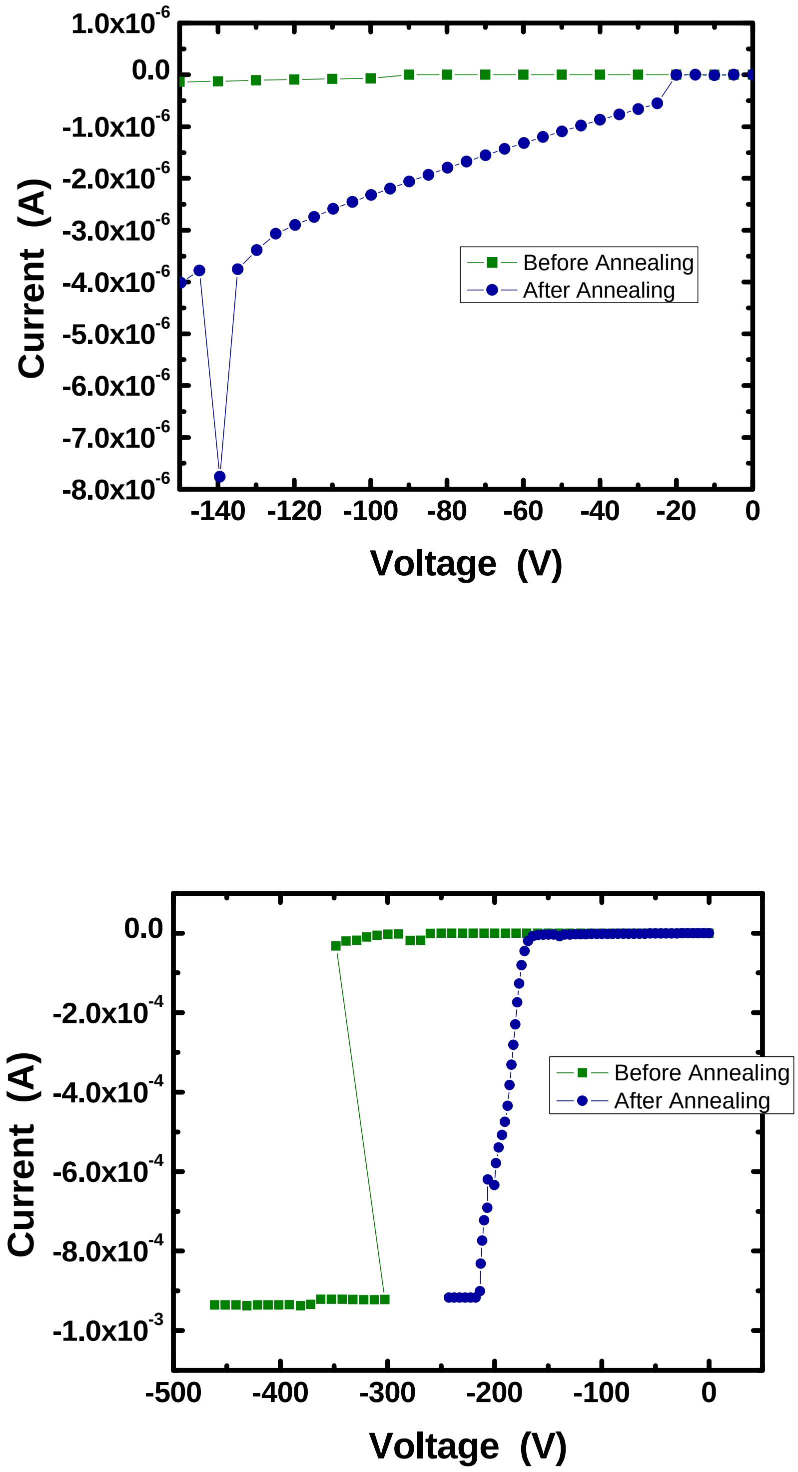

Figure 3.6 Breakdown voltage before and after Schottky contact annealing

3.4 Summary and Conclusions

In conclusion, vertical structure Schottky barrier diodes based on n-/n+ GaN wafer were fabricated. The low doped epi-layer and high doped bulk-layer were both grown by HVPE technology, which simplified the crystal growth procedures and reduced the cost. The diodes showed low turn-on voltage and low on-state resistance. Moreover, these characteristics were further improved by Pt contact annealing for a short time at 500oC. However, the breakdown characteristics were sacrificed.

CHAPTER 4

IN SITU RAMAN DIAGNOSTICS FOR SCHOTTKY DIODES ON BULK GAN SUBSTRATE

4.1 Introduction

Gallium nitride (GaN) based electronic devices have shown great potential for high power and high frequency applications due to GaN's intrinsic properties such as a large energy band gap, high electron mobility, and high critical breakdown field. Although significant progress has been made in fabrication of the GaN-based power electronic devices, growing concerns about their reliability have been raised in the past few years[68]. For example, AlGaN/GaN high electron mobility transistors (HEMTs) under operation suffer from a so-called "self-heating" problem which severely limits their performance and lifetime of the devices[68]. Therefore, it is of great importance to prudently assess the device heating problem if a reliable power electronic device is to be developed.

Recently, many research groups have reported successful operation of GaN-based Schottky rectifiers. With increasing power ratings of these devices, device degradation due to Joule heating needs to be considered. Since higher operating temperature is required for GaN devices, characterization of thermal property is of great importance. However, it is difficult to measure accurate device temperature, especially when the devices are under operation. Among the technique which can be used to monitor the temperature of the device under operation, micro-Raman spectroscopy is interesting due to its high spatial resolution. Raman spectroscopy also provides a great non-contact method to diagnose device temperature without disturbing its operation.

Several researchers have applied Micro-Raman spectroscopy to temperature measurement of the AlGaN/GaN HEMT devices under operation[69, 70, 71, 72]. However, there is limited research about GaN Schottky rectifier temperature measuring using Raman spectroscopy. Kim *et al.* has investigated the effect of thermal stress on Raman determination of device temperature for Schottky rectifier fabricated using GaN epilayer grown on Al_2O_3 substrate[73]. Recent technologies make it possible to produce high quality freestanding (FS) GaN substrate using Hydride Vapor Phase Epitaxy (HVPE). Therefore, vertical Schottky rectifiers based on FS GaN attract more attention, due to its low dislocation density and fabrication simplicity. Zhou *et al.* have reported that a vertical Schottky rectifier can exhibit higher reverse breakdown voltage compared to lateral structure[74]. Premature breakdown is closely related to device working temperature. It is necessary to study Schottky diode temperature effect in order to further improve its electrical characteristics. There is no report on Raman determination of operating device temperature of bulk GaN-based Schottky rectifiers can be found. Therefore, the Schottky diodes on bulk GaN were fabricated, and Raman spectroscopy were used to “measure” the temperature of the device under operation.

4.2 Experiment

N-type bulk GaN wafer with 500 μm in thickness was prepared using HVPE at Kyma Technologies, Inc. The carrier concentration of the wafer (determined using capacitance-voltage measurement) was ~2.4×10^{16} cm^{-3}. The Ga-face of the wafer was mechanically polished. Vertical structure Schottky diodes were fabricated using the bulk GaN wafer as follows; initially, the sample was cleaned using Trichloroethylene (TCE), Acetone, and Methanol, followed by etching in HCl at 100°C. As a full backside ohmic contact, Ti(50nm)/Al(100nm)/Pt(50nm)/Au(200nm) layers were deposited on the N-face of the wafer using direct-current (DC) magnetron sputtering, followed by rapid thermal annealing at 750ºC in N_2 atmosphere for 30s. Standard photolithography was used to pattern the circular Schottky contact on the Ga-face of the wafer. After that, semi-transparent Ni (20nm) contacts with 300 μm in diameter were prepared in an Ar ambient using DC magnetron sputtering, followed by lift off.

Low-field current-voltage (I-V) measurement was carried out using a Keithley 6517 electrometer with its built-in power supply. High-field I-V measurements were performed using a Tektronix 471 curve-tracer. The capacitance-voltage (C-V) measurements were performed using a Keithley Mod 82-WIN Simultaneous C-V System.

The 441.6 nm line (80 mW) from HeCd laser (Kimmon Electric) was illuminated on the semi-transparent Schottky contact through the microscope objective while the device was forward biased. It is shown in figure 4.1. Raman spectra were collected *in-situ* using a spectrometer (JY-Triax 550) with grating with a groove density of 3600 lines/mm and a thermoelectrically-cooled charge coupled device (CCD). The spectral resolution of the grating used is 0.2 cm^{-1}. For comparison, the Raman spectra were also measured while the sample was heated by a hot plate (without applying an external bias), as shown in figure 4.2. For bias-dependent Raman measurement, HP 6481P was used as a power supply. The photoluminescence spectrum was measured with a 325 nm line (20 mW) from the Helium-Cadmium (He-Cd) laser.

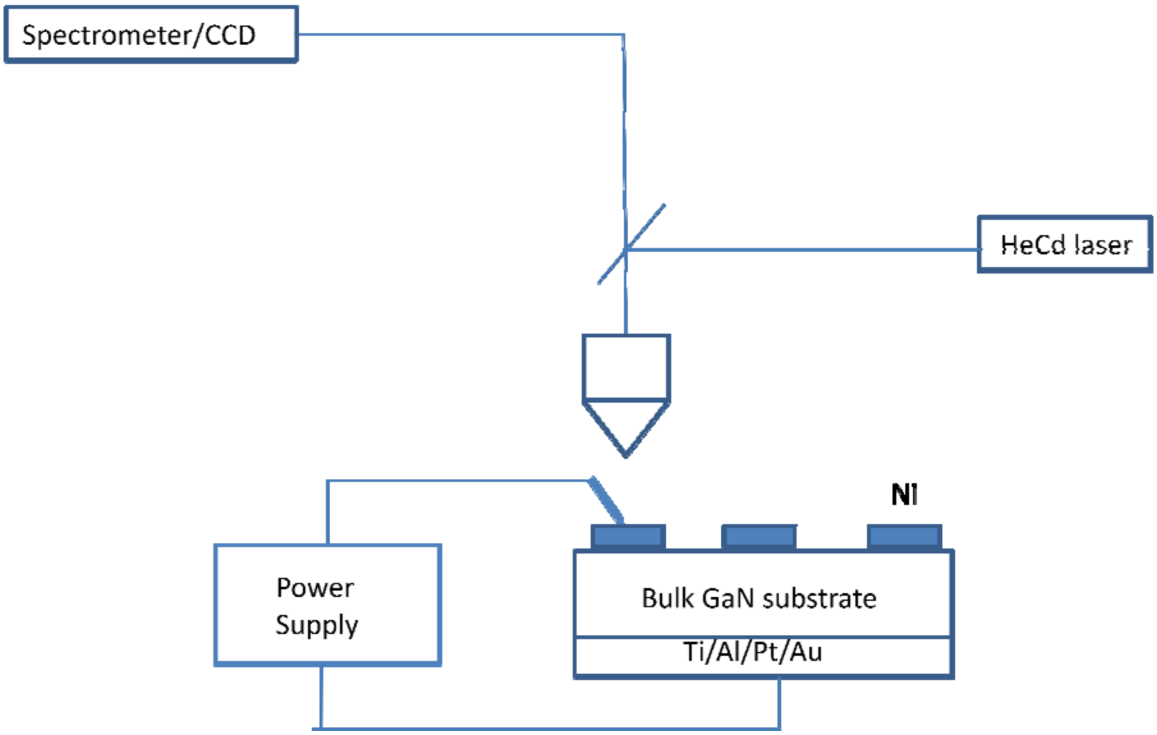

Figure 4.1 Equipment setup for Raman measurement on biased Schottky diode

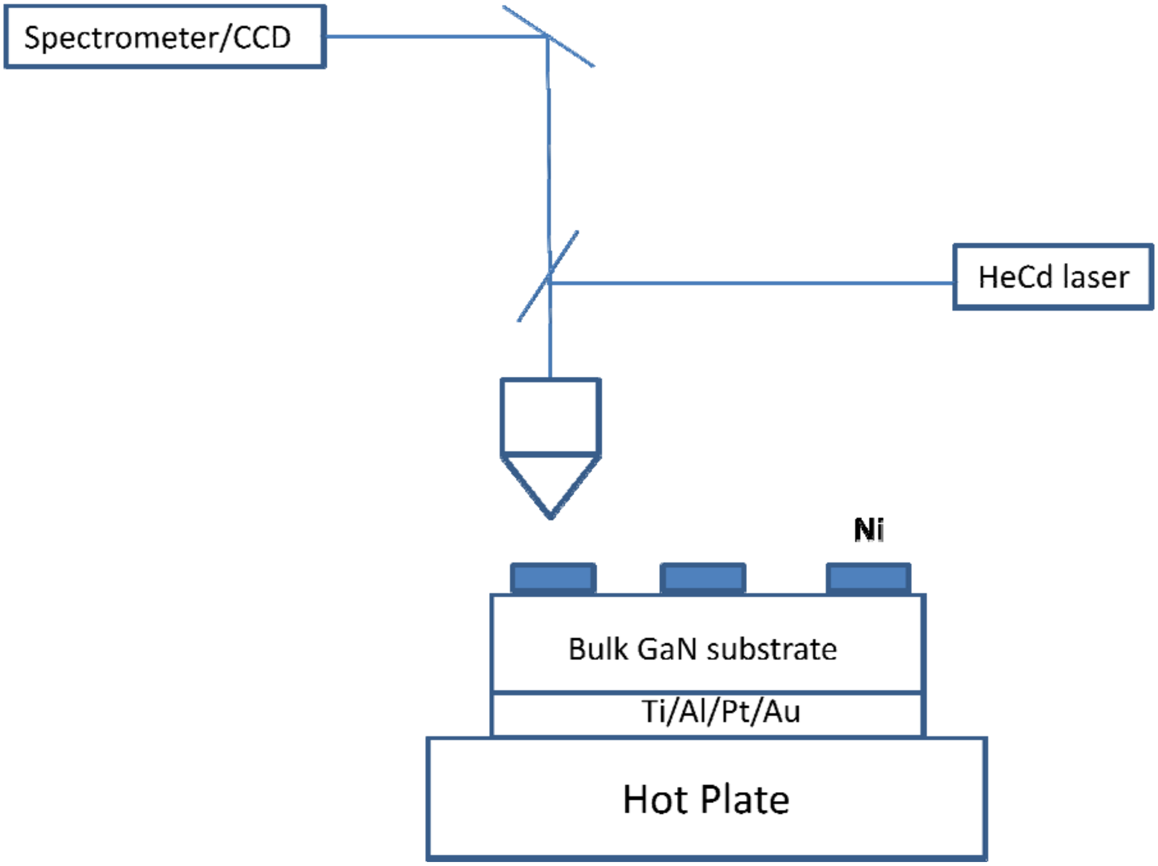

Figure 4.2 Equipment setup for Raman measurement on direct heated Schottky diode

4.3 Results and Discussion

Figure 4.3 shows the forward and reverse bias current-voltage (I-V) characteristics of the Schottky diode investigated. High-field I-V characteristics are shown in the inset of the Figure 4.3. The carrier concentration of the wafer determined by C-V measurement is 2.4×10^{16} cm^{-3}. The specific on-state resistance, $R_{sp,on}$, determined from low-field and high-field I-V plots are 58.8 mΩ·cm and 71.6 mΩ·cm, respectively. The barrier height determined from the I-V plot, $\Phi_s^{I\text{-}V}$, can be as follows[75];

$$\Phi_s^{I-V} = -\frac{k_B T}{q} ln\left(\frac{I_0}{AA^* T^2}\right) \qquad (1)$$

where k_B is the Boltzmann constant, T is the absolute temperature, q is the electron charge, I_0 is the saturation current, A is the effective diode area, and A^* is the effective Richardson constant where theoretically evaluated value of 26.4 $Acm^{-2}K^{-2}$ was used. In addition, diode ideality factor, n, was calculated from the slope of the linear region of the plot of *ln I vs. V* as follows;

$$n = \frac{q}{k_B T \cdot slope} \qquad (2)$$

The evaluated barrier height, $\Phi_s^{I\text{-}V}$, and diode ideality factor, n, are 0.54 V and 1.02, respectively. In order to evaluate barrier height from C-V measurement, built-in potential, V_{bi} , was obtained from the following expression[76];

$$\left(\frac{1}{C}\right)^2 = \frac{2}{\varepsilon\varepsilon_0 q N_d A^2}\left(V_{bi} - V - \frac{k_B T}{q}\right) \qquad (3)$$

where C is the capacitance, ε is the dielectric constant of GaN, ε_0 is the permittivity of free space, and N_d is the electron concentration (2.4×10^{16} cm^{-3}). The barrier height determined from C-V measurement ($\Phi_s^{C\text{-}V}$ = 0.6 V) was obtained using the following expression;

$$\Phi_s^{C-V} = V_{bi} + \frac{k_B T}{q} \ln \frac{N_C}{N_d} \qquad (4)$$

where N_C is the conduction band effective density of states.

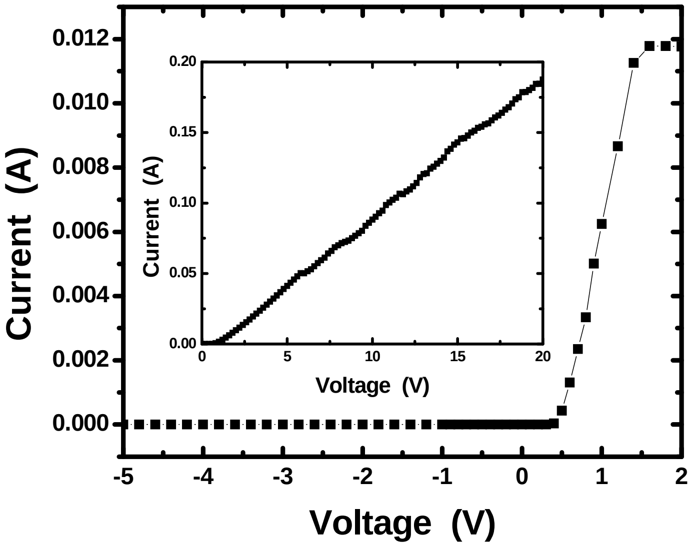

Figure 4.3 The forward and reverse bias current-voltage (I-V) characteristics of the Schottky diode investigated. Inset shows the high-field I-V characteristics.

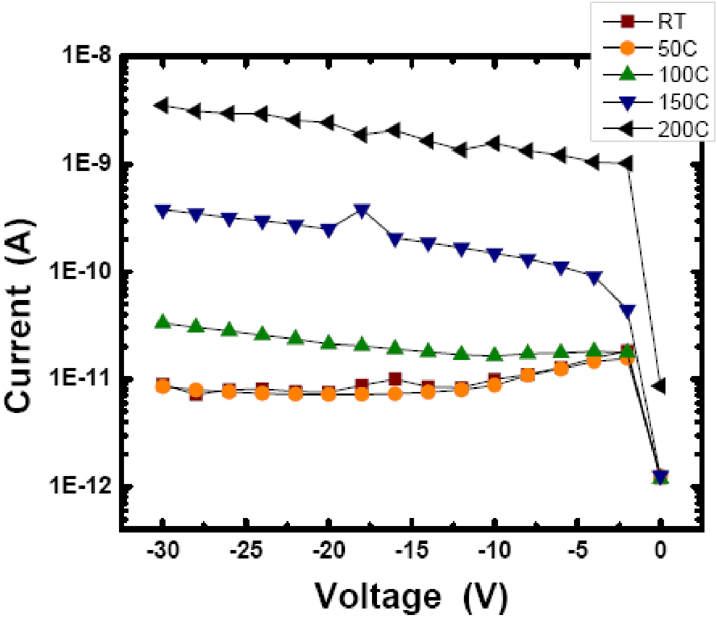

Figure 4.4 The characteristics of the reverse leakage current as a function of the device temperature.

Figure 4.4 shows the characteristics of the reverse leakage current as a function of the device temperature. The leakage current increased as the temperature of the device increases, which is possibly attributed to defect-assisted tunneling at the metal-semiconductor interfaces[77].

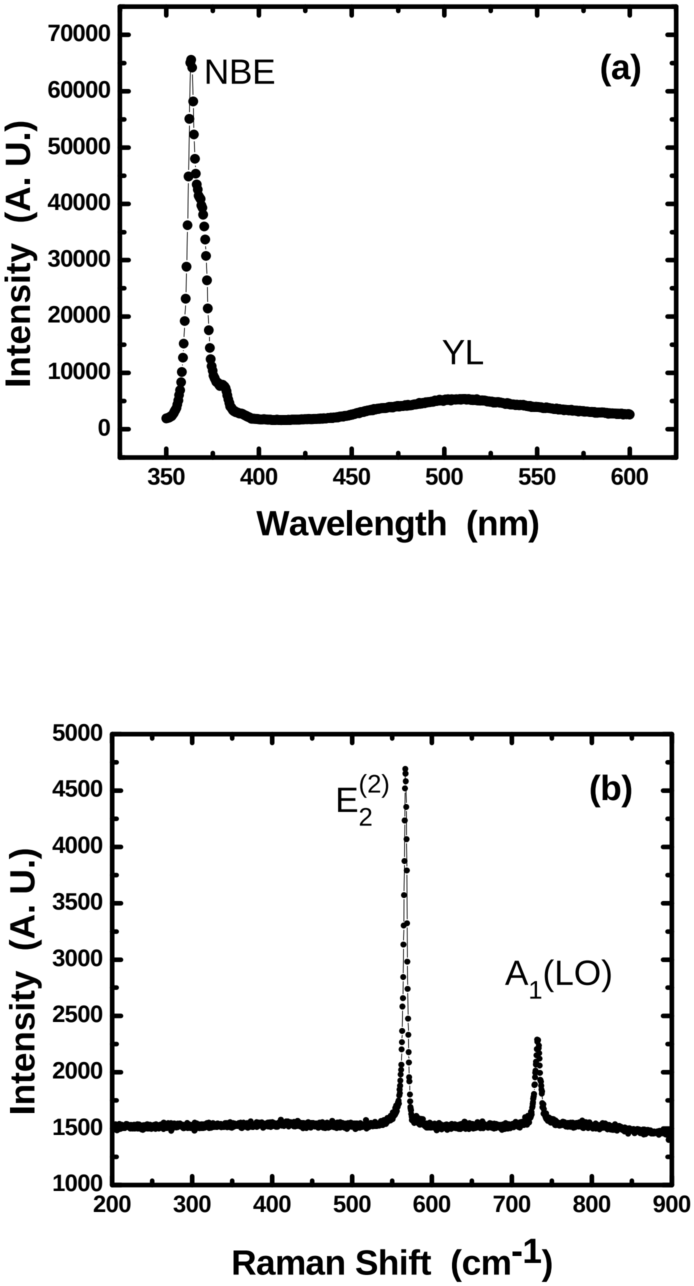

Figure 4.5 (a) Photoluminescence and (b) Raman spectra of the GaN.

Figure 4.5(a) shows micro-photoluminescence spectrum of the GaN wafer. A near-band-edge (NBE) UV peak at around 365 nm and a weak broad band (@~500 nm) due to yellow luminescence (YL) can be clearly seen from the spectrum. The full-width-at-half-maximum (FWHM) of the NBE peak is around 8 nm. In addition, a shoulder peak and a low intensity peak at longer wavelength regime have been observed, and further research is required to elucidate the nature of these peaks.

Figure 4.5(b) exhibits micro-Raman spectrum of the GaN wafer. From the group theory, $A_1(z) + 2B_1 + E_1(x,y) + 2E_2$ optical modes are expected at the Γ point of the Brillouin zone of wurtzite GaN[78]. Among these optical modes, the A_1 and E_1 modes are both Raman and infrared active, and the two E_2 modes are Raman active. The A_1 and E_1 modes split into longitudinal optical (LO) and transverse optical (TO) components due to their polar nature. In this experiment, $z(-,-)\underline{z}$ scattering geometry is used, implying that only the $E_2^{(1)}$, $E_2^{(2)}$, and A_1(LO) modes are allowed based on the Raman selection rule.

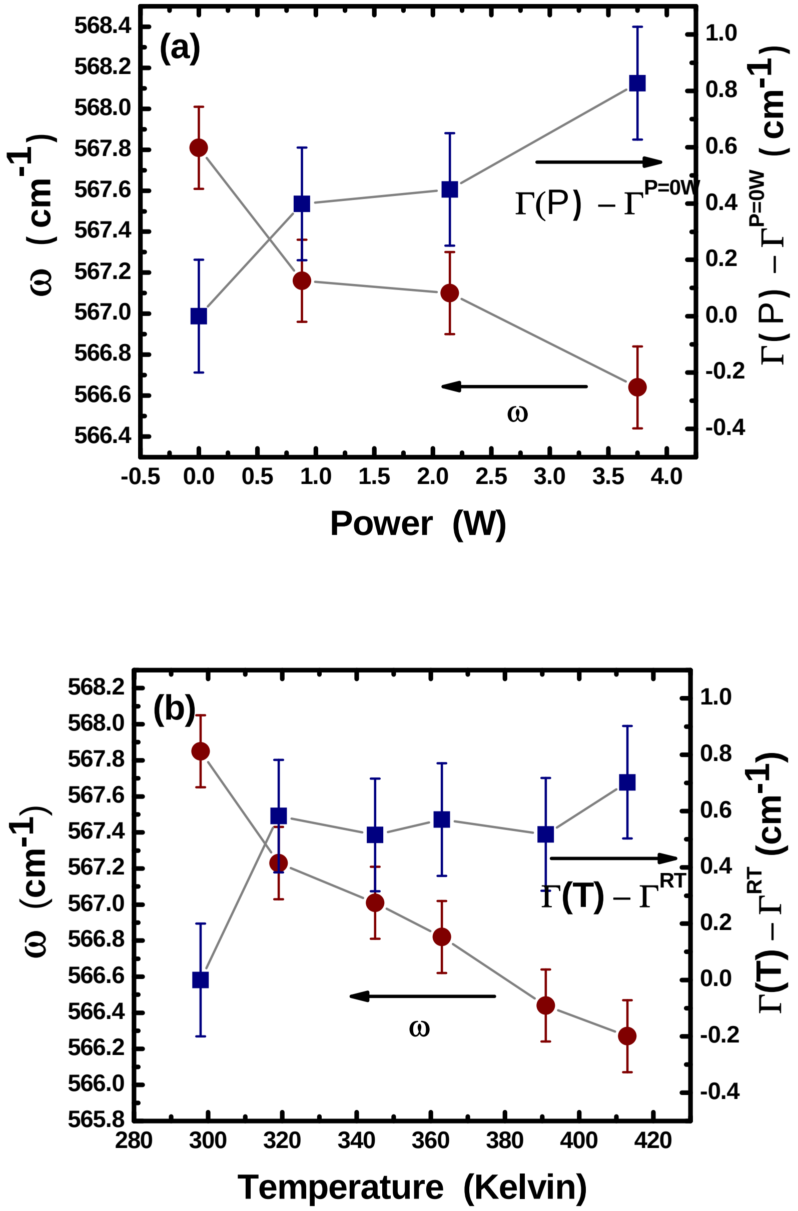

Figure 4.6 (a) Bias (power) and (b) temperature dependent Raman peak position and relative change in FWHM of the Raman peak.

Bias-dependent evolution of Raman spectra are summarized in Figure 4.6(a). Raman $E_2^{(2)}$ peak position and relative change in FWHM were plotted against forward bias voltage. The spectral position and FWHM of the Raman peak were determined by fitting the spectra with a Lorentzian function. Raman spectra were measured when the Schottky diode was forward biased at 0, 10, 15, and 20 V, which corresponds to 0, 0.9, 2.1, and 3.7 W of power, respectively. As can be seen from the graph, the Raman $E_2^{(2)}$ mode shifted to a lower wavenumber upon biasing, which is considered to be caused by self-heating of the device.

In order to investigate the spectral evolution of the GaN Raman peak as a function of device temperature, the device was heated using a hot plate. Prior to colleting Raman spectra, the device is thermally equilibrated by heating it for 10 minutes. Since the energy band gap of GaN (~3.4 eV) is greater than the energy of the incident laser light, absorption of the laser light by the sample is minimal. Therefore, laser-induced heating can be neglected in this investigation[73]. From the figure 4.6(b), all Raman peaks shift to lower wavenumber with increasing temperature of the device. The heat-induced Raman peak shift can be described by the following expression[79, 80];

$$\omega = \omega^0 - \frac{\alpha}{e^{\beta\hbar\omega_0/k_B T} - 1} \qquad (5)$$

where α and β are fitting parameters, and ω^0 is the Raman frequency at 0 K. This equation is commonly employed to describe the temperature dependence of Raman mode shift. Figure 4.7 shows the data points and fitting curve. From the fitting curve, α is 0.13, β is -2.3×10^9, and ω^0 is 571.6cm^{-1}. Since there are not enough data points, the fitting curve is a rough calculation. All the Raman modes exhibit a nonlinear decrease in frequencies with increasing temperature. A second order polynomial expression can be used to represent the Raman shifts[80]:

$$\omega = \omega_0 - AT - BT^2$$

As seen in figure 4.8, this polynomial equation can also provide a good fitting curve to the limited data. Based on the above two fitting curves, it was found that the devices under operation had a temperature increase of 73K, from room temperature (298K) to 371K.

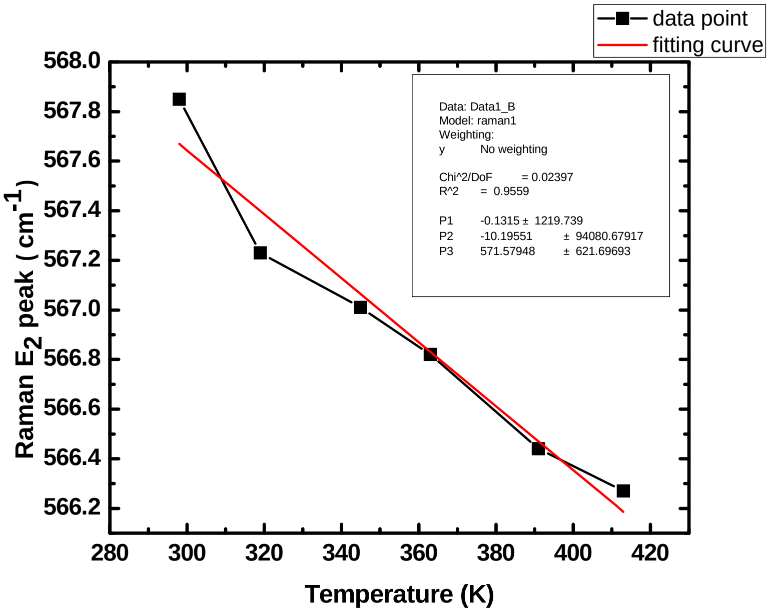

Figure 4.7 Raman peak shift *vs*. temperature data fitting by exponential equation

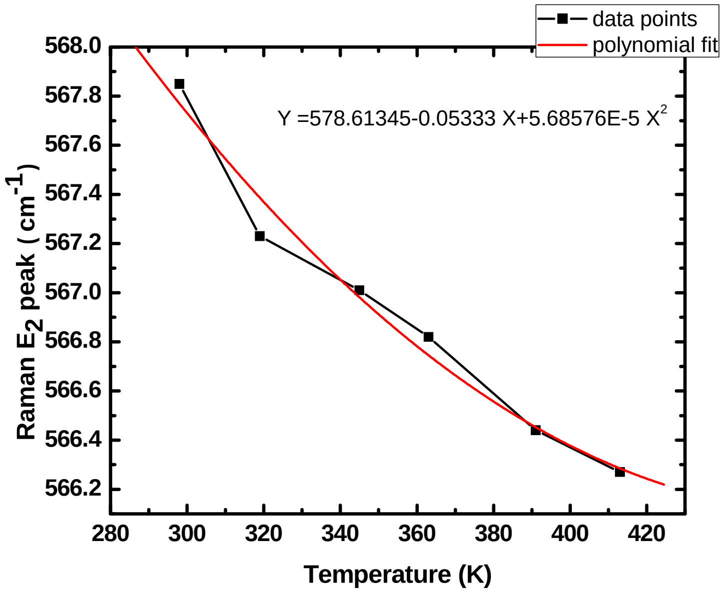

Figure 4.8 Raman peak shift vs. temperature data fitting by polynomial equation

The Raman peak shift is mainly caused by thermal expansion induced vibration frequency change and anharmonic coupling of phonon with other phonons[81]. At higher temperature, the interaction between the optical phonons increases, which results in an increase in the phonon scattering and decrease in the phonon life times. Meanwhile, the population of the acoustic phonons increases. All these cause an increase in the line widths. Raman shift is the real part of the phonon self-energy, which can be written as[81]:

$$\Omega(T) = \Omega_0 + \Delta^{(1)}(\mathrm{T}) + \Delta^{(2)}(\mathrm{T})$$

where Ω_0 is the harmonic frequency of the optical mode, $\Delta^{(1)}(\mathrm{T})$ is the thermal expansion contribution to the shift, and $\Delta^{(2)}(\mathrm{T})$ is the term due to anharmonic coupling. In addition, $\Omega_0 + \Delta^{(2)}(\mathrm{T} = 0)$ equals to the Raman frequency as T = 0K.

$$\Delta^{(1)}(\mathrm{T}) = \Omega_0[\exp\left\{-3\gamma\int_0^{\mathrm{T}} \alpha(\mathrm{T}')\mathrm{d}\mathrm{T}'\right\} - 1]$$

where γ is the Gruneisen parameter for the optical Raman mode and $\alpha(\mathrm{T})$ is the linear thermal expansion coefficient[80]. The correction of phonon self-energy due to anharmonic coupling can be modeled as[80]:

$$\Delta^{(2)}(\mathrm{T}) = \mathrm{M}_1\left\{1 + \sum_{\mathrm{i}=1}^{2}\frac{1}{\mathrm{e}^{\mathrm{x}_\mathrm{i}} - 1}\right\} + \mathrm{M}_2\left\{1 + \sum_{\mathrm{j}=1}^{3}[\frac{1}{\mathrm{e}^{\mathrm{y}_\mathrm{j}} - 1} + \frac{1}{(\mathrm{e}^{\mathrm{y}_\mathrm{j}} - 1)^2}]\right\}$$

where M1 and M2 are constants. The first term is three phonon process and the second term is four phonon term. With enough data, it is more accurate to use above equations to do curve fitting.

The results agree with those from Liu *et al.*'s report on temperature dependent Raman peak shift of GaN[82]. The device underwent the temperature increase from room temperature (RT) to ~371 K when the device was biased from 0 to 20 V. As a comparison, the Raman E_2 phonon mode shift through passive heating was used as a measure of the device temperature under operation.

Figure 4.6(a) also shows the relative change in FWHM of the E_2 mode as a function of the forward bias (power) applied to the Schottky diode. Continuous broadening of FWHM with power was observed. Liu *et al.* used the following equation to describe the temperature dependent peak broadening[82, 83];

$$\Gamma(T) = \Gamma^0 \left[1 + \frac{2}{e^X - 1}\right] \qquad (6)$$

where Γ^0 is the FWHM of the Raman peak at 0 K, and $X = \hbar\omega_0 / 2k_B T$.

Since GaN is a piezoelectric material due to the lack of inversion symmetry, it also exhibits the converse piezoelectric effect, implying that strain will be induced when an electric field is applied. Therefore, it is worth considering the piezoelectric strain induced phonon shift. Sarua *et al.* have investigated bias induced strain in AlGaN/GaN heterojunction field effect transistor (HFET) structure and have reported that the strain in GaN layer is proportional to the applied electric field[84]. For our experiment, the maximum electric field is 400 V/cm, which leads to strain of ~10^{-7} along the c-axis. According to Kisielowski *et al.*, a biaxial stress of 1 GPa will shift the Raman $E_2^{(2)}$ peak of GaN by 4.2 cm^{-1}.[85] The strain along the *a*- and *c*-axes of GaN will be on the order of 10^{-7}, which corresponds to the phonon mode shift of only ~0.001 cm^{-1}. Therefore, in the experiment, phonon mode shift due to piezoelectric effect can be neglected. This confirms that the Raman phonon mode shifts observed are mainly from the thermal effect (device heating), not from piezoelectric effect.

4.4 Summary and Conclusions

Vertical Schottky rectifiers using a HVPE grown bulk GaN wafer with 500 μm thickness were fabricated and measured the temperature of the device under operation *in-situ* using micro-Raman spectroscopy. The carrier concentration of the wafer, determined by C-V measurement, was ~3×10^{16} cm^{-3}. A systematic shift and broadening of the Raman E_2 peak with increasing bias (power) were observed, which is attributed to the device heating. As a comparison, the Raman spectra of the GaN device under passive heating were also collected. It has been demonstrated that micro-Raman spectroscopy can serve an excellent *in-situ* diagnostic tool for analyzing thermal characteristics of the GaN Schottky diode. The strain caused by piezoelectric effect is calculated, and it will only shift the Raman peak at the level of 0.001 cm^{-1}. This confirms that the Raman peak shift observed is predominantly produced by thermal effect, not by the piezoelectric effect.

CHAPTER 5

SCHOTTKY DIODES UNDER GAMMA-RAY RADIATION

5.1 Introduction

GaN materials are suitable for high temperature and high power electronic devices, as well as radiation environment applications, due to the high breakdown field and low thermal carrier generation rates[86]. Many groups used high energy radiation to study the material properties of GaN. Exposure to energetic radiation is considered as a tool to controllably introduce point defects and other defects. It is also benefit to obtain insights into the nature of intrinsic defects, for examples, vacancies, interstitials, and their influence on optical and current transport properties. It has been found that energetic radiation can degrade electron mobility, because defects are introduced, which will act as scattering centers[87]. Frenkel defect, also named frenkel pair, are considered as primary defects after high energy radiation in semiconductor materials. Frenkel pair is formed when an atom leaves its original place and occupies a nearby position in the lattice. During this process, two kinds of defects are produced, vacancy and interstitial. It is named after the Russian physicist Yakov Frenkel. From the definition, the number of vacancies equals the number of interstitials.

5.2 Experiment

The devices were fabricated on bulk GaN substrates. After ultrasonic cleaning in Acetone, TCE, Acetone, Methanol, Methanol 5 minutes each, GaN wafers were immersed in HCl: H_2O ratio 1:1 solution for 10 minutes, heated at 100^0C to remove native oxide. Then four layer ohmic contacts Ti/Al/Pt/Au were sputtered on the full backside of the N-face. The ohmic contacts were annealed in N_2 atmosphere at 750^0C for 30 seconds. The Schottky contacts of 3 different circular sizes were patterned by photolithography. Pt was sputtered as the Schottky metal, followed by lift-off. Then low field current-voltage and high field current-voltage measurement were performed before any γ ray radiation treatment. ^{60}Co was used as the irradiator with an average dose rate of 11.6 krad/min. The radiation was executed in air ambient at room temperature. The devices were finally exposed to cumulative γ ray doses of 17.4 Mrad. After the γ ray exposure, low field and high field I-V measurement were carried out. The crystallinity of the bulk GaN was tested by Bruker X-ray diffraction (XRD) D8. Raman spectra were collected through 514 nm line (20 mW) from an air-cooled ion laser (Model 163-C42, Spectra-Physics Lasers, Inc.) as the excitation source and a Renishaw inVia Raman microscope system with 1800 grating.

5.3 Results and Discussion

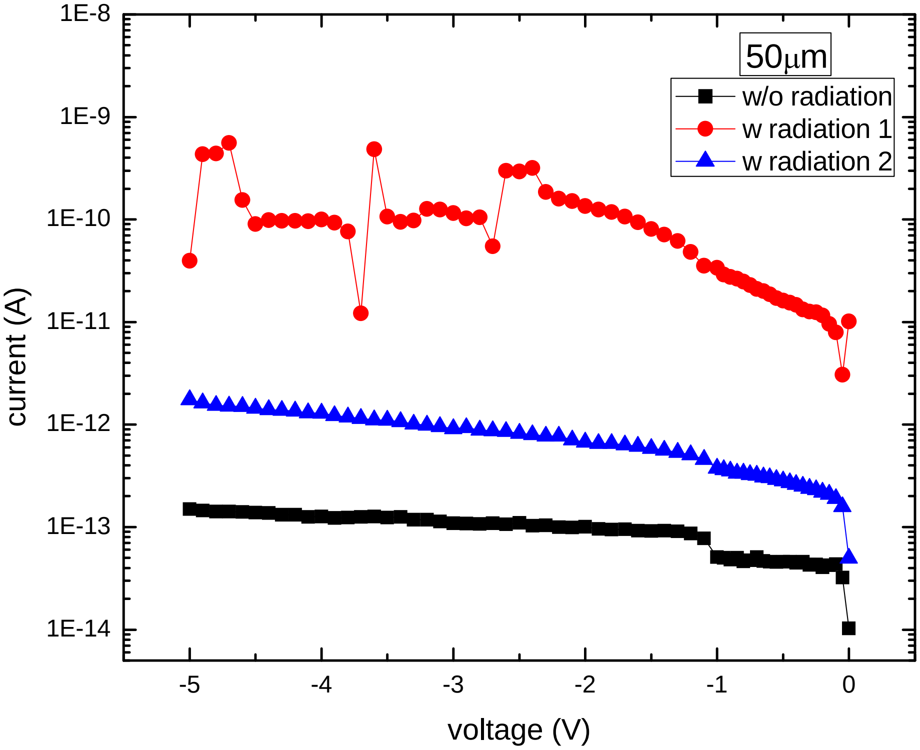

Figure 5.1.1 reverse leakage current of 50μm diameter devices

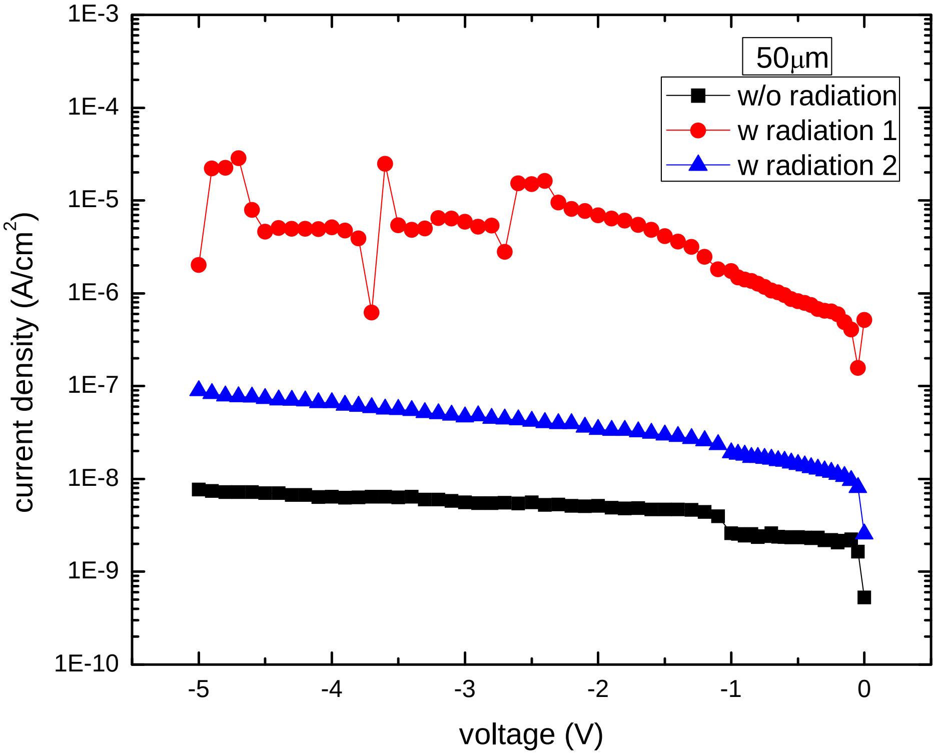

Figure 5.1.2 reverse leakage current density of 50μm diameter devices

Figure 5.1.1 and 5.1.3 shows the reverse leakage current and forward current profile for the devices with 50μm-diameter circles. Figure 5.1.2 and 5.1.4 shows the corresponding current density. Similarly, figure 5.2.1, 5.2.2, 5.2.3, 5.2.4, 5.3.1, 5.3.2, 5.3.3 and 5.3.4 display the results of 150μm-diameter and 300μm-diameter circular devices. A detailed look at the smallest devices first; at the reverse bias of 5 V, leakage current density increased to 0.089μA/cm^2, in which one of devices even went up to 2.0199μA/cm^2, compared to the un-radiated level 0.0075μA/cm^2. This trend is consistent with the work done by other groups[88,89]. The carrier concentration determined from the C-V measurement after radiation is 3~7×10^{16} cm^{-3}. Unfortunately, C-V measurement was not taken before radiation. However, from another piece of the same substrate, where different Schottky metal Ni was used, it found that the carrier concentration is ~ 2.4×10^{16} cm^{-3}.

Table 5.1 Summary of Schottky diodes Parameters Extracted from I-V curve

Dose (Mrad)	Ideality factor: n	Barrier height: Φ_B(ev)	Series Resistance: R_s (Ω)	Carrier concentration N (cm^{-3})
0	1.14	0.92	94.9	2.4×10^{16}
17.6	1.21	0.89	113.5	5×10^{16}

The data in table 5.1 were calculated through the simple ideal equations described previously. For the simple model, it is presumed that the metal-semiconductor interface is intimate, defect-free and homogeneous. From the experimental results, reported GaN Schottky diodes behaved non-ideal electrical characteristics. In addition, discrepancies generally exists for the reported GaN Schottky barrier height, where Pt was the contact metal. There are many effects giving rise to the variations of the reported values. Defect-assisted tunneling can help electrons pass through the barrier if there are many defects at the surface region[90]. The details of this kind of tunneling process are not known. Electrons, which were trapped in the interface state, are excited during the operation.

New states are created to assist the tunneling current[91]. In addition, the introduction of radiation-induced defects near the metal-GaN interface needs to be considered[88]. There are some reports demonstrating the improvement of diode performance after radiation at low doses [92]. However, high doses irradiation as studied here has caused device degradation. One of the possible degradation mechanisms comes from the increase in interfacial defect density from gamma-ray radiation[93]. Desorption of Ga and N happened near the surface of GaN. G. A. Umana-Membreno *et al.* indicated that energetic irradiation resulted in point defects of Ga and N species from their individual sublattices. The carrier concentration in GaN substrate after exposure to gamma ray irradiation increases, which was also observed[87]. Frenkel defects are considered to contribute to this increase of carrier concentration. Attention was paid to the vacancies on sublattices, V_N^+ and V_{Ga}^{3-}, which are the electrically active components of primary defects in n-GaN. V. V. Emtsev *et al.* suggested that at least one kind of native defects is mobile in GaN at room temperature, therefore the impurity atoms can work as effective traps for migrating defects[87].

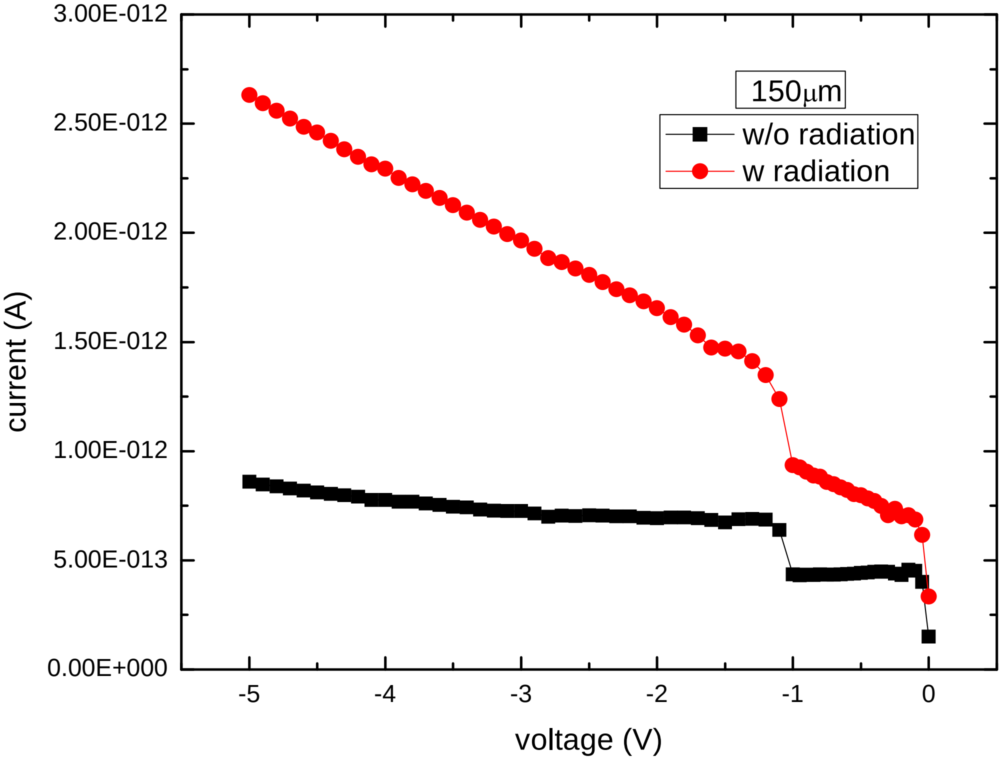

Figure 5.2.1 reverse leakage current of 150μm diameter devices

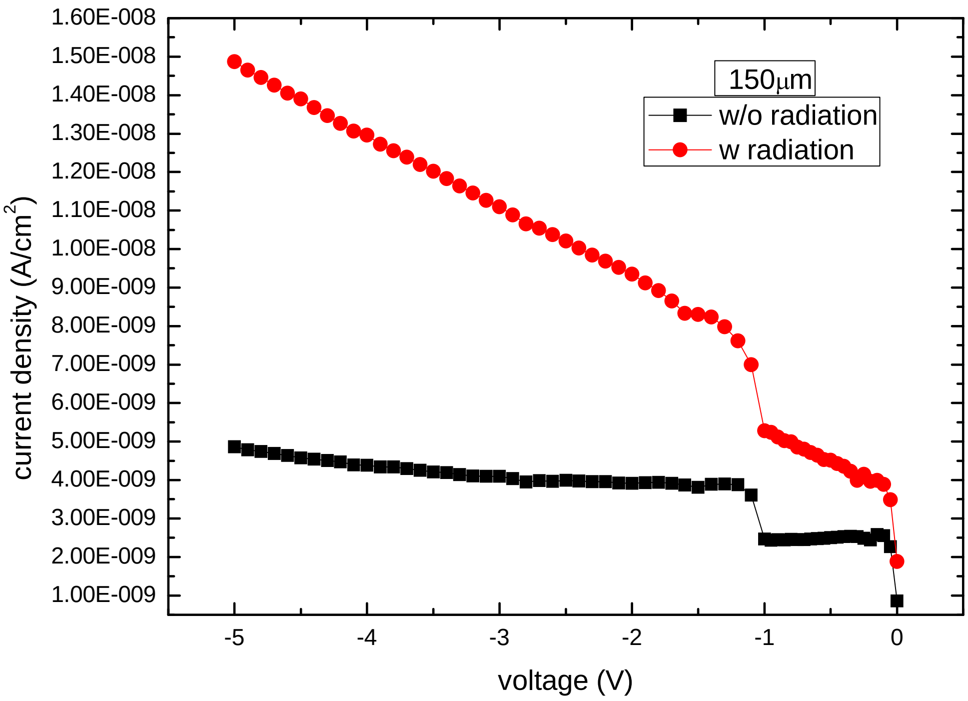

Figure 5.2.2 reverse leakage current density of 150μm diameter devices

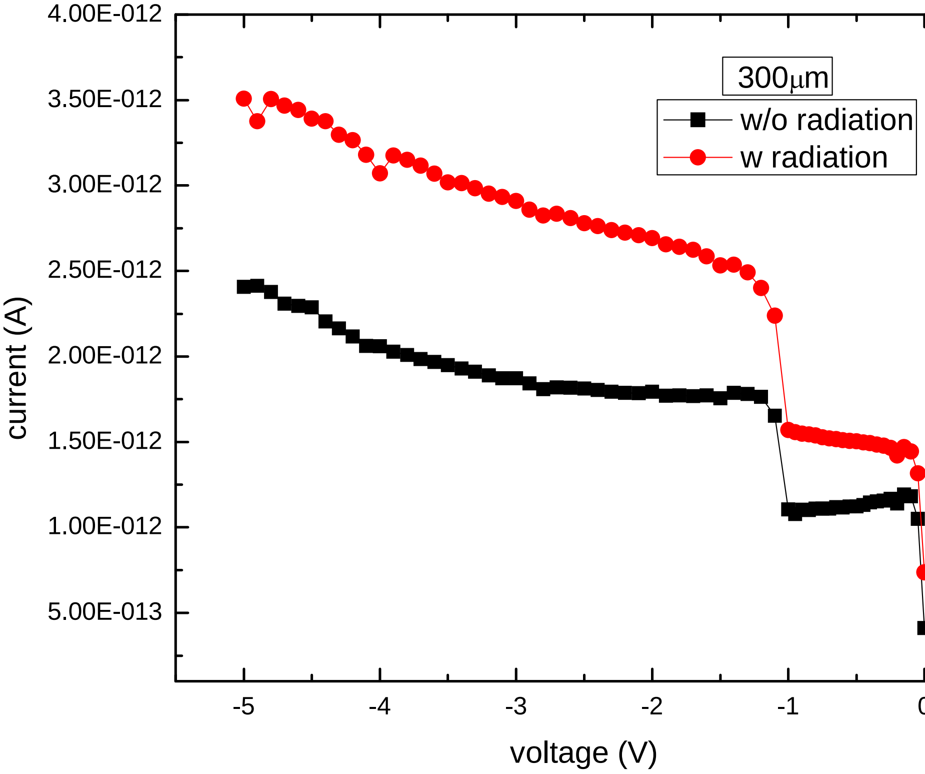

Figure 5.3.1 reverse leakage current of 300μm diameter devices

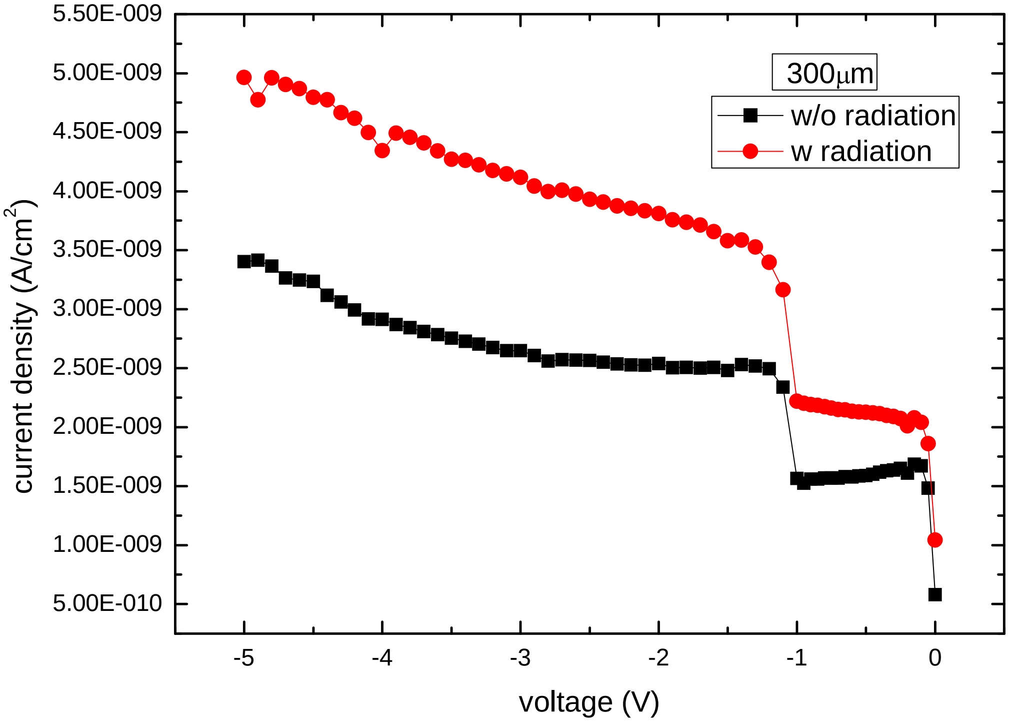

Figure 5.3.2 reverse leakage current density of 300μm diameter devices

On the reverse I-V characteristics, the radiation had a larger effect on the smaller size diode. As observed from experiment data, is the reverse leakage current shift of the order: small size (50μm) > middle size (150μm) > large size (300 μm), which are 10 times, 2 times and less than 1.4 times respectively compared to each original data in figure 5.1.1, 5.2.1 and 5.3.1. However, for larger size diodes, the leakage current goes much faster as the reverse bias increases, as seen from the slope of the curve. Another thing need to pay attention to is that before radiation the leakage current density at 5V for increasing size diodes are 8×10^9 A/cm^2, 5×10^9 A/cm^2, and 3.5×10^9 A/cm^2 from figure 5.1.2, 5.2.2, and 5.3.2. Generally, it is believed that smaller size should have smaller reverse leakage current, because there are fewer chances that the defects, such as dislocation will be included in the smaller size diodes. This data shows the different result. One possible explanation is due to the nonuniformity of dislocation densities. Although larger size diode covers more area in the GaN top surface, if the dislocation density varies spot by spot, it is possible that the average defect density could be smaller. From the formation of Schottky barrier at the metal-semiconductor interfaces, the experimental data are consistent with the presence of SBH inhomogeneity[94]. The experimental leakage current observed from diode to diode varied in agreement with isolated "leakage spots" because of the existence of low local SBH[95]. At the low SBH area, the local current density maybe orders of magnitude higher than the average. Higher than average SBH patches are also possible, however, they have little contribution to the electron transport.

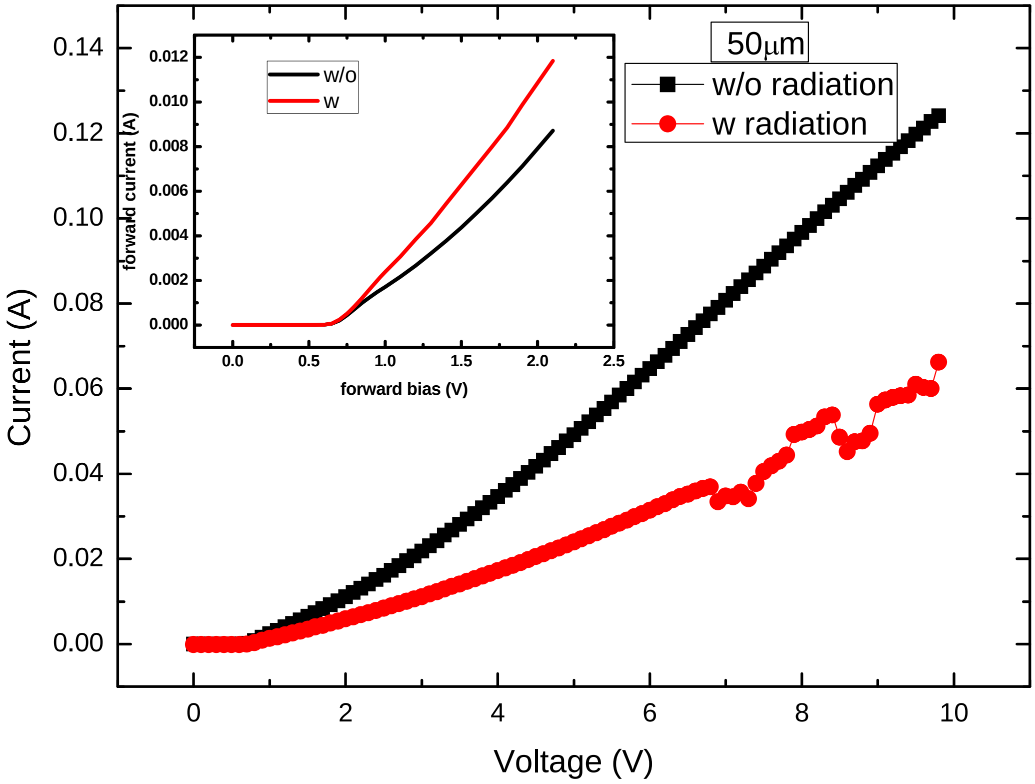

Figure 5.1.3 forward current of 50μm diameter devices

Forward I-V curves characteristics should be considered in two parts. First, look at the small diode of 50 μm diameter in figure 5.1.3. It is interesting to find that from 0 to 2 V bias, the diode after gamma ray radiation showed better performance, a lower turn on voltage and a smaller on-state resistance (inset of figure 5.1.3). However, as bias continues to increase, the damage of gamma ray radiation can be observed. At 10 V, the forward current reduced to only half of the original value. This anomaly is very similar to the temperature dependent current behavior of Schottky diodes[96]. The presence of

Schottky barrier height inhomogeneity over the metal-semiconductor contact area was used to explain this phenomenon[97]. Electron transport has been treated as the summation of current flowing through all the individual patches. Each patch has its own area and Schottky barrier height[95]. The interaction of neighboring patches with different Schottky barrier height need to be considered. In this experiment, the gamma ray radiation adds inhomogeneity of Schottky barrier height to the metal-semiconductor interface. Larger size diodes 150 μm diameter and 300 μm also showed the same trend in figure 5.2.3 and 5.3.3.

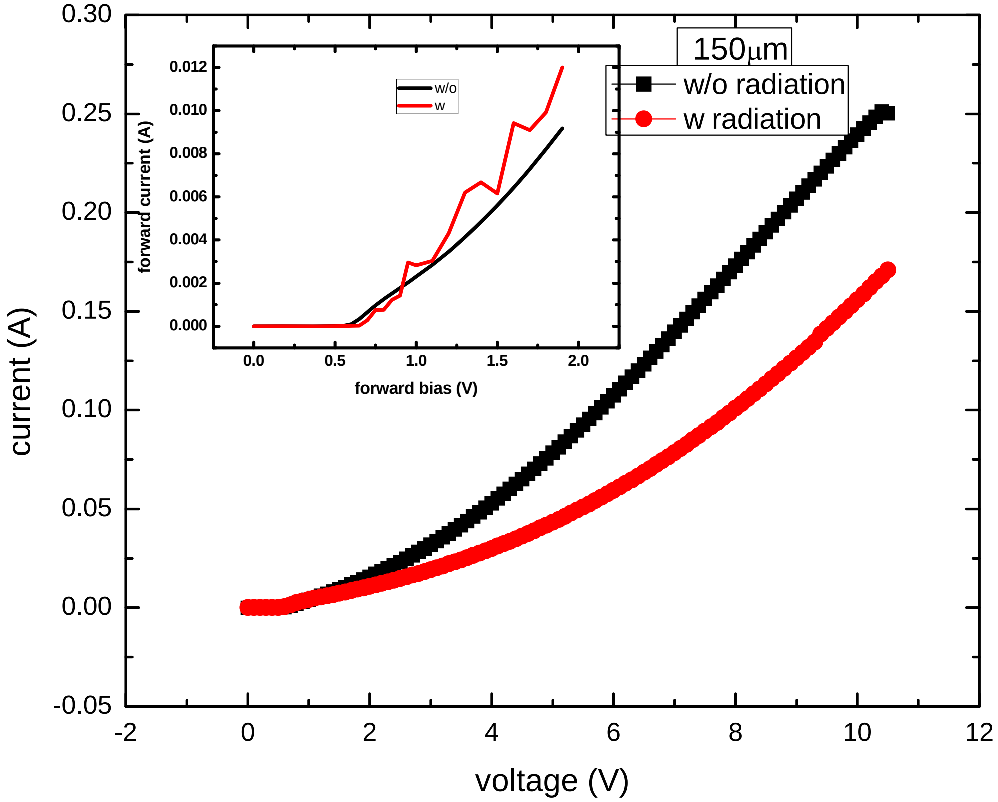

Figure 5.2.3 forward current of 150μm diameter devices

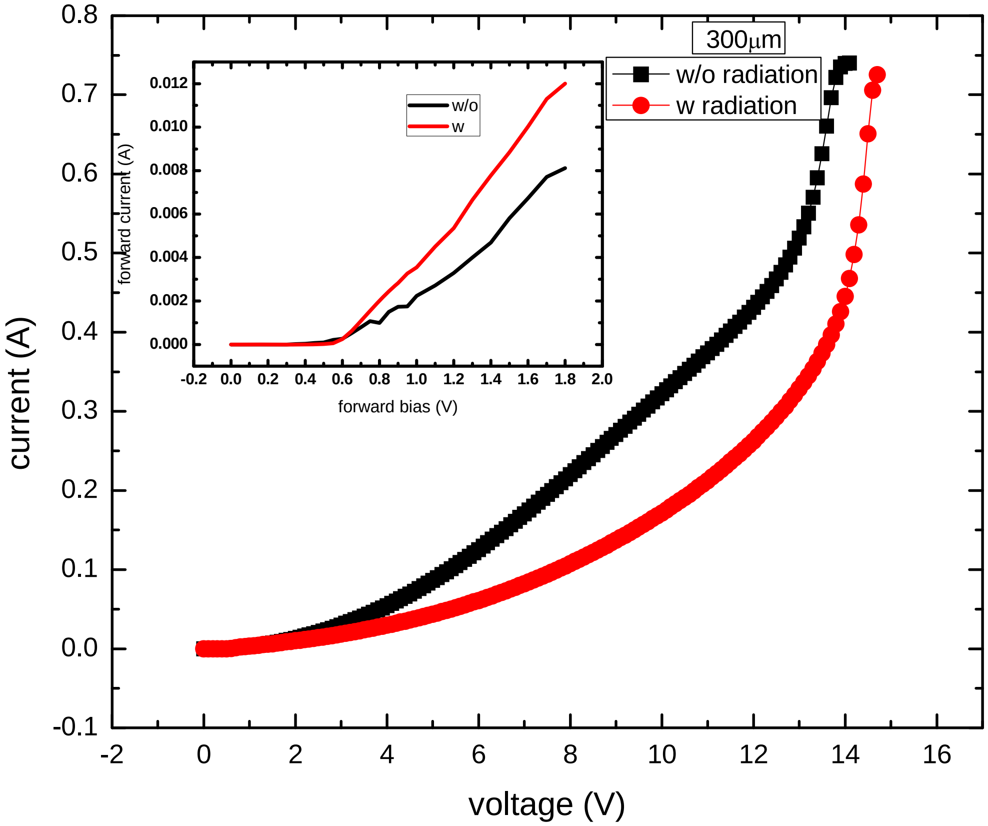

Figure 5.3.3 forward current of 300μm diameter devices

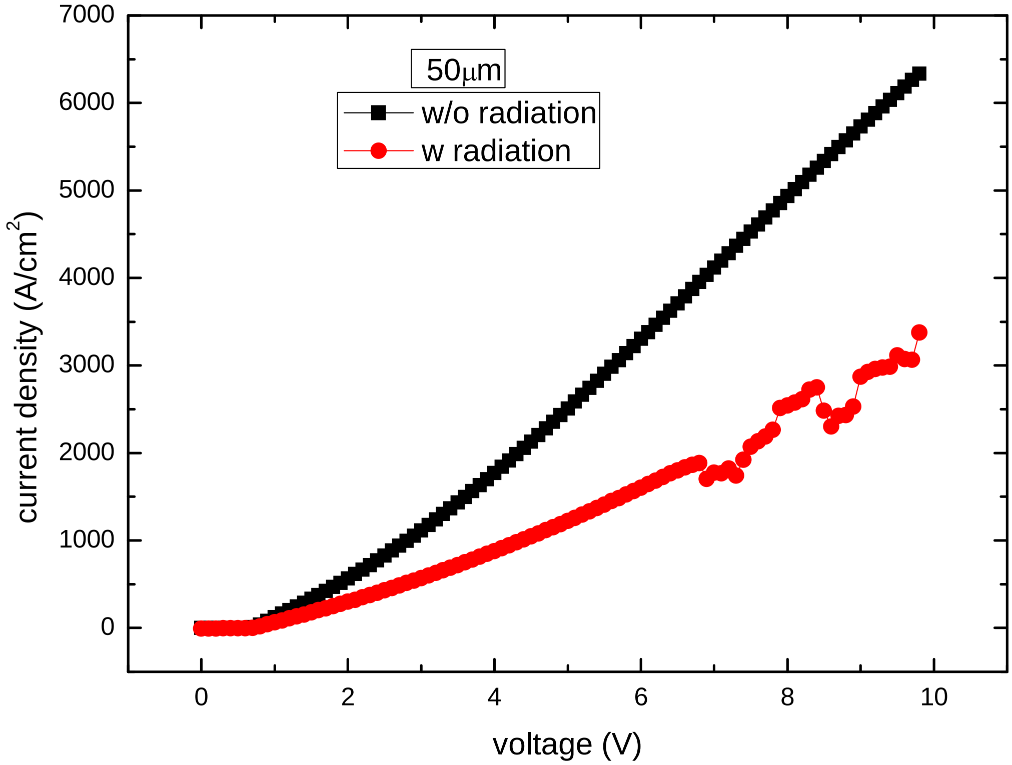

Figure 5.1.4 forward current density of 50μm diameter devices

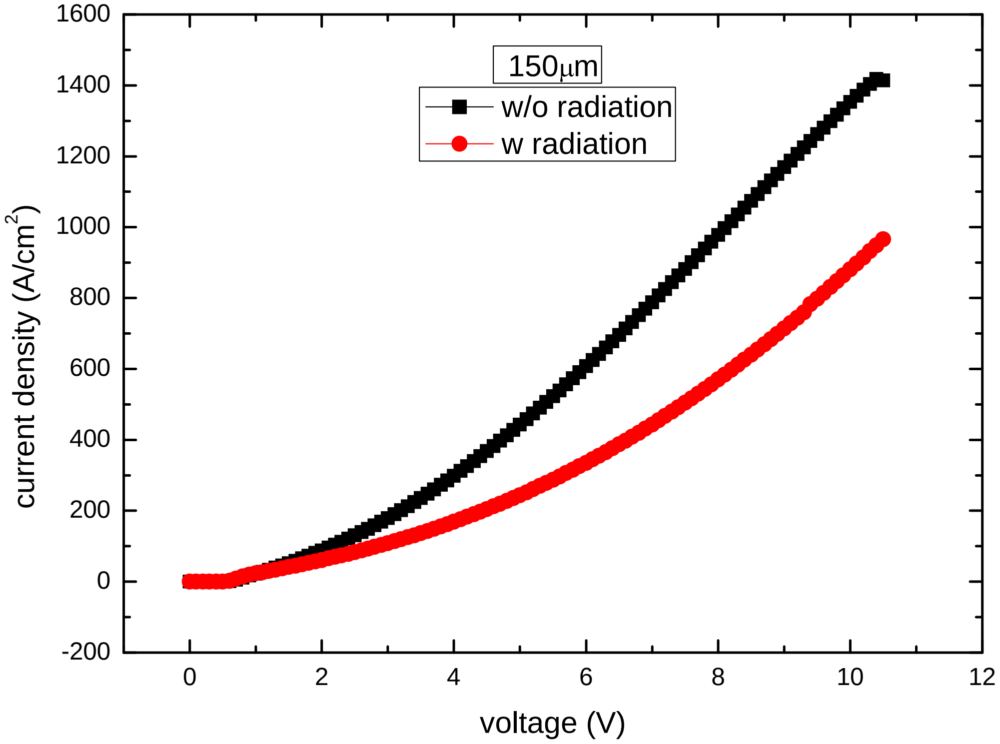

Figure 5.2.4 forward current density of 150μm diameter devices

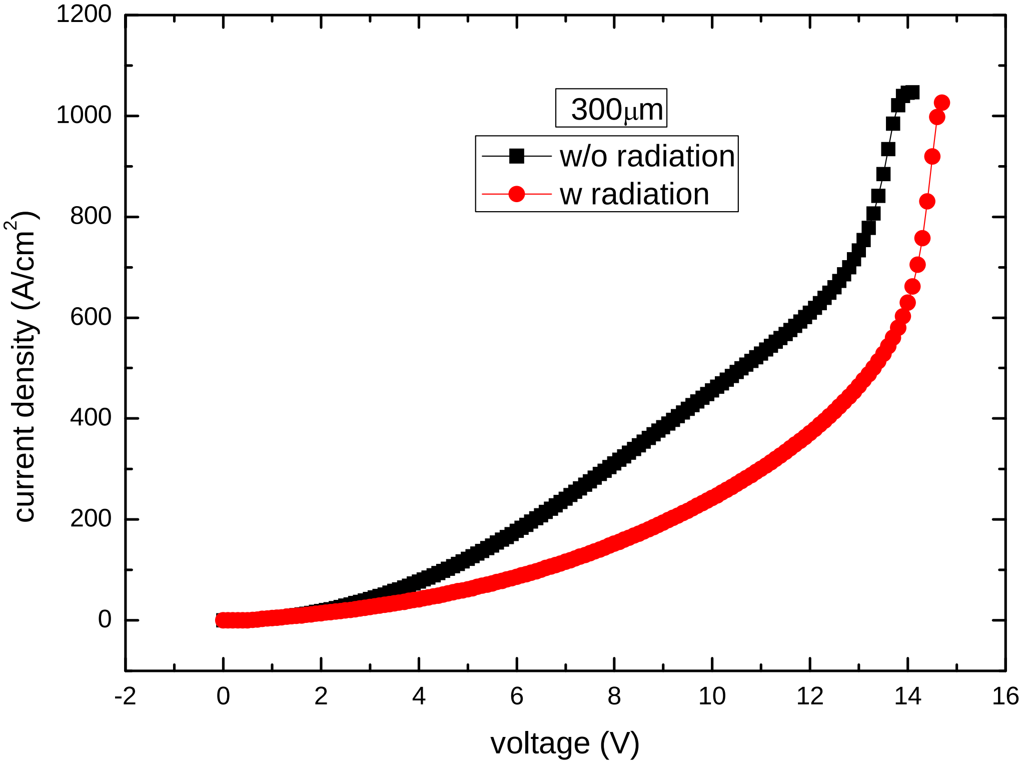

Figure 5.3.4 forward current density of 300μm diameter devices

Consider forward current density, different size diodes reduced forward conductor at the similar rate at higher voltages. This means forward current characteristic is not as sensitive to size of the contact as that for reverse leakage current.

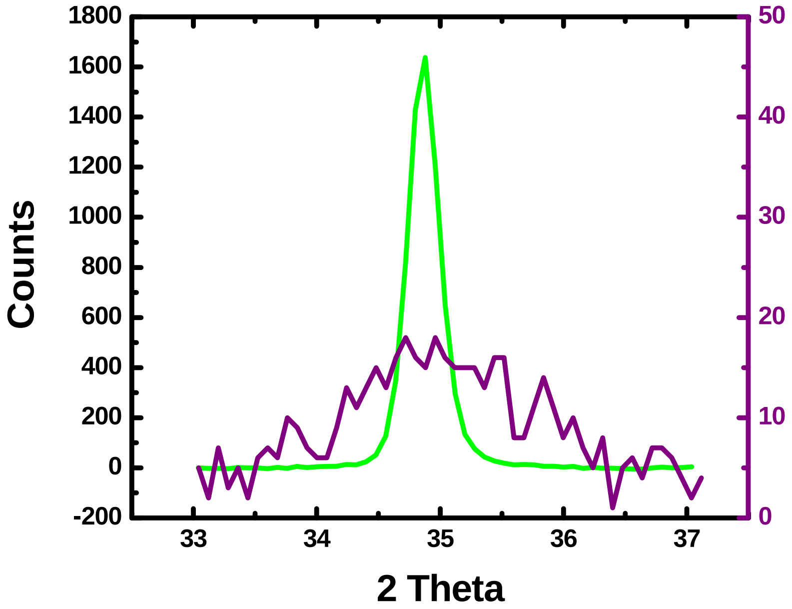

Figure 5.4 XRD spectra for GaN treated by gamma ray.

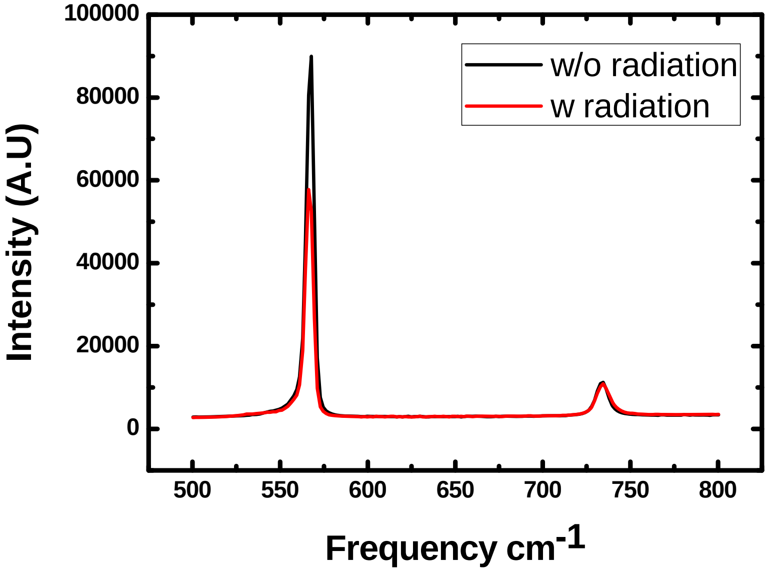

Figure 5.5 Raman Spectra for GaN before and after gamma ray radiation

Figure 5.4 gives the X-ray diffraction profile for preirradiated and gamma ray radiated GaN. The profile indicates that the crystallinity of GaN was greatly influenced by the radiation. The dominant peak of GaN is located at 2theta = 35°, from GaN (0002) plane[98]. The intensity of this peak decreased dramatically after the exposure to gamma ray and the peak broadened severely. One conclusion is that irradiation energy had played a destructive role in the crystallinity of GaN. However, compared to the GaN thin film, this bulk GaN is more tolerant to radiation[99].

Figure 5.5 shows the Raman spectra for GaN substrate. The only difference between the spectra is the Raman E_2 peak intensity before and after radiation. The spectra provide evidence to explain that the crystal structure is destroyed by energetic radiation, and then the amount of GaN which can contribute to the spectrum is reduced. This data is consistent with the X-ray diffraction results.

5.4 Summary and Conclusions

The effect of of gamma ray radiation on the performance of vertical Schottky diodes based on bulk GaN was investigated through reverse leakage current and forward current. Frenkel defects probably caused the increase of carrier concentration in GaN after exposure to gamma ray radiation. By comparing the electrical characteristics before and after gamma ray radiation, Schottky barrier height inhomogeneity over the metal-semiconductor contact area was utilized to explain the different current behavior at lower voltages and higher voltages. XRD and Raman data show the crystal structure of GaN was badly destroyed by the energetic radiation. However, the electrical properties are not as bad, which proves GaN especially bulk GaN is tolerant to radiation environment.

CHAPTER 6

SUMMARY AND FUTURE WORK

For the experiment in Chapter 3, Schottky contact was fabricated on front side of bulk GaN with no other treatment. With the n^- epi and on n^+ bulk substrate design, the forward current characteristic is improved by reducing the specific on-state resistance through the high doping near the ohmic contact. However, the breakdown voltage is not as high as expected. Schottky diode on GaN is known to suffer from premature breakdown. With edge termination schemes, electrical crowding at the corner of the metal contact can be released effectively. There are only a few reports of edge termination methods employed to GaN Schottky rectifiers. A. P. Zhang *et al.* investigated three different edge termination techniques, such as p guard ring formed at the edge of Schottky barrier metal, p floating field ring to extend the depletion boundary along the surface of SiO_2 dielectric and p-n junction grid integrated into the drift region of Schottky rectifier structure[100,101]. The most widely used edge termination method is adding field plate to smooth out the electric field distribution around the contact periphery. Therefore, in order to increase the breakdown voltage, field plate can be added to the edge of Schottky metal contact. Edge termination design and simulation done by K. H. Baik *et al.* showed that SiO_2 produced the highest breakdown voltage due to the large band-gap and low dielectric constant[102]. Yi Zhou pointed that high quality SiO_2 is necessary to achieve high breakdown voltages. SiNx is another candidate good for field plate. Other factors, such as the extent of metal electrode overlap, dielectric thickness and ramp oxide angle (if ramp oxide is used) also greatly influence the performance of the dielectric materials[102]. It is necessary to make sure that the thickness of the dielectric materials is large enough to prevent the breakdown initiating from the dielectric.

There are several improvements which can be applied to the *in-situ* Raman diagnosis of bulk GaN-based Schottky rectifier under operation experiment. First of all, the contact damage from the needle to the Schottky contact is an issue. Wire bonding is an excellent tool to make interconnections between devices and the outside. There will be two advantages, if wire is used to extend the Schottky contact. One is to avoid the scratch from the probe needle; the other is to enlarge the effective contact area between the Schottky contact metal and the probe needle. Therefore, heat will not accumulate at the tip of needle in order to avoid melting the metal contact. All these can increase the maximum current (power), which can be applied to the device. With more power available, more data points showing the relationship of Raman peak shift and added power will be achieved. Secondly, if an XY stage for sample is usable, a 2-D mapping of the E_2 frequency change is acquired, which can illustrate the Raman frequency shift not limited to the random position probed on Ga-face. It can spread the measurement over the whole area of the device. Device degradation can originate from local “hot spots” due to imperfection. It is of great importance to study hot spot in GaN as the thermal conductivity lead to high power dissipation in the hot spot, which result in the higher temperature in the hot spot[72]. Large gradient of temperature exists in the hot spot. Meanwhile, a lateral heat dissipation profile on the Schottky contact of the device is examined. Currently, most of the hot spot detection was realized on the AlGaN/GaN

HEMT structures. It is necessary to study the hot spot on Schottky diodes based on bulk GaN because the reliability of the device is important for high power applications. Thirdly, piezoelectric strain is another source for Raman E_2 phonon peak shift on GaN when the Schottky diode is biased. The piezoelectric strain induced Raman phonon shift is calculated through the data provided by published papers from different groups in Chapter 4 and the shift is found to be very small compared to the shift observed. However, it will be more convincing if corresponding experimental data can be provided. It was pointed out that the temperature dependence of Raman phonon frequency is sensitive to the biaxial strain which comes from the heteroepitaxial growth on sapphire or other foreign substrate[82]. So compared to freestanding GaN wafer, the GaN epilayer on sapphire was considered under compressive or tensile strain depending on various layer structure and layer thickness, while bulk GaN was considered as stress free[73]. An experiment can be set up, where the wafer is attached to a well heat-sink carrier. In addition, limited power should be applied to the device to prevent self-heating. Under these conditions, the contribution of temperature increase from self-heating can be neglected. When electric field is added to the device through the power source, micro Raman spectroscopy can monitor the strain/stress in the bulk GaN layer via the change of phonon frequencies. By this method, the effect of piezoelectric strain on phonon frequency can be detected experimentally to support the theoretical calculation.

In chapter 5, the performance of Schottky diodes on bulk GaN under gamma ray radiation is discussed. The samples can be exposed to different gamma ray doses in order to get a complete profile of Schottky diode parameters extracted from C-V and I-V curves under the influence of various doses. By doing this, the gradual effect of gamma ray radiation on GaN devices can be observed. Moreover, post-radiation low temperature annealing was reported to fully restore the reverse I-V characteristics to pre-radiation levels[88]. However, the annealing temperature after radiation scattered for different groups[87, 88, 103]. It is meaningful to study the effect of different post-radiation annealing temperatures on the recovery of Schottky diode characteristics under gamma ray radiation. In polar semiconductors, it is known that the electronic parameters of materials, such as the electron concentration and mobility can be achieved via Raman spectroscopy. The coupling between longitudinal-optical (LO) phonons and plasmons result in the formation of longitudinal-optical-phonon-plasmon (LPP) mode, which is closely related to the carrier concentration and mobility of free carriers[87] through plasmon frequency ω_P and plasmon damping constant γ. The electron concentration extracted via C-V characteristic in GaN subjected to gamma ray radiation was observed to increase from the pre-radiation level. Raman spectroscopy can offer another method to prove the increase of carrier concentration due to the radiation-induced defects.

BIBLIOGRAPHY

[1] J. I. Pankove, E. A. Miller and J. E. Berkeyheiser, RCA Rev. **32**, 383 (1971). "GaN electroluminescent diodes"

[2] H. Amano, N. Sawaki, I. Akasaki and Y. Toyoda, Appl. Phys. Lett. **48**, 353 (1986). "Metalorganic vapor phase epitaxial growth of a high quality GaN film using an AlN buffer layer"

[3] S. Nakamura, Japan. J. Appl. Phys. Part 2, **30**, L1705 (1991). "GaN Growth Using GaN Buffer Layer"

[4] S. Nakamura, T. Mukai, and M. Senoh, Japan. J. Appl. Phys. **31**, 2883 (1992). "Si- and Ge- doped GaN Film Grown with GaN Buffer Layers"

[5] H. Amano, M. Kito, K. Hiramatsu and I. Akasaki, Japan. J. Appl. Phys. **28**, L2112 (1989). "P-type Conduction in Mg-Doped GaN Treated with Low-Energy Electron Beam Irradiation (LEEBI)"

[6] S. Nakamura, M. Senoh, T. Mukai, Japan. J. Appl. Phys. **30**, L1708 (1991). "Highly P-Typed Mg-Doped GaN Films Grown with GaN Buffer Layers"

[7] S. Nakamura, T. Mukai, M. Senoh and N. Iwasa, Japan. J. Appl. Phys. **31**, L139 (1992). "Thermal Annealing Effects on P-Type Mg-Doped GaN Films"

[8] Joachim Piprek, "Nitride semiconductor devices book" Germany, Wiley-VCH, 2007

[9] P. Lawaetz, Phys. Rev. B **5**, 4039 (1972). "Study of the Wurtzite Structure"

---

[10] Michael E. Levinshtein, Sergey L. Rumyantsev and Michael S. Shur, Properties of Advanced Semiconductor Materials. New York, John Wiley & Sons, 2001.

[11] S. M. Sze, Kwok K. Ng, Physics of Semiconductor devices. New York, John Wiley & Sons, 2007.

[12] S. J. Pearton, F. Ren, A. P. Zhang and K. P. Lee, Mater. Sci. Engi. **R30**, 55 (2000). “Fabrication and Performance of GaN devices”

[13] M. Trivedi and K. Shenai, J. Appl. Phys. **85**, 6889 (1999). “Performance evaluation of high-power wide band-gap semiconductor rectifiers”

[14] B. Gelmont, K. S. Kim, and M. Shur, J. Appl. Phys. **74**, 1818 (1993). “Monte Carlo simulation of electron transport in GaN”

[15] M. S. Shur, B. Gelmont, and M. Asif Khan, J. Electron. Mater. **25**, 777 (1996). “Electron Mobility in Two-Dimensional Electron Gas in AlGaN/GaN Heterostructures and in Bulk GaN”

[16] http://www.fujitsu.com/global/news/pr/archives/month/2005/20051205-02.html

[17] R. Gaska, J.W. Yang, A. Osinsky, Q. Chen, M.A. Khan, A.O. Orlov, G.L. Snider, and M.S. Shur, Appl. Phys. Lett. **72**, 707 (1998). “Electron transport in AlGaN–GaN heterostructures grown on 6H–SiC substrates”

[18] M. Dur, S. M. Goodnick and P. Lugli, Phys. Rev. B, **54**, 17794 (1996). “Monte Carlo simulation of intersubband relaxation in wide, uniformly doped GaAs/AlxGa1-xAs quantum wells”

[19] H. Morkoc, S. Strite, G. B. Gao, M. E. Lin, B. Sverdlov and M. Burns, J. Appl. Phys. **76**, 1363 (1994). “Large-band-gap SiC, III-V nitride, and II-VI ZnSe-based semiconductor device technologies”

---

[20] S. D. Lester, F. A. Ponce, M. G. Craford and D. A. Steigerwald, Appl. Phys. Lett. **66**, 1249 (1995). “High dislocation densities in high efficiency GaN-based light-emitting diodes”

[21] W. C. Johnson, J. B. Parsons, and M. C. Crew, J. Phys. Chem. **36**, 2651 (1932). “Nitrogen Compounds of Gallium. III”

[22] H. P. Maruska and J. J. Tietjen, Appl. Phys. Lett. **15**, 327 (1969). “The preparation and properties of vapor-deposited single-crystalline GaN”

[23] M. K. Kelly, R. P. Vaudo, V. M. Phanse, L. Gorgens, O. Ambacher and M. Stutzmann, Jap. J. Appl. Phys. **38**, L217 (1999). “Large Free-Standing GaN Substrates by Hydride Vapor Phase Epitaxy and Laser-induced Liftoff”

[24] http://www.oxford-instruments.com/products/etching-deposition-growth/processes-techniques/hvpe/PublishingImages/HVPE.png

[25] X. H. Wu, P. Fini, E. J. Tarsa, B. Heying, S. Keller, U. K. Mishra, S. P. DenBaars and J. S. Speck, J. Crys. Growth. **189**, 231 (1998). “Dislocation generation in GaN heteroepitaxy”

[26] M. A. Khan, R. A. Skogman, R. G. Schulze, and M. Gershenzon, Appl. Phys. Lett. **42**, 430 (1983). “Electrical properties and ion implantation of epitaxial GaN, grown by low pressure metalorganic chemical vapor deposition”

[27] P. Hacke, T. Detchprohm, K. Hiramatsu, and N. Sawaki, Appl. Phys. Lett. **63**, 2676 (1993). “Schottky barrier on n-type GaN grown by hydride vapor phase epitaxy”

[28] J. S. Foresi and T. D. Moustakas, Appl. Phys. Lett. **62**, 2859 (1993). “Metal contacts on gallium nitride”

---

[29] Lei Wang, M. I. Nathan, T-H. Lim, M. A. Khan and Q. Chen, Appl. Phys. Lett. **68**, 1267 (1996). “High barrier height GaN Schottky diodes: Pt/GaN and Pd/GaN”

[30] J. D. Guo, M. S. Feng, R. J. Guo, F. M. Pan and C. Y. Chang, Appl. Phys. Lett. **67**, 2657 (1995). “Study of Schottky barrier barrier on n-type GaN grown by low-pressure metalorganic chemical vapor deposition”

[31] Q. Z. Liu and S. S. Lau, Solid State Electron. **42**, 677 (1998) and references cited. “A review of the Metal GaN contact technology”

[32] Z. Z. Bandic, P. M. Bridger, E. C. Piquette, T. C. Mcgill, R. P. Vaudo, V. M. Phanse, and J. M. Redwing, Appl. Phys. Lett. **74**, 1266 (1999). “High voltage (450) GaN Schottky rectifiers”

[33] G. T. Dang, A. P. Zhang, M. M. Mshewa, F. Ren, J. –I. Chyi, C. –M. Lee, C. C. Chuo, G. C. Chi, J. Han, S. N. G. Chu, R. G. Wilson, X. A. Cao and S. J. Pearton, J. Vac. Sci. Technol. A **18**, 1135 (2000). “High breakdown voltage Au/Pt/GaN Schottky diodes”

[34] A. P. Zhang, J. W. Johnson, F. Ren, J. Han, A. Y. Polyakov, N. B. Smirnov, A. V. Govorkov, J. M. Redwing, K. P. Lee and S. J. Pearton, Appl. Phys. Lett. **78**, 823 (2001). “Lateral AlxGa1ÀxN power rectifiers with 9.7 kV reverse breakdown voltage”

[35] M. Misra, A. V. Sampath, and T. D. Moustakas, Appl. Phys. Lett. **76**, 1045 (2000). “Investigation of vertical transport in n-GaN films grown by molecular beam epitaxy using Schottky barrier diodes”

[36] Kwok K. Ng, Complete guide to semi devices book. McGraw-Hill series, 1995

[37] S. J. Pearton, J. C. Zolper, R. J. Shul and F. Ren, J. Appl. Phys. **86**, 1 (1999). “GaN: Processing, defects, and devices”

---

[38] S. M. Sze, Kwok K. Ng, Physics of Semiconductor devices. New York, John Wiley & Sons, 2007.

[39] C. Fontaine, T. Okumura and K.N. Tu, J. Appl. Phys. **54**, 1404 (1983). “Interfacial Reaction and Schottky Barrier Between Pt and GaAs”

[40] D. K. Schroder. Semiconductor Material and Device Characterization. New York, John Wiley & Sons, 2006.

[41] T. Okumura and K.N. Tu, J. Appl. Phys. **61**, 2955 (1987). “Electrical Characterization of Schottky Contacts of Au, Al, Gd and Pt on n-Type and p-Type GaAs”

[42] http://en.wikipedia.org/wiki/File:Raman_energy_levels.jpg

[43] T. Azuhata, T. Sota, K. Suzuki, and S. Nakamura, J. Phys. Condens. Matter **7**, L129 (1995). “Polarized raman spectra in GaN”

[44] C. A. Arguello, D. L. Rousseau, and S. P. S. Porto, Phys. Rev. **181**, 1351 (1969). “First-Order Raman Effect in Wurtzite-Type Crystals”

[45] T. Beechem, A. Christensen, S. Graham, and D. Green. J. Appl. Phys. **103**, 124501 (2008).

[46] M. Diale, F. D. Auret, N. G. van der Berg, R. Q. Odendaal, W. D. Roos, Appl. Surf. Sci. **246**, 279 (2005). “Analysis of GaN procedures”

[47] S. W. King, J. P. Barnak, M. D. Bremser, K. M. Tracy, C. Ronning, R. F. Davis and R. J. Nemanich, J. Appl. Phys. **84**, 5248 (1998). “Cleaning of AlN and GaN surfaces”

[48] M. E. Lin, Z. Ma, F. Y. Huang, Z. F. Fan, L. H. Allen and H. Morkoc, Appl. Phys. Lett. **64**, 1003 (1994). “Low resistance ohmic contacts on wide band-gap GaN”

[49] D. W. Jenkins and J. D. Dow, Phys. Rev. **B 39**, 3317 (1989). “Electronic structures and doping of InN, InxGa1-xN, and InxAl1-xN”

---

[50] B. P. Luther, S. E. Mohney, T. N. Jackson, M. Asif Khan, Q. Chen and J. W. Yang, Appl. Phys. Lett. **70**, 57 (1997). "Investigation of the mechanism for Ohmic contact formation in Al and Ti/Al contacts to *n*-type GaN"

[51] S. N. Mohammad, J. Appl. Phys. **95**, 7940 (2004). "Contact Mechanisms and design principles for alloyed ohmic contacts on *n*-GaN"

[52] L. F. Lester, J. M. Brown, J. C. Ramer, L. Zhang, S. D. Hersee, and J. C. Zolper, Appl. Phys. Lett. **69**, 2737 (1996). "Nonalloyed Ti/Al ohmic contacts to n-type GaN using high temperature premetallizational anneal"

[53] http://www.memsnet.org/mems/processes/etch.html

[54] http://www.ul.ie/~childsp/CinA/Issue53/issue53_files/main_files/cinina62.jpg

[55] H. P. Maruska and J. J. Tietjen, Appl. Phys. Lett. **15**, 327 (1969). "THE PREPARATION AND PROPERTIES OF VAPOR-DEPOSITED SINGLE-CRYSTAL-LINE GaN"

[56] T. L. Chu, J. Electrochem. Soc. **118**, 1200 (1971). "Gallium Nitride films"

[57] Y. Morimoto, J. Electrochem. Soc. **121**, 1383 (1974). "Few characteristics of Epitaxial GaN-etching and thermal Decomposition"

[58] S. J. Pearton, C. R. Abernathy, F. Ren, J. R. Lothian, P. W. Wisk, A. Katz, and C. Constantine, Semicond. Sci. Technol. **8**, 310 (1993). "Dry etching of thin-film InN, AlN and GaN"

[59] R. J. Shul, G. B. McClellan, S. J. Pearton, C. R. Abernathy, C. Constantine, and C. Barratt, Electron. Lett. **32**, 1408 (1996). "Comparison of dry etch techniques for GaN"

---

[60] I. Adesida, A. Mahajan, E. Andideh, M. Asif Khan, D. T. Olsen, and J. N. Kuznia, Appl. Phys. Lett. **63**, 2777 (1993). "Reactive ion etching of gallium nitride in silicon tetrachloride plasmas"

[61] E. H. Rhoderick and R. H William, "Metal-Semiconductor Contacts". Oxford 1988.

[62] B. S. Kang, F. Ren, Y. Irokawa, K. W. Baik, S. J. Pearton, C.-C. Pan, G.-T. Chen, J.-I. Chyi, H.-J. Ko, and H.-Y. Lee, J. Vac. Sci. Technol. B **22**, 710 (2004). "Temperature dependent characteristics of bulk GaN Schottky rectifiers on free-standing GaN substrates"

[63] L. Lewis, B. Corbett, D. O. Mahony, and P. P. Maaskant, Appl. Phys. Lett. **91**, 162103 (2007). "Low-resistance Ni-based Schottky diodes on freestanding n-GaN"

[64] Hai Lu, Rong Zhang, Xiangqian Xiu, Zili Xie, Youdou Zheng, and Zhonghui Li, Appl. Phys. Lett. **91**, 172113 (2007). "Low leakage Schottky rectifiers fabricated on homoepitaxial GaN"

[65] S. Hashimoto, Y. Yoshizumi, T. Tanabe, and M. Kiyama, J. Crys. Growth **298**, 871 (2007). "High-purity GaN epitaxial layers for power devices on low-dislocation-density GaN substrates"

[66] R. M. Cibils and R. H. Buitrago, J. Appl. Phys. **58**, 1075 (1985). "Forward *I-V* plot for nonideal Schottky diodes with high series resistance"

[67] Q. Z. Liu, L. S. Yu, S. S. Lau, J. M. Redwing, N. R. Perkins and T. F. Kuech, Appl. Phys. Lett. **70**, 1275 (1997). "Thermally stable PtSi Schottky contact on n-GaN"

[68] T. Beechem, A. Christensen, S. Graham, and D. Green. J. Appl. Phys. **103**, 124501 (2008). "Micro-Raman thermometry in the presence of complex stresses in GaN devices"

---

[69] Y. Ohno, M. Akita, S. Kishimoto, K. Maezawa, and T. Mizutani, Jpn J. Appl. Phys. **41**, L452 (2002). “Temperature Distribution Measurement in AlGaN/GaN High-Electron-Mobility Transistors by Micro-Raman Scattering Spectroscopy”

[70] I. Ahmad, V. Kasisomayajula, M. Holtz, J. B. Berg, S. R. Kurtz, C. P. Tigges, A. A. Alleman, and A. G. Baca, Appl. Phys. Lett. **86**, 173503 (2005). “Self-heating study of an AlGaN/GaN-based heterostructure field-effect transistor using ultraviolet micro-Raman scattering”

[71] W. D. Hu, X. S. Chen, Z. J. Quan, C. S. Xia, W. Lu, and P. D. Ye. J. Appl. Phys. **100**, 074501 (2006). “Self-heating simulation of GaN-based metal-oxide-semiconductor high-electron-mobility transistors including hot electron and quantum effects”

[72] I. Ahmad, V. Kasisomayajula, D. Y. Song, L. Tian, J. M. Berg, and M. Holtz. J. Appl Phys. **100**, 113718 (2006). “Self-heating in a GaN based heterostructure field effect transistor: Ultraviolet and visible Raman measurements and simulations”

[73] J. Kim, J. A. Freitas, Jr., P. B. Klein, S. Jang, F. Ren, and S. J. Pearton. Electrochem. Solid-State Lett. **8**, G345 (2005). “The Effect of Thermally Induced Stress on Device Temperature Measurements by Raman Spectroscopy”

[74] Y. Zhou, M. Li, D. Wang, C. Ahyi, C. C. Tin, J. Williams, and M. Park. Appl. Phys. Lett. **88**, 113509 (2006). “Electrical characteristics of bulk GaN-based Schottky rectifiers with ultrafast reverse recovery”

[75] S. M. Sze and K. K. Ng. Physics of Semiconductor Devices. 3rd Ed. New York, John Wiley & Sons, 2007.

[76] D. K. Schroder. Semiconductor Material and Device Characterization. New York, John Wiley & Sons, 2006.

---

[77] J. –I. Chyi, C. –M. Lee, C. –C. Chuo, X. A. Cao, G. T. Dang, A. P. Zhang, F. Ren, S. J. Pearton, S. N. G. Chu and R. G. Wilson. Solid State Electronics **44**, 613 (2000). "Temperature dependence of GaN high breakdown voltage diode rectifiers"

[78] W. Hayes and R. Laudon. Scattering of Light by Crystals. New York, John Wiley & Sons, 1978.

[79] J. B. Cui, K. Amtmann, J. Ristein, and L. Ley. J. Appl. Phys. **83**, 7929 (1998). "Noncontact temperature measurements of diamond by Raman scattering spectroscopy"

[80] W. S. Li, Z. X. Shen, Z. C. Feng, and S. J. Chua. J. Appl. Phys. **87**, 3332 (2000). "Temperature dependence of Raman scattering in hexagonal gallium nitride films"

[81] H. Tang and I. P. Herman. Phys. Rev. B **43**, 2299 (1991). "Raman microprobe scattering of solid silicon and germanium at the melting temperature"

[82] M. S. Liu, L. A. Bursill, S. Prawer, K. W. Nugent, Y. Z. Tong and G. Y. Zhang. Appl. Phys. Lett. **74**, 3125 (1999). "Temperature dependence of Raman scattering in single crystal GaN films"

[83] M. Balkanski, R. F. Wallis, and E. Haro. Phys. Rev. B. **28**, 1928 (1983). "Anharmonic effects in light scattering due to optical phonons in silicon"

[84] A. Sarua, H. Ji, M. Kuball, M. J. Uren, T. Martin, K. J. Nash, K. P. Hilton, and R. S. Balmer. Appl. Phys. Lett. **88**, 103502 (2006). "Piezoelectric strain in AlGaN/GaN heterostructure field-effect transistors under bias"

[85] C. Kisielowski, J. Krüger, S. Ruvimov, T. Suski, J. W. Ager III, E. Jones, Z. Liliental-Weber, M. Rubin, E. R. Weber, M. D. Bremster, and R. F. Davis. Phys. Rev. B **54**, 17745 (1996). "Strain-related phenomena in GaN thin films"

[86] U. K. Mishra, Y.-F. Wu, B. P. Keller, S. Keller, and S. P. DenBaars, IEEE

Trans. Microwave Theory Tech. **46**, 756 (1998). “GaN microwave electronics”

[87] V. V. Emtsev, V. Y. Davydov, V. V. Kozlovskii, V. V. Lundin, D. S. Poloskin, A. N. Smirnov, N. M. Schmidt, A. S. Usikov, J. Aderhold, H. Klausing, D. Mistele, T. Rotter, J. Stemmer, O. Semchinova, and J. Graul, Semicond. Sci. Technol. **15**, 73 (2000). “Point defects in γ–irradiated n-GaN”

[88] G. A. Umana-Membreno, Student Member, IEEE, J. M. Dell, G. Parish, Member, IEEE, B. D. Nener, Senior Member, IEEE, L. Faraone, Senior Member, IEEE, and U. K. Mishra, Fellow, IEEE, IEEE. Trans. Electron. Devices. **50**, 2326 (2003). “^{60}Co Gamma Irradiation Effects on n-GaN Schottky diodes”

[89] Z.-Q. Fang, J. W. Hemsky, D. C. Look, and M. P. Mack, Appl. Phys. Lett. **72**, 448 (1998). “Electron-irradiation-induced deep level in *n*-type GaN”

[90] L. S. Yu, Q. Z. Liu, Q. J. Qiao, S. S. Lau, and J. Redwing, J. Appl. Phys. **84**, 2099 (1998). “The role of the tunneling component in the current–voltage characteristics of metal-GaN Schottky diodes”

[91] J. C. Carrano, T. Li, P. A. Grudowski, C. J. Eiting, R. D. Dupuis, and J. C. Campbell, J. Appl. Phys. **83,** 6148 (1998). “Comprehensive characterization of metal–semiconductor–metal ultraviolet photodetectors fabricated on single-crystal GaN”

[92] Ching-Wu Wang, J. Vac. Sci. Tech. B, **20**, 1821 (2002). “Neutron irradiation effect on radio-frequency magnetron-sputtered GaN thin films and Au/GaN Schottky diodes”

[93] G. A. Umana-Membreno, J. M. Dell, G. Parish, B. D. Nener, L. Faraone, S. Keller and U. K. Mishra, J. Appl. Phys. **101**, 054511 (2007). “Annealing of ^{60}Co gamma radiation-induced damage in *n*-GaN Schottky barrier diodes”

---

[94] R. T. Tung, Appl. Phys. Lett. **58**, 2821 (1991). “Electron transport of inhomogeneous Schottky barriers”

[95] R. T. Tung, Phys. Rev. B, **45**, 13509 (1992). “Electron transport at metal-semiconductor interfaces: General theory”

[96] S. Zhu, R. L. Van Meirhaeghe, C. Detavernier, F. Cardon, G.. P. Ru, X. P. Qu and B. Z. Li, Solid-State Electron **44**, 663 (2000). “Barrier height inhomogeneities of epitaxial CoSi2 Schottky contacts on n-Si (100) and (111)”

[97] S. Karadeniz, M. Sahin, N. Tugluoglu and H. Safak, Semicond. Sci. Technol. **19**, 1098 (2004). “Temperature-dependent barrier characteristics of Ag/p-SnS Schottky barrier diodes”

[98] T. I. Shin and D. H. Yoon, Cryst. Res. Technol. **40**, 827 (2005). “Growth behaviour of bulk GaN single crystals grown with various flux ratios using solvent-thermal method”

[99] Ching-Wu Wang, Bo-Shao Soong, Jing-Yu Chen, Chih-Liang Chen, and Yan-Kuin Su, J. Appl. Phys. **88**, 6355 (2000). “Effects of gamma-ray irradiation on the microstructural and luminescent properties of radio-frequency magnetron-sputtered GaN thin films”

[100] A. P. Zhang, G. T. Dang, X. A. Cao, H. Cho, F. Ren, J. Han, J.-I. Chyi, C.-M. Lee, T.-E. Nee, C.-C. Chuo, G.-C. Chi, S. N. G. Chu, R. G. Wilson and S. J. Pearton, MRS Internet J. Nitride Semicond. Res. **5S1**, W11.67 (2000). “Processing and Device Performance of GaN Power Rectifiers”

[101] J. W. Johnson, A. P. Zhang, W. B. Luo, F. Ren, S. J. Pearton, S. S. Park, Y. J. Park, and J.-I. Chyi, IEEE Trans. Electron Devices **49**, 32 (2002). “Breakdown Voltage and Reverse Recovery Characteristics of Free-Standing GaN Schottky Rectifiers”

---

[102] K. H. Baik, Y. Irokawa, F. Ren S. J. Pearton, S. S. Park and S. K. Lee, J. Vac. Sci. Technol. B, **20**, 2169 (2002). “Edge termination design and simulation for bulk GaN rectifiers”

[103] L. Polenta, Z.-Q. Fang, and D. C. Look, Appl. Phys. Lett. **76**, 2086 (2000). “On the main irradiation-induced defect in GaN”